Adaptive Integrated Guidance and Control for Air-breathing Phase of Reusable Launch Vehicle

A thesis submitted

in partial fulfillment for the award of the degree of

Doctor of Philosophy

by

Rani Radhakrishnan

Department of Avionics

Indian Institute of Space Science and Technology

Thiruvananthapuram, India

February 2025

Certificate

This is to certify that the thesis titled ***Adaptive Integrated Guidance and Control for Air-breathing Phase of Reusable Launch Vehicle*** submitted by **Rani Radhakrishnan**, to the Indian Institute of Space Science and Technology, Thiruvananthapuram, in partial fulfillment for the award of the degree of **Doctor of Philosophy** is a bonafide record of the original work carried out by her under my supervision. The contents of this thesis, in full or in parts, have not been submitted to any other Institute or University for the award of any degree or diploma.

Name of the Supervisor
Dr. Priyadarshnam
Professor,
Department of Avionics, IIST

Name of the Co-Supervisor
Dr. K. Sivan
Former Chairman,
ISRO.

Name of the Department Head
Dr. N. Selvaganesan
Professor and Head,
Department of Avionics, IIST.

Place: Thiruvananthapuram
Date: February 2025

Declaration

I declare that this thesis titled ***Adaptive Integrated Guidance and Control for Air-breathing Phase of Reusable Launch Vehicle*** submitted in partial fulfillment for the award of the degree of **Doctor of Philosophy** is a record of the original work carried out by me under the supervision of **Dr. Priyadarshnam**, and has not formed the basis for the award of any degree, diploma, associateship, fellowship, or other titles in this or any other Institution or University of higher learning. In keeping with the ethical practice in reporting scientific information, due acknowledgments have been made wherever the findings of others have been cited.

Place: Thiruvananthapuram
Date: February 2025

Rani Radhakrishnan
(SC13D017)

This thesis is dedicated to my Husband and Parents

Acknowledgements

The work presented in this thesis would not have been possible without my close association with many people. I take this opportunity to extend my sincere gratitude and appreciation to all those who made this Ph.D thesis possible.

First and foremost, I would like to extend my sincere gratitude to my research supervisor ***Dr. Priyadarshnam***, Professor, IIST. His guidance, perseverance, encouragement and continuous support enabled me to push forward and successfully complete my thesis. I would also extend my sincere gratitude to ***Dr. M. S. Harsha Simha***, Assistant Professor, IIST for his dedicated help, guidance and advice in publishing my journal papers. I am deeply grateful to my research supervisor ***Dr. K. Sivan***, the Former Chairman, ISRO to accept me as his project student and inspire me to complete this work amid his busy life. I deeply express my sincere gratitude to ***Dr. S. Somanath***, Ex. Chairman, ISRO for his timely intervention as Director IIST and for helping me to speed up in submitting the journal papers and motivating me to complete the work. I gratefully acknowledge the chairman of the doctoral committee, ***Dr.N. Selvaganesan***, Professor & Head, Department of Avionics, IIST and extend my sincere thanks to the other members of my doctoral committee ***Dr. Asok Joshi***, Professor, IIT Mumbai, ***Dr. Das Gupta***, Retd. Deputy Director, VSSC and ***Dr. V. R. Lalithambika***, Retd. Director, HSFC, ISRO for their periodic assessments of my research work.

I also take this opportunity to thank ***Shri. M. V. Dhekane***, Retd Director, IISU, ISRO, ***Dr. S. Geetha***, Retd. Programme Director, VSSC and ***Dr. G. Ayyappan***, Retd. Associate Director, VSSC for their kind technical support and assistance.

I am thankful to my institutes, **IIST, VSSC**, for picking me up as a doctoral student and providing me with an excellent research environment. I would like to express my sincere gratitude to the current Director ***Dr. Dipankar Banerjee*** of IIST and the Director of VSSC ***Dr. Unnikrishnan Nair*** for their encouragement and continuous support.

I would like to thank my ***(Parents)***, my ***(Son, Daughter)*** and other relatives and all my friends for their unconditional love and support. Last but not least, a heartfelt thanks goes out to my husband ***(Dr. K. Muraleedharan Nair)***, who stood by me through all the thick and thins and for his immense technical support.

-Rani Radhakrishnan

Abstract

Air-breathing satellite launch vehicles are winged vehicles containing all features and challenges of reusable launch vehicle with additional complexity of air-breathing propulsion. Air-Breathing Satellite Launch Vehicle (ABSLV) uses scramjet propulsion during the ascent phase which makes the system complex due to severe interaction between propulsion, aerodynamics and structural subsystems. Guidance and control design for an air-breathing launch vehicle is highly challenging due to the small frequency of separation between the two and high control structure interaction due to slender geometry of the vehicle. In conventional launch vehicle open loop guidance scheme is preferred in the atmospheric phase. But for air-breathing vehicle as the trajectory is sensitive to propulsion and aerodynamic forces, a closed loop guidance scheme is essential in this phase.

The thesis deals with the design of 6D trajectory, guidance and controller for the air-breathing phase of ABSLV. The 6D trajectory development for a hyper-sonic air-breathing vehicle involves the development of models for aerodynamics, propulsion, vehicle dynamics, earth model, guidance and control covering the ascent phase of the flight regime. The vehicle propulsion model is based on the scramjet engine. Ascent phase guidance problem is formulated as an optimal control problem to find the control input u, which drives the vehicle to follow the trajectory where the performance index will be minimized. The performance index selected is to optimize the fuel taking velocity, altitude and mass as the states with angle of attack as the control input. The control philosophy is to simultaneously control the states to follow the reference trajectory without defining any authority to particular state. Thus, an integrated multi input multi output control law is developed with input/output decoupling using state feedback and then classical controllers are designed in each channel to ensure stability and robustness. All the control surfaces work together to handle the aero-propulsive couplings and parameter uncertainties. Integrated guidance and controller for the air-breathing phase handles the coupling between longitudinal and lateral dynamics as well as translational and rotational dynamics and provides robustness to 40% of parametric perturbations.

In general, the integrated guidance and controller for ABSLV is subjected to sudden changes in the parameters due to the dynamic flight envelope, the vehicle has to cater. Hence uncertainties associated with parameters and the possible presence of unmodelled

dynamics during scramjet operation are state and time dependent. To address this problem, an adaptive control and guidance law augmentation is developed for the integrated guidance and controller in the air-breathing phase. Due to this unmodelled dynamics and plant uncertainties, there is fast variation in the ideal weights as system undergo sudden changes in dynamics. Thus the new adaptive control law using derivative free update algorithm can improve the robustness by tuning the adaption gain instead of compromising for the closed loop performance as in the case of derivative or projection based update laws. Similarly a novel predictor-corrector guidance method based on all-coefficient adaptive control theory is developed to take care of control surface failure condition or for degraded propulsion performance. This is achieved by re-commanding the angle of attack to achieve the predicted final states following a sub optimal trajectory to save the mission in case of degraded performance.

Finally, the usefulness and performance of the integrated controller augmented with adaptive control and guidance algorithm has been successfully demonstrated and established through 6D and Monte-Carlo (MC) simulations.

Contents

List of Figures

List of Tables

Abbreviations

ABSLV	Air Breathing Satellite Launch Vehicle
MIMO	Multi Input Multi Output
DCNLP	Direct Collocation with Nonlinear Programming
PNN	Polynomial Neural Networks
ECKF	Extended Consider Kalman Filter
LQG	Linear Quadratic Gaussian
LQR	Linear Quadratic Regulator
ALQ	Adaptive Linear Quadratic
MRAC	Model Reference Adaptive Control
GPM	Gauss Pseudo spectral Method
BELBIC	Brain Emotional Learning Based Intelligence Controller
NPCG	Numerical Predictor- Corrector Guidance
QEGC	Quasi-Equilibrium Glide Condition
MC simulation	Monte-Carlo simulation

Nomenclature

A	axial force, N
A_c	engine capture area, m^2
b	lateral-directional reference length, span, m
c	longitudinal reference length, mean aerodynamic chord, m
C_A	axial force coefficient
C_D	total drag coefficient
C_{D0}	drag increment coefficient for basic vehicle
$C_{D\delta_{eL}}$	drag increment coefficient for left elevon
$C_{D\delta_{eR}}$	drag increment coefficient for right elevon
$C_{D\delta_{ru}}$	drag increment coefficient for rudder
C_L	total lift coefficient
C_{L0}	lift increment coefficient for basic vehicle
$C_{L\delta_{eL}}$	lift increment coefficient for left elevon
$C_{L\delta_{eR}}$	lift increment coefficient for right elevon
$C_{L\delta_{ru}}$	lift increment coefficient for rudder
C_N	normal force coefficient
C_Y	total side force coefficient
$C_{Y\beta}$	side force with side-slip derivative for basic vehicle
$C_{Y\delta_{eL}}$	side force increment coefficient for left elevon
$C_{Y\delta_{eR}}$	side force increment coefficient for right elevon
$C_{Y\delta_{ru}}$	side force increment coefficient for rudder
C_l	total rolling moment coefficient
$C_{l\beta}$	rolling moment with side-slip derivative for basic vehicle
$C_{l\delta_{eL}}$	rolling moment increment coefficient for left elevon
$C_{l\delta_{eR}}$	rolling moment increment coefficient for right elevon
$C_{l\delta_{ru}}$	rolling moment increment coefficient for rudder
C_{lp}	rolling moment with roll rate dynamic derivative

C_{lr}	rolling moment with roll rate dynamic derivative
C_m	total pitching moment coefficient
$C_{m\delta_{eL}}$	pitching moment increment coefficient for left elevon
$C_{m\delta_{eR}}$	pitching moment increment coefficient for right elevon
$C_{m\delta_{ru}}$	pitching moment increment coefficient for rudder
C_{mq}	pitching moment with pitch rate dynamic derivative
C_n	total yawing moment coefficient
$C_{n\beta}$	yawing moment with side-slip derivative for basic vehicle
$C_{n\delta_{eL}}$	yawing moment increment coefficient for left elevon
$C_{n\delta_{eR}}$	yawing moment increment coefficient for right elevon
$C_{n\delta_{ru}}$	yawing moment increment coefficient for rudder
C_{np}	yawing moment with roll rate dynamic derivative
C_{nr}	yawing moment with yaw rate dynamic derivative
C_T	thrust coefficient
D	drag force, N
F_{Aero}	total Aero force, N
F_A	total Aero force in body frame, N
F_B	total force in body frame, N
F_{CB}	total control force in body frame, N
F_{TB}	total thrust force in body frame, N
G_0	gravitational acceleration magnitude at the surface of the Earth, m/s^2
L	lift force, N
M_{Aero}	total Aero moment, Nm
M_A	total Aero moment in body frame, Nm
M_B	total moment in body frame, Nm
M_{CB}	total control moment in body frame, Nm
M_{TB}	total thrust moment in body frame, Nm
M_a	Mach number
m	mass of the vehicle, kg
$\dot{m}$	mass flow rate, kg/s
N	normal Force, N
I_{sp}	engine specific impulse, s
I_{xx}, I_{yy}, I_{zz}	inertia along roll/pitch/yaw, kg/m^2
P	engine pressure
p	roll rate, rad/s

Q	dynamic pressure, Pa
q	pitch rate, rad/s
r	yaw rate, rad/s
S_{ref}	reference area, m^2
T	total thrust of the vehicle, N
u_I, v_I, w_I	components of velocity in inertial frame, m/s
V_{AB}	relative velocity in body frame, m/s
V_{AI}	relative velocity in inertial frame, m/s
V_{IG}	velocity in gravitational frame, m/s
W	vehicle weight, kg
W_0	initial vehicle weight, kg
$\dot{W}$	fuel flow rate, kg/s
x_I, y_I, z_I	components of position in inertial frame, m
α	angle of attack, rad
β	side slip angle, rad
γ	flight path angle, rad
Θ	azimuth angle, rad
Φ	fuel to air ratio , equivalence ratio
ω	angular body rate, rad/s
θ	pitch angle, rad
ψ	yaw angle, rad
ϕ	roll angle, rad
η	generalized structural mode displacement, rad
ρ	atmosphere density, kg/m^2

Chapter 1

Introduction

Air Breathing Satellite Launch Vehicle (ABSLV) uses air breathing propulsion system which brings a dramatic reduction in the flight time. These vehicles are capable of horizontal take-off and landing. For the ascent phase, the propulsive system of ABSLV is usually powered by hydrogen fuel based scramjet engine. To obtain maximum propulsive efficiency, the scramjet engine must be operated at high dynamic pressure. Since aerodynamic heating and drag increases with dynamic pressure, the benefits of high propulsive efficiency must be balanced against temperature and structural constraints. Slender geometry and light structure causes flexible effects [6]. Further, propulsive efficiency will depend on the vehicle trajectory [7]. Thus, a strong coupling exists between aerodynamics, airframe and propulsion [8], [9]. The development of fuel/time optimal trajectory for ABSLV using scramjet engine pose strong coupling to other subsystems because of the large velocity and altitude demanded by such trajectories. The mission performance and stability robustness of the system requires development of a highly integrated guidance and control techniques [10].

In space transportation problems, translational dynamics is controlled by guidance system and rotational dynamics is controlled by digital autopilot. In conventional launch vehicles, a decoupled translational and rotational design can be considered due to frequency separation existing between these dynamics. However, in ABSLV, a strong coupling exists between translational and rotational dynamics due to the closeness in frequency and the use of common control surface for both the dynamics [11]. Propulsion system uses throttle controlled engine, where, thrust is function of angle of attack and thus guidance control interaction is through propulsion and aerodynamics [12]. The interaction diagram of different subsystems is shown in Figure 1.1.

This thesis mainly investigate the following

1. 6-D trajectory development,

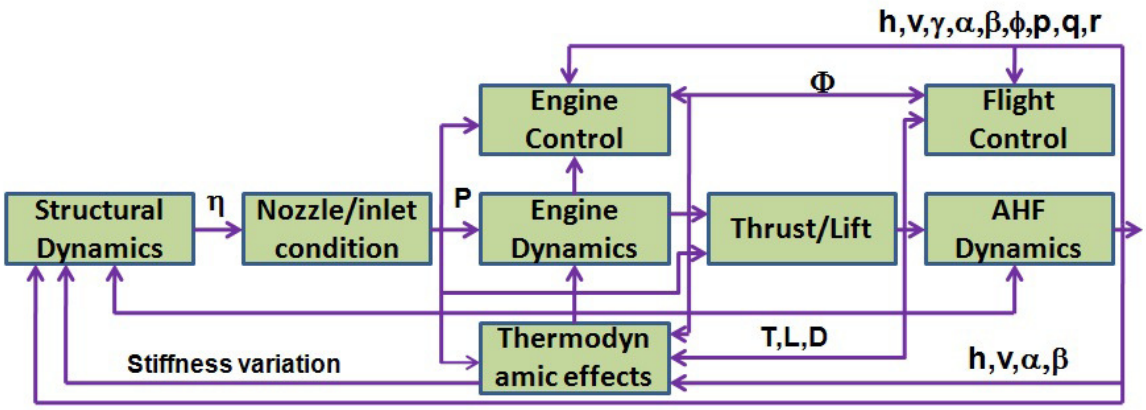

Figure 1.1: Interaction of different subsystems

2. Integrated guidance and control law development for air-breathing phase of ABSLV,

3. An adaptive guidance and control law augmentation for handling the large parameter uncertainties and unmodelled dynamics to ensure the robust performance of integrated controller.

1.1 Literature Survey and Motivation

Numerous optimal trajectory design, linear and nonlinear control design studies have been reported on air-breathing launch vehicles over the years, attempting to investigate the physics underlying air-breathing propulsion and associated coupling issues. A detailed literature review of these studies is presented here.

1.1.1 Air-breathing Vehicle Design and Modeling

Air-breathing hypersonic vehicle has air-frame integrated hydrogen fueled scramjet engine resulting in the following vehicle properties.

- decrease in drag, increase in lift-to-drag ratio, which bring the coupling between aerodynamics and thrust,

- to obtain maximum propulsive efficiency, the scramjet engine must be operated at a high dynamic pressure,

- aerodynamic heating and drag increases with dynamic pressure, thus the benefits of high propulsive efficiency is limited due to structural constraints,

- the trajectory demands wide range of flight conditions which calls for dynamic characterization of vehicle over wide flight envelope,

- moreover, slender geometry and light structure causes structural vibration of the vehicle [6].

Thus, there is strong coupling between different subsystems and variations due to wide flight conditions, making the characterization of the ABSLV flight dynamics highly challenging [13].

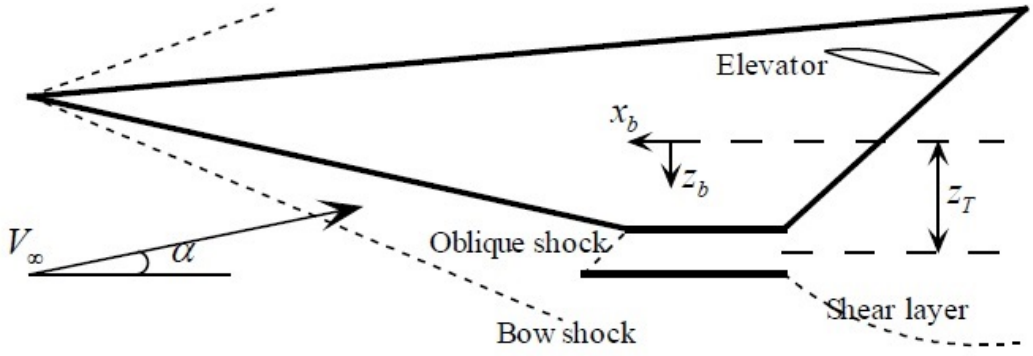

Figure 1.2: Geometry of the vehicle [1]

Figure 1.2 illustrates the general geometry of the vehicle. An optimal combination of oblique shock and bow shock in the intake is required for maximum pressure recovery which depends on the range of possible angle of attack and structural bending conditions [14], [15]. To maintain the shock configuration in the inlet [1], [16], pressure at inlet is to be maintained which is determined by angle of attack, dynamic pressure and the free stream characteristics. Since the angle of attack determines the air flow inside the scramjet engine chamber, the thrust developed depends heavily on the angle of attack. Moreover, the under-slung engine produces a nose-up pitching moment which is proportional to thrust. The coupling between aerodynamics and propulsion has to be taken into account in the control model.

Design optimization of the air breathing scramjet engine of hypersonic vehicle [15], [17], [18] is manipulated through five vehicle design parameters, including the size and position of the engine - fore-body cone half angle in the vehicle symmetry plane (φ), the aspect ratio of the (elliptical) fore-body (AR), the capture width of the scramjet engines (w_{cap}), the leading edge sweep angle of the wing (Ψ), and the wing span (b). A large value of φ causes a high fore-body shock and more compression, resulting in a high thrust at the

expense of increased aerodynamic drag. Increasing the fuselage aspect ratio AR enables the integration of the scramjet with a larger capture area resulting in a large thrust. On the other hand, a wide fuselage results in higher aerodynamic drag. The capture width of the scramjet engine w_{cap} is adjusted to fit inside the fuselage geometry and should satisfy shock-on-lip condition. Optimization variables for the wings, the span b and the leading-edge sweep angle Ψ are designed for lift generation. When the engine is shifted towards the nose, center of gravity shift forward and vehicle become more stable and trim angle of attack increases with mach number. When the engine is shifted rearward, instability will increase but it will make the vehicle more maneuverable for flight path angle tracking as bandwidth can be increased for maximum right half plane zero.

A nonlinear, wind tunnel-CFD based model of the longitudinal and lateral-directional dynamics for a wing-cone air-breathing hypersonic vehicle is developed in [19]. Two additional effects were considered in this work, the first effect considered was the on-design and off-design propulsion system performance resulting from an oscillating bow shock and the second effect they considered was the presence of coupling between the rigid-body accelerations and flexible body dynamics. Aerodynamic database was also generated based on test results from hyper-X air-frame integrated scramjet propulsion experiment [20]. However the equations of motion used in the simulation account for the time varying center of mass, the center of gravity (c.g.) and the moments of inertia. The total mass of the vehicle, its c.g. location and the products of inertia vary as fuel is consumed. It is assumed that the c.g. moves only along the body x-axis as the fuel is consumed.

1.1.2 Optimal Guidance and Trajectory Design

Three dimensional ascent phase trajectory studies of ABSLV with guidance law based on optimal two-point boundary value problem [5], [21], [22], [23], linear logarithmic steering law [24] with direct collocation optimization, singular perturbation theory [25] using two time scale approach [26] by apportioning vehicle states to slow and fast variables, on line trajectory optimization using convex programming [27] were attempted in the past few years. Autonomous ascent guidance with multiple terminal constraints [28] based on two point boundary value problem was demonstrated for all solid small vehicles.

Takayuki Yamamoto [24] proposed a new guidance strategy derived from the optimal condition for the steering function which had linear and logarithmic terms, with only four parameters. The commanded attitude angle was solved analytically and expressed as $\phi = c1 + c2 + \lambda * \log t_f$. Acquired terminal horizontal velocity computed through the

parameterized liner logarithmic steering law was almost same with that obtained by the direct numerical optimization. It was difficult to discuss analytically the general steering law because the adjoint variables include the lift and thrust which depend on flight time. But by implementing the numerical analysis, it was able to show the sinusoidal behavior of the optimal steering. Here the algorithm used for optimal control problems was Direct Collocation with Nonlinear Programming (DCNLP), which is one of the direct optimization methods to handle the state constraints. Here the author also formulated a guidance update algorithm considering path constraints based on time to go according to the fuel remained. The parameters in the steering function were re-calculated if there is a deviation from nominal ascent path. This was by solving simple two-by-two linear algebraic equations along with forward integration on-board, which guarantee the robust and real-time solutions excluding any optimization process.

J. E. Corban et al [25] addressed the problems associated with on-board trajectory optimization and the synthesis of guidance laws for ascent to low earth orbit of ABSLV. An algorithm for generating fuel-optimal climb profiles was derived via singular perturbation theory. States considered were specific energy, mass, flight path angle and altitude with altitude and flight path angle as fast variables and specific energy and mass as slow variables. The control variables were rocket engine throttle, and vehicle lift (L). The objective was to minimize the fuel consumed in gaining energy by applying minimum principle to a low order dynamic model showing the functional dependence of normal component of thrust on angle of attack. Maximum dynamic pressure and maximum aerodynamic heating rate constraints were considered in addition to acceleration limits. The use of bank angle to modulate the magnitude of the vertical component of lift was shown to improve the index of performance.

In time scale decomposition of states approach [26], the guidance law allows the design of feedback controllers for slow and fast modes and finally they were combined to form a composite feedback controller for the full order dynamics. The assumption made for simplification was, thrust is aligned with the velocity. The dynamics were brought to standard perturbation form with specific energy and mass were taken as slow manifolds and altitude and flight path angle as the fast dynamics. Guidance law design is approached from a geometric perspective. State space is composed of a family of control dependent slow manifolds and control independent fast manifolds honoring transversality conditions. Near optimal guidance was obtained from a composite control law. One set of control was based on feedback control law for flying the vehicle on slow manifold and the other set based on regulation law on fast manifold for tracking the vehicle in the reduced order

trajectory. Thus design was for non-optimal control law which will stabilize the fast dynamics so that the intersection of slow manifold and fast manifold was an asymptotically stable equilibrium point. Fast dynamics were linearized using feedback linearization and then stabilized using state feedback. Using bang-bang controller for the throttle, the optimal altitude was computed honouring dynamic pressure constraint and a stagnation-point heating rate constraint. For fixed specific energy E, both constraints were functions of altitude so that throttle switching logic is unaffected. A flight path angle correction was used to improve the accuracy of reduced solution.

Anthony J. Calise et al [29] developed an optimal three-dimensional trajectory of a launch vehicle in the atmosphere satisfying a set of operational constraints and a set of tangency conditions at main engine cutoff. A hybrid analytic/numerical approach was applied to this problem. The resulting guidance algorithm had the maximum utilization of the analytically tractable portions of the solution to construct a set of interpolating functions. These functions were then used in the numerical treatment of the total problem based on the method of collocation. The application of this algorithm on single stage vehicle model indicate that guidance algorithm converged reliably and accurately and that the execution time required for a single guidance update is well within the realm of real-time implementation. The initial solution can be computed prior to launch and later updated in real time at intervals along the flight trajectory. Guidance analytically solved the optimal state and co-state equations. State and co-state equations were propagated from the initial time using a function based on Simpon's rule to approximate the thrust. Here the co-state scalar for state mass was neglected and initial values of velocity and position states were solved by developing a nearly algebraic relationship for the dependence on terminal constraints. Gleb Merkulov [30] derived semi analytical solution for optimal guidance law for intercepting a stationary target with quadratic approximation of the kinematic equations and fixed terminal time.

John D. Schierman [10] developed Integrated Adaptive Guidance and Control program for Boeing X-40A during approach and landing phase using dynamic inversion approach along with optimal control allocation to avoid command saturation. Band width was proportionally reduced for all three control channels in case of command saturation. Guidance law was based on back stepping approach with proportional feedback gains to track the reference trajectory. The trajectory reshaping was based on optimum-path-to-go methodology where the possible scenarios of trajectory were computed offline and best trajectory was computed on board from this data base based on the current state of the vehicle. Basically the guidance law was for successive loop closure architecture with

- altitude loop,
- flight path angle loop and,
- angle of attack loop - generates a quaternion command which finally drives the inner control loop.

The Optimum-Path-to-Go trajectory reshaping consists of four steps

1. optimization problem formulation - optimization problem was formulated through successive quadratic programming with cost function to minimize the vertical acceleration which ensured less aggressive trajectories.
2. off-line trajectory database generation - a data base of the optimal trajectories were generated by varying the initial states, upper bound and lower bound perturbation for critical parameters like lift and drag coefficients.
3. off-line trajectory database modeling and encoding - from the trajectory data base, states of the system were best fitted using polynomial fit of fifth or sixth order. Further a non linear function modeling was used to generate Polynomial Neural Networks (PNN) which map the initial states and parameter perturbations to the coefficients of basic function, describing the associated trajectory. and
4. online trajectory reshaping - estimation of critical parameters in flight was done using the onboard measurements of the initial conditions and PNN interrogation and using this trajectory was reshaped.

Entry guidance algorithm for aero-capture was formulated as a robust optimization problem in [31]. Successful guidance law requires a precise knowledge of system states, environmental conditions and vehicle performance parameters. This work incorporated the uncertainty in entry flight problems into an overall optimization objective using robust optimization principles. Robust optimization involves modification of a deterministic cost objective to incorporate the effects of uncertainty. The parameters representing uncertainties or unmodeled dynamics were included as consider variables in the Kalman filter. Errors in parameters were reflected in the associated covariance update equations of the consider filter, while nominal parameter estimates remained static. This way an Extended Consider Kalman Filter (ECKF) was used to predict propagated uncertainty due to dynamics and measurement updates. The ECKF equations were used for propagating state and parameter uncertainties, as well as for predicting the conditioning effect of future measurements

on the estimation error covariance. Thus guidance prediction errors were desensitized by optimization procedure decreasing the necessary ΔV budget by about 50%.

A continuous-time predictive control-based novel integrated guidance and control for missile target was proposed in [32]. Targeted acceleration was considered as external disturbance and predicted using an extended state observer. Feedback control gain and disturbance compensator gain was computed using optimal nonlinear feedback control law. The response of the nonlinear dynamical system was predicted by appropriate functional expansion. In the performance index, a quadratic cost function based on the predicted errors, control expenditure and having an additional term involving rate of change of predicted error similar to derivative feedback in classical controller to improve the performance, was minimized. Integrated guidance and control design based on various theories like dynamic inversion, θ-D method, optimal control, sliding mode control, feed back linearization, sequential loop closure were applied to descent phase of reusable launch vehicle, missile guidance and control problems etc.

Most of the researches to date focus on the development of different guidance algorithm using three dimensional trajectory of the ascent phase of air-breathing vehicle. In the present work guidance law is developed using the 6D trajectory, considering the effect of controller on guidance states. Here during the formulation of the guidance algorithm, sum of the force contribution from control surface deflection and from the basic vehicle is considered in the co-state equations. Aero control surfaces are deflected for trim angle of attack required for static equilibrium, then rotational dynamics are solved with controller and cumulative aerodynamic force components and thrust has been considered for solving co-state equations in guidance law. Moreover mass is taken as an optimal state in the Hamiltonian formulation for the guidance to account for mass update in air-breathing phase.

1.1.3 Control Design Techniques for ABSLV

Several tracking controller design to steer the states to the reference trajectory was attempted during the past few years. Control schemes based on LQ controller design [11], H_∞ control and μ-synthesis methods [33], linear parameter varying control [34], sliding mode control [35] and output regulation [36], [37] for the longitudinal dynamics of ABSLV are effective in tracking the reference trajectory. Wilcox et al [38] studied Lyapunov-based continuous robust controller with implicit learning method for the exponential reference model tracking of ABSLV considering aero-thermal effects and unmodeled distur-

bances. Hypersonic flight conditions cause severe interaction between structural dynamics and flight dynamics. To tackle this, Z. D. Wilcox and et al developed a nonlinear temperature dependent, parameter varying model with nonlinear additive bounded disturbance. A Lyapunov-Based tracking controller was developed which ensured robustness and stability. Controller consists of the state feedback, an initial condition term, and the implicit learning term based on update law which allowed the controller to obtain an exponential stability to reject the exogenous disturbance terms.

A new control strategy for tracking problem of air-breathing hypersonic vehicle [39] uses the aero-propulsive coupling effect as well as elevator to lift non-minimum phase effect instead of canceling them. The suppression of flexible effect was achieved by integrating this control with H_∞ control. In order to improve the robustness of the controller, a non linear disturbance observer was proposed to estimate uncertainties from unmodeled dynamics and is used in design.

The effect of right half plane zero in elevator to flight path angle transfer function and how to control the vehicle was briefed in [40]. Unlike aircraft control, the bandwidth of the longitudinal controller was severely limited by the frequency of transmission zeros which is small compared to conventional aircraft transmission zeros. Another important difference was the more lag between flight path angle and pitch angle for a given elevator input for hypersonic vehicle compared to aircraft. Other than this, the high speed of the hypersonic vehicle affected the altitude stability as small change in flight path angle cause large changes in altitude. The author suggested that the frequency of right half zero can be increased by altering the control effector configuration of the vehicle ie a canard is ganged with elevator using a constant elevator to canard interconnect gain. The effect of fixed canard length and varying interconnect gain - varying the position of canard location from the nose of the aircraft close to the center-of-mass, on the transmission zero were also highlighted in this paper. Moreover when flexibility effects were added to the model, achievable bandwidth was limited by the complex coupling between the structural modes and rigid modes.

A non linear control law for longitudinal dynamics of hypersonic vehicle was briefed in [41]. The states controlled are altitude and velocity using elevator deflection and fuel to air ratio as the control inputs. Additional complexity was added to the system by introduction of aero-elastic modes, its coupling and unstable zero dynamics introduced by the aerodynamic forces. Here approximate feedback linearization was attempted to stabilize the non minimum phase system. An approximate reduced model (flexible modes and unstable internal dynamics was identified and removed) was generated having the full

vector relative degree with original system and then feedback linearization control law was developed. Simulation studies were carried out with this control law on the truth model and the tracking performance was established. Simulations were also done with mild plant parametric variations to demonstrate the robustness of the design.

A control oriented model was developed after thorough understanding of the theoretic properties of the system. In order to handle the zero dynamics of the system another control surface, canard was included to ensure stability by eliminating non-minimum phase behavior and also for high-frequency aero-elastic mode introduced by the heave coupling. Heave coupling is the excitation of flexible modes by changes in the body axis vertical acceleration resulting in coupling between rigid body and flexible modes.

1.1.4 Adaptive Augmentation of Guidance and Controller

Control schemes integrated with adaptive control were able to maintain the performance [42], [43], [44], [45], [46] in the case of model uncertainties, actuator failure and command saturation [47], [48], [49]. Non linear controller based on sequential loop closure [50] and dynamic inversion augmented with robust adaptive techniques [51] were also designed for tracking the velocity and attitude reference profiles. The adaptive linear quadratic controller designed for the altitude and velocity tracking of longitudinal model of air-breathing hypersonic vehicle [51], [52] had taken velocity, flight path angle, altitude, angle of attack, pitch rate and three flexible modes as states. The structural modes were not used in the control design and were considered as unstructured uncertainty. Linear Quadratic Gaussian (LQG) problem formulation follows a linear quadratic proportional-integral-filter (PIF) control structure, for this controller robustness was not guaranteed as flexible modes may destabilize the system. To tackle the uncertainty in aero and propulsion dynamics, robust adaptive law based on gradient method with projection modification was incorporated. The certainty equivalence principle was used to induct adaptive law with the control structure of linear quadratic regulator. Simulations of both control law, traditional linear quadratic (LQ) control design and the adaptive linear quadratic(ALQ) control design were compared and established that ALQ increases the robustness to unmodeled dynamics associated with structural modes.

B. J. Bialy et al [53] developed an adaptive back stepping controller for longitudinal dynamics of hypersonic flight to asymptotically track the velocity reference profile and regulate other states. The controller was based on adaptive update laws and Lyapunov-based stability analysis was carried out to ensure the asymptotic stability of the controlled

states. Hao An [54] did a novel bound estimation method, which minimized the update law of the adaptive controller for the dynamic variation of the inlet length of scramjet engine. This handled time-varying uncertain parameters and external disturbance by ensuring an efficient thrust. In the adaptive control proposed, a novel bound estimation method was developed minimizing the parameter update laws. In back stepping which guarantees good tracking performance, attitude controller command filtering technique was used to overcome the problem associated with analytical solution of time varying virtual control derivatives.

Several research work had focused on adaptive control of longitudinal dynamics of air breathing vehicles to build robustness for unmodeled dynamics and parameter uncertainties. Tansel Yucelen and Anthony J. Calise examined robustness to unmodeled dynamics using derivative free adaptive control law [55], where adaption gain is increased to improve robustness without the use of modification terms. The study further demonstrated the limitation of derivative law with modification terms and also the projection based adaptive laws where author demonstrated that the performance of the closed loop system was compromised to improve robustness to unmodeled dynamics. J. Tian and X.J. Xie [56] discussed the adaptive state feedback for high-order stochastic non-linear systems with uncertain control coefficients. The issues related to model reference adaptive control (MRAC) which had with opposite to the expected sign of control signal demanded by multi input multi output (MIMO) plant ie they fail to satisfy sufficient condition for satisfying adaptive approximation errors in a fixed point solution was discussed in [57]. Inverse gain switching control was proposed as an adaptive control law where the adaptive gain as a function of control signal was utilized. This created a non-causal dependence that was broken by solving explicitly for the control signal. As a result, there is a singularity in a term containing the said adaptive gain. This was remedied with a switching control law to appropriately move it around the singularity and retain stability. Proposed architecture used Chebyshev polynomial adaptive control in addition to the proposed inverse switching gain control.

The stability conditions of uncertain dynamic system subjected to actuator amplitude saturation was established in [58]. Here the author discussed quadratic stability condition, bounded tracking error and on the added design flexibility using a modification term by reducing the allowable saturation limit while ensuring closed loop system stability. T. Yucelen [59] proposed observer architecture to estimate the uncertain input dynamics and established asymptotic stability of the system error dynamics for the adaptive command following case. In [60], output feedback architecture used a linear quadratic Gaussian structure to produce a baseline control in which an optimal state feedback control law

provided command tracking and stabilization. An observer, modified with loop transfer recovery, was used to estimate the states in the baseline control. Then e adaption law was computed with estimation error. Here Gibson's rule was used for tuning the adaptive learning rates which made the adaptive design simple and easy to implement.

The article [61] presented a state feedback method for adjusting the adaptive gain for abnormal conditions with increased tracking error by warping the Lyapunov level sets. Tracking error bound analysis was done to avoid high increase in the gain. A gain function to adjust the aggressiveness of adaption law was used for varying the adaptive gain with tracking error expressed in weight estimation error and high frequency gain estimation error. In [53] B. J. Bialy and et al developed an adaptive back stepping controller for longitudinal dynamics of hypersonic flight to asymptotically track the velocity reference profile and regulate other states. The controller was based on adaptive update laws and Lyapunov-based stability analysis was carried out to ensure the asymptotic stability of the controlled states. ALQ based altitude and velocity tracking control algorithm for the longitudinal states of generic hypersonic vehicle was discussed in [62], where the author combined the certainty equivalence principle to a linear quadratic control law to bring the robust adaptive nature to the LQR control law. Adaptive law used here was gradient method with projection modification. L. Fiorentini [63] used a non-linear sequential loop closure method to design dynamic state feedback control laws for the longitudinal dynamics of the air-breathing hypersonic vehicle. Appropriate intermediate controllers on certainty equivalence principle with adaption law based on projection method were used for different subsystems.

Great deals of research had been carried out in adaptive guidance especially in the re-entry phase including trajectory reshaping and adaptive guidance methods. M. Li and J. Hu presented a novel predictor-corrector guidance method [64] based on all-coefficient adaptive control theory in the approach and landing phase of reusable launch vehicle. Algorithm used a first-order characteristic model to predict the states and control command was reshaped to achieve the new predicted state. It had the advantage of high accuracy and was independent of the predetermined reference trajectories. Predictor corrector re-entry guidance algorithm was discussed in [2], [3], [65] for the medium to high lift-to-drag ratio re-entry vehicles with later guidance for cross range control by commanding bank angle.

The adaptive predictor-corrector reentry guidance [2] was divided into two phases as shown in Figure 1.3. In the first phase predictor -corrector guidance law between two self defined way points was developed. In the second phase just before the end point, on-board trajectory was computed from the existing point to end point and guidance tracking was achieved using LQR control. The way points were determined by optimal trajectory via a

Gauss pseudo-spectral method (GPM) with the control variable as angle of attack and bank angle. Here a brain emotional learning based intelligence controller(BELBIC), was used to develop the predictor-corrector algorithm. The results were validated through simulations for various dispersion cases and endpoint maneuvering cases.

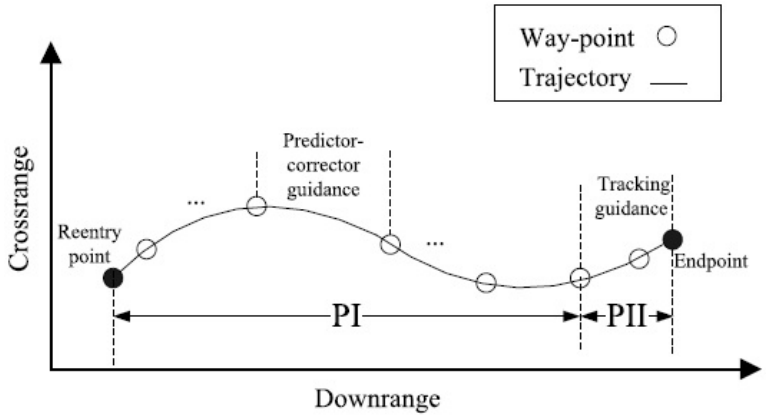

Figure 1.3: Re-entry guidance scheme [2]

A guidance law to command the optimum glide dynamic pressure to maximize lift to drag ratio as well as to suppress the phugoid oscillations was developed for an aerodynamically controlled hypersonic boost-glide class of flight vehicle [66]. Authors presented the robustness analysis using statistical theory to demonstrate the capability of guidance algorithm. A detailed study on an adaptive multi-step predictor-corrector iterative guidance algorithm in interplanetary re-entry capsules to earth [67] used two quantities, gross error adjustment for cross range error and fine error adjustment for position error. The algorithm generated bank angle profiles till preset cross range was reached.

Overall guidance scheme for numerical predictor- corrector guidance (NPCG) for re entry vehicles briefed in [68], [69], [3] had three modules

1. trajectory predictor-corrector module which had trajectory prediction and parameter iterative correction,

2. constraint management module which handled the different constraints - path constraints, terminal constraints and control constraints,

3. a lateral guidance module which executed the bank angle reversals.

The entry flight was decomposed to initial descent phase, quasi equilibrium glide phase, and pre-TAEM phase. Upper and lower angle boundaries of bank angle were derived for each phase and a compound bank angle corridor was constructed by connecting these boundaries. Another difference from convection methods was that the control variables were parameterized for the weighted sum of upper and lower boundaries compared to initial bank angle adjustment which had large range planning capability. In this algorithm bank angle was parameterized for the range constraint using the weighted sum of upper and lower bank angle boundaries and the weighting coefficient, w which can take the value from 0 to 1. Multiple constraints were handled in this compound bank angle corridor construction and were not considered in trajectory planning which improved the computational speed. In the constraint management module as shown in Figure 1.4, terminal constraint was enforced through state feedback and control constraint by limiting the bank angle rate based on a command filter. Lateral guidance module executed the reversal of bank angle to achieve accurate heading control to enhance the robustness and accuracy of three-dimensional entry guidance.

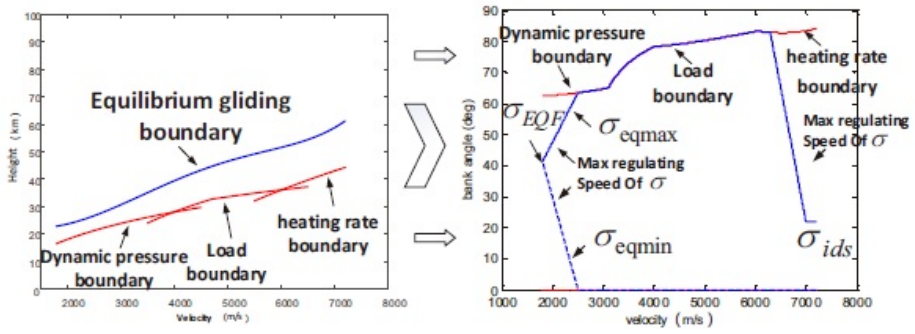

Figure 1.4: Constrained transformation relationship [3]

A second order difference equation was used to describe the slow varying dynamics in characteristic model based adaptive control law for drag free satellite addressed in [70] . Different all coefficient adaptive law for this second order model like 1) Maintaining/tracking control law 2) Golden-section adaptive control law 3) Logic differential control law 4) Logic integral control law 5) Logic double integral control law were discussed, out of which the logic double integral control law was effective to reduce the second-order disturbance. The golden-section adaptive control was simple to use, convenient to adjust and test, and able to generate highly robust systems and guaranteed closed-loop stability for transient process or when parameter estimates were not converged to true values. A combination of golden-section, logic integral and logical double integral control law was

finally designed for drag-free control of the gravity satellite in the accelerator mode and the performance comparison for all-coefficient adaptive control was done through simulations.

A quasi-equilibrium glide adaptive guidance methodology based on the quasi-equilibrium glide condition (QEGC) was proposed for hypersonic vehicles in [4]. The algorithm was independent of the standard trajectory and analytically computed the guidance commands using precise analytical prediction of range and terminal velocity. It developed an analytical relationship between the terminal velocity and flight altitude by separating the effects of the drag deceleration and gravity from the velocity calculation. All the path constraints were conveniently converted to upper and lower bounds of the angle of attack and were easily satisfied as the guidance law operated along the quasi-equilibrium glide boundary most of the time. Principle of quasi-equilibrium adaptive guidance is shown in Figure 1.5. With the adaptive guidance law proposed, the vehicle adapted to variable mission requirements without adjusting the guidance parameters within the vehicle's flight ability.

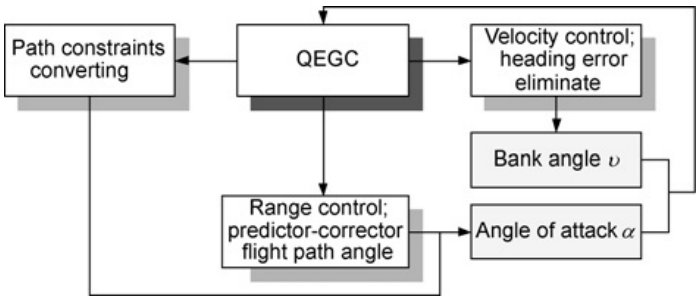

Figure 1.5: Principle of quasi-equilibrium adaptive guidance algorithm [4]

All-coefficient adaptive control was found effective in controlling the shock and had good disturbance rejection capability as demonstrated in scramjet engine control [71] by predicting scramjet plant and in the [72] the ascent phase of hypersonic vehicle. Predictor corrector re-entry guidance algorithm was discussed in [73], [74], [2], [3], [75], [65], [76] for the medium to high lift-to-drag ratio re-entry vehicles for cross range control by commanding bank angle.

The ascent trajectory of air-breathing hypersonic vehicle demands highly varying angle of attack and Mach number which leads to sudden variation of propulsive and aerodynamic forces. To handle such dynamics and associated uncertainties there is a strong requirement for an integrated guidance and control law in the ascent phase of air-breathing hypersonic vehicle. Along with the usual coupling issues that exist between subsystems, it is also observed that the coupling between longitudinal and lateral dynamics makes the problem more intrinsic and is not properly addressed in the literature, especially for air-breathing

phase. Most of the researches till date focus on the development of different guidance algorithm using three dimensional trajectory of the ascent phase of air-breathing vehicle. From the past research work, it is apparent that the control design of hypersonic vehicle dealt with development of control laws for longitudinal dynamics with altitude, velocity, flight path angle, pitch rate and angle of attack as state variables. Different control laws were attempted on this model based on sliding mode control, dynamic inversion and adaptive control.

This motivate to propose an integrated guidance and control for air breathing phase of ABSLV with emphasis to handle unmodelled dynamics and uncertainties. In the present work, six dimensional trajectory is developed solving both translational and rotational dynamics. Here the winged cone configuration of hypersonic vehicle is taken for study and modeled the coupling dynamics between varies subsystems. Further guidance law is developed using the 6D trajectory, considering the effect of controller on guidance states. Here during the formulation of the guidance algorithm, sum of the force contribution from control surface deflection and from the basic vehicle is considered in the co-state equations. Aero control surfaces are deflected for trim angle of attack required for static equilibrium, then rotational dynamics are solved with controller and cumulative aerodynamic force components and thrust has been considered for solving co-state equations in guidance law. Similarly present work focused on the development of an integrated controller taking longitudinal, lateral and translational states simultaneously. Controller design is based on hybrid control law-a new approach with i)decoupling controller to decouple the states which is essential for air-breathing hypersonic vehicle and ii) classical controller designed in each channel to ensure robustness.

Further, a novel concept of augmenting the integrated controller with adaptive guidance and control is attempted which improves the robustness and performance of integrated controller in the enhanced flight and uncertainty parameter envelope. Design of the adaptive control and guidance for an air-breathing vehicle in ascent phase is different from conventional control problems due to strong coupling between different subsystems and the possible presence of unmodelled dynamics during scramjet operation. Usually the adaptive control laws are applied to systems having time-invariant or slowly time-varying disturbance and dynamics. In air-breathing vehicle the uncertainties associated with are state and time dependent as the system undergoes sudden changes in dynamics. Unmodelled dynamics is also time-varying with respect to plant dynamics. To handle highly time-varying dynamics and disturbance, adaptive control without derivative-based update or modification terms is preferable. In derivative-free update laws, the designer has the freedom to

increase the adaptive gain for fast adaptation without affecting the stability of the overall system, while increasing the adaptive gain the fact to be considered is that increased control effort demands the deflection of control surfaces. This can increase the angle of attack at air intake zone resulting in the dynamic interaction between aerodynamics and propulsion.

In air breathing vehicles, due to strong interaction between different subsystems and the slender geometry, a narrow vehicle trajectory corridor only exists to meet high propulsive efficiency, different structural and thermal constraints and stability. Added to this is the possibility of failure of control power plant or the degraded propulsive performance. Other than the parameter uncertainties and unmodeled dynamics, ascent phase flight is susceptible to large initial state errors. These calls for the requirement of advanced guidance law with adaption capabilities to account for the degraded performance. Hence, along with adaptive control law, an all-coefficient adaptive predictor-corrector guidance algorithm is also proposed to reshape the trajectory to meet the terminal conditions at air-breathing phase.

1.2 Research Contribution

The research contributions of the thesis are summarized as follows:

1. 6D-Trajectory Development for the Air-breathing Phase of ABSLV

    - 6D-trajectory development for a hypersonic air-breathing vehicle involves the development of models for aerodynamics, propulsion, mass model, vehicle dynamics, and kinematic relations during the air-breathing phase of the flight regime.
    - The vehicle propulsion model is based on the scramjet engine.

2. Guidance Design

    - During the air-breathing phase, guidance is formulated as an optimal control problem to find the control parameter - angle of attack, to optimize the fuel taking velocity, altitude and mass as the states.
    - The two point boundary value problem is numerically solved using pseudo-spectral approach.

3. Integrated Controller Design

- The control philosophy is to develop an integrated multi input multi output controller taking longitudinal, lateral and translational states simultaneously to follow the reference trajectory without defining any authority to particular state.
- Integrated controller is based on hybrid control law- with i)input/output decoupling controller using state feedback and ii) further, classical controller is designed in each channel to ensure stability and robustness. All the control surfaces work together to handle the aero propulsive couplings and parameter uncertainties.

4. Adaptive Guidance and Control Augmentation to Integrated Controller

   - An adaptive control law based on derivative-free update law is augmented to the existing controller to handle wide range of parametric uncertainties by tuning the adaption gain without compromising the stability of the overall system.
   - An all-coefficient adaptive guidance law is developed to predict the terminal states and re-commanded the control input to achieve the predicted terminal states at air-breathing phase in case of initial state errors, control surface saturation or for degraded propulsion performance.
   - The new adaptive guidance and control algorithm is validated through various parameter perturbations for aerodynamic parameters, control effectiveness and propulsive parameters and evaluated the limit of perturbation that the overall system can handle. Finally, the new scheme's robustness is demonstrated via Monte Carlo (MC) simulations.

1.3 Overview of Thesis

- Chapter 2 introduces the 6D trajectory development for air breathing phase of reusable vehicle which involves model development, governing equations and the numerical scheme for integration. It addresses the mathematical model for the various subsystems, different coordinate systems used, vehicle dynamics and the kinematic relations. Validation of the trajectory and open loop simulation results are also discussed in this chapter.

- Chapter 3 explains the guidance law development of air-breathing phase. Details of the optimal control guidance formulation, the numerical scheme using pseudo-

spectral method for the solving the optimal problem and the closed loop results are discussed here.

- In Chapter 4, explores the integrated controller development which addresses the longitudinal, lateral and translational dynamics. Controller consists of a decoupling controller which decouples the states using input-output state feedback. Further, classical controller with compensator is designed in each channel to ensure robustness. The frequency response and time response of the controller have been presented to give an overall picture of the robustness of the design. The longitudinal and lateral time domain responses along with perturbation cases are also discussed here and shows how effectively the integrated system achieves the mission requirements considering all the coupling effects within various subsystems.

- Adaptive guidance and control law augmentation to the integrated controller is described in Chapter 5. The adaptive control law is based on derivative free control law and adaptive guidance is based on characteristic model based predictor-corrector guidance law. Stability analysis of the adaptive augmentation to the integrated controllers is also brought out and the effectiveness of augmented adaptive guidance and control law is demonstrated through extreme parameter perturbations and MC simulations.

- Chapter 6 concludes the work and indicates the future direction of this work.

Chapter 2

6D Trajectory Development

2.1 Introduction

The air-breathing hypersonic vehicle features an airframe integrated scramjet engine, which may result in static and dynamic coupling between different subsystems in the narrow flight envelope demanded by the vehicle. The vehicle configuration considered for the study is the Winged Cone configuration [77] as shown in Figure 2.1. The vehicle is estimated to have a gross take-off weight of 12700kg and an overall fuselage length of 60m. The fuselage central line mounted wing has independently controllable trailing edge elevons with their hinge line perpendicular to the fuselage center-line. Deflections of elevons are with respect to hinge line with positive deflection being the trailing edge up. The fuselage has an antisymmetric conical fore body, a cylindrical engine nacelle section, and a cone frustum engine nozzle section. A vertical tail mounted in the center line of the fuselage has a full-length rudder with its hinge line at the 25% chord from the trailing edge. Deflections of the rudder are measured with respect to its hinge line, and positive deflections are with the trailing edge left. Canards are placed relative to the fuselage center line with positive deflection being the trailing edge down.

In expendable launch vehicles, a decoupled guidance and control design is attempted considering translational states-position and velocity as slow manifolds for guidance and rotational states-body rates and attitude angles as fast manifolds for control. These two subsystems were integrated and tested for different parameter perturbations. Modifications in each loop were carried out independently which calls for different design iterations and may result in a sub optimal response during flight. In three degrees- of- freedom (3D) model only the translational dynamics are taken into account along the three axes of a reference frame. In six-degrees-of-freedom (6D) model in addition to translational dynamics, rotational dynamics are also solved along the pitch, yaw and roll planes. In air-breathing ve-

hicles where a high degree of coupling exists between different subsystems, the 6D model will represent a more real operating environment due to the effect of rotational dynamics on the translational dynamics and vice versa.

The mathematical model for the air-breathing vehicle under consideration, requires the development of models for various subsystems including propulsion, mass model, aerodynamics, vehicle dynamics and kinematic relations. The mathematical models for the above subsystems are discussed in the subsections below.

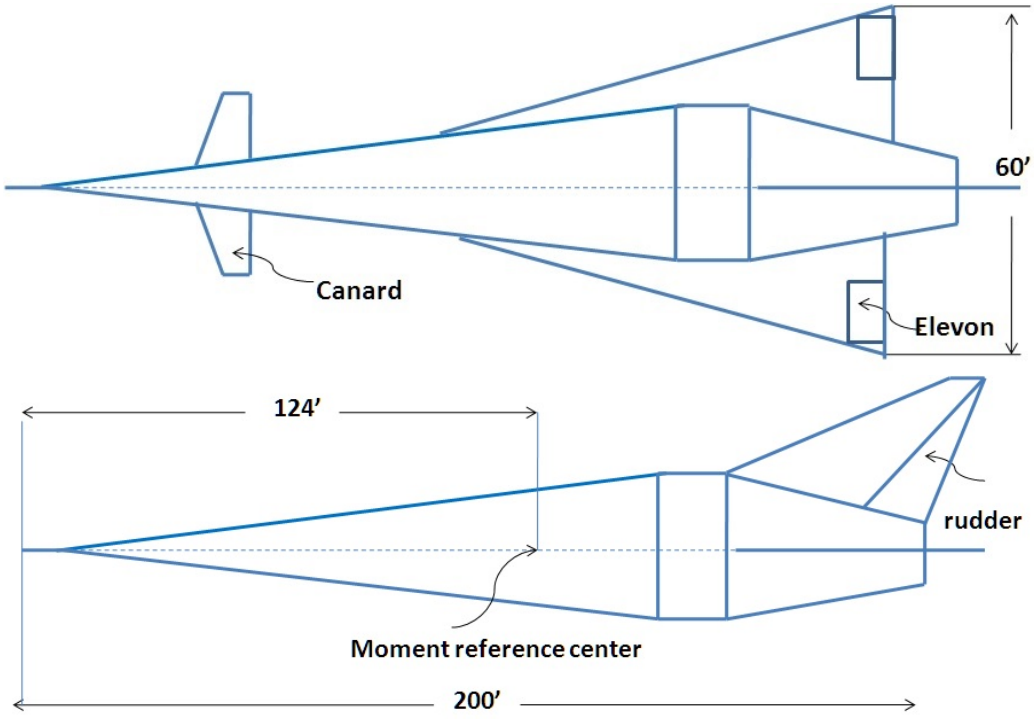

Figure 2.1: Winged cone research vehicle

2.2 Propulsion

The most critical technology of an air-breathing vehicle is the high speed hydrogen fuelled scramjet propulsive system. In scramjet engine, supersonic compression of the hydrogen fuel take place in an air frame compressed by the forward speed of the vehicle. Since the engine operates at supersonic speed, there is less time for the fuel and scooped oxygen to mix which requires a long combustion chamber. The main objective of the propulsion system is to dynamically produce thrust to faithfully track the thrust command as closely as possible. For this, the engine inlet must capture as much air flow as possible. Moreover,

the system has to manage the shock configuration [78] in the intake as forward as possible to achieve maximum pressure recovery and minimize the fuel requirement. Details of scramjet engine is briefed in Appendix A.

The air-frame integrated scramjet engine causes significant interaction between propulsion, aerodynamics and control system [79]. In the longitudinal plane, the inlet flow pressure along the fore body causes nose up pitching moment whereas the external nozzle flow causes pitch down moment. Similarly the aerodynamics affects the propulsion as the bow shock at the inlet determines the the air intake and compression rate of the engine. Thus, engine model is dependent on the state of the vehicle so the coupling between propulsion, aerodynamics and trajectory of the vehicle has to be properly addressed. Because of the wide speed range of the vehicle, multiple engine cycles are needed for trajectory development. For speed less than Mach 2, turbojet is used and for speed between Mach 2 and 5, ramjet is used and for speed above Mach 5 scramjet is used. In this work, the trajectory development for speed above Mach 5 is addressed assuming the engine to be working in scramjet mode.

The thrust delivered by the engine is the product of weight flow rate and specific impulse given by

$$T = \dot{m} G_0 I_{sp} \tag{2.1}$$

where I_{sp} is the engine specific impulse, $\dot{m}$ is the mass flow rate and G_0 is the gravitational acceleration at the surface of the earth. Weight flow rate is the air that passes through the intake of the engine and is given by

$$\dot{m} G_0 = G_0 \rho V_{AB} A_c \tag{2.2}$$

where ρ is the atmosphere density, V_{AB} is the relative velocity in body frame and A_c is the engine capture area. For scramjet engine the air enters the cowl non-uniformly and thrust coefficient (C_T) is a function of angle of attack (α) and Mach number M_a. Thus, thrust is given by

$$T = G_0 \rho V_{AB} C_T(\alpha, M_a) A_c I_{sp}(M_a, \Phi) \tag{2.3}$$

The propulsion model uses linear interpolation/extrapolation scheme to compute the thrust coefficient C_T as a function of (M_a, α), shown in Figure 2.2 and specific impulse I_{sp} as a function of (M_a, equivalence ratio - Φ) shown in Figure 2.3. Fuel flow is varied by engine throttling command Φ_c which can vary between 0 to 10 for Mach less than 25.

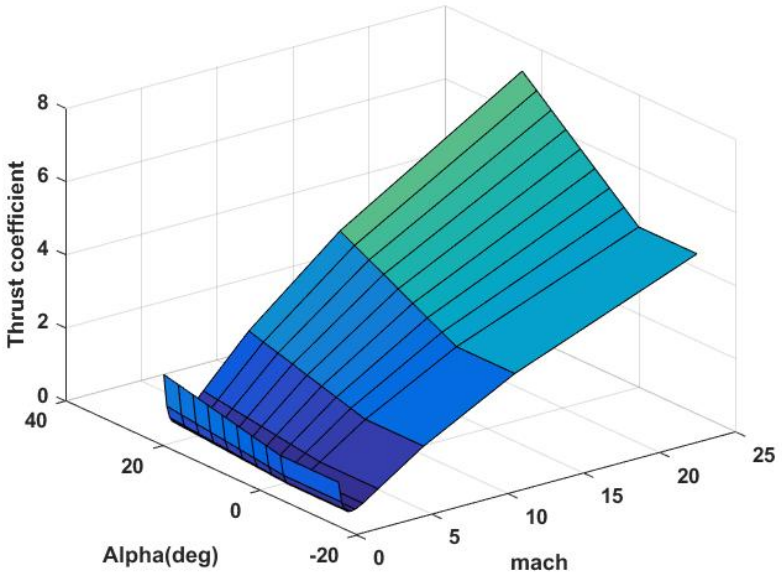

Figure 2.2: Thrust coefficient (C_T) as a function of α and M_a

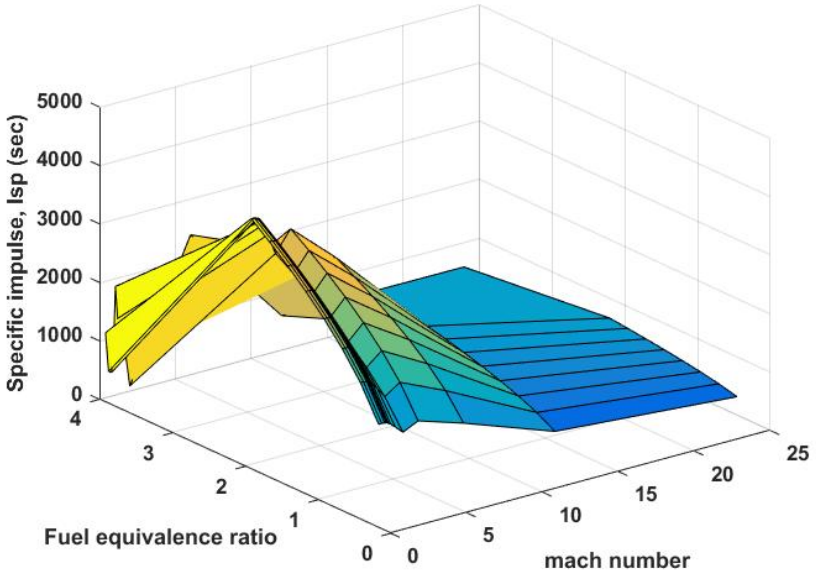

Figure 2.3: Specific impulse (I_{sp}) as a function of Φ and M_a

2.2.1 Mass Model

The mass model is based on the assumption that the vehicle is rigid and mass, centre of gravity and moment of inertia vary with respect to time as the fuel is consumed. Once thrust is computed, fuel flow rate is given by

$$\dot{w} = \frac{T}{I_{sp}} \tag{2.4}$$

and vehicle weight is updated as

$$W = W_0 - \dot{w}dt \tag{2.5}$$

where W_0 is the vehicle initial weight. With respect to the updated mass, centre of gravity and moment of inertia are interpolated from the data base. Fuel sloshing is not considered and cross product of moment of inertia is neglected. It is assumed that centre of gravity varies along the x-axis of the body as the fuel is consumed.

2.2.2 Aerodynamics

Aerodynamic model for generic, single stage to orbit, winged cone configuration of AB-SLV is taken as the study configuration. Aerodynamic force and moment coefficients are the function of Mach number, angle of attack and control surface deflection. Trim deflection requirement for the control surface is generated for the static stability of the vehicle. The longitudinal and lateral directional force and moment coefficients are then generated along the trajectory using linear interpolation/extrapolation of aero-data (data base generated from [77] with respect to Mach number, angle of attack and control surface deflection as briefed in Appendix B).

The drag, lift and side force coefficients are computed as sum of the corresponding coefficients of the basic vehicle and the control surfaces. Now the total force coefficients are computed as

$$C_D = C_{D0} + C_{D\delta_{eL}} + C_{D\delta_{eR}} + C_{D\delta_{ru}} \tag{2.6}$$

$$C_L = C_{L0} + C_{L\delta_{eL}} + C_{L\delta_{eR}} + C_{L\delta_{ru}} \tag{2.7}$$

$$C_Y = C_{Y\beta}\beta + C_{Y\delta_{eL}} + C_{Y\delta_{eR}} + C_{Y\delta_{ru}} \tag{2.8}$$

where β is the side slip angle of the vehicle, C_{D0}, C_{L0} are the drag, lift force coefficients of the basic vehicle, $C_{Y\beta}$ is the side force coefficient with side slip derivative of the basic

vehicle and $C_{D\delta_i}$, $C_{L\delta_i}$, $C_{Y\delta_i}$ (where i is eL, eR and ru for left elevon, right elevon and rudder respectively) are the drag, lift, side force increment coefficients of the corresponding control surfaces. Similarly, the moment coefficients in roll, pitch and yaw [80] are computed as

$$\begin{aligned} C_l = {} & C_{l\beta}\beta + C_{l\delta_{eL}} + C_{l\delta_{eR}} + C_{l\delta_{ru}} \\ & + C_{lp}\frac{pb}{2V_{AB}} + C_{lr}\frac{rb}{2V_{AB}} \end{aligned} \tag{2.9}$$

$$\begin{aligned} C_m = {} & C_{m0} + C_{m\delta_{eL}} + C_{m\delta_{eR}} + C_{m\delta_{ru}} \\ & + C_{mq}\frac{qc}{2V_{AB}} \end{aligned} \tag{2.10}$$

$$\begin{aligned} C_n = {} & C_{n\beta}\beta + C_{n\delta_{eL}} + C_{n\delta_{eR}} + C_{n\delta_{ru}} \\ & + C_{np}\frac{pb}{2V_{AB}} + C_{nr}\frac{rb}{2V_{AB}} \end{aligned} \tag{2.11}$$

where p, q, r are the vehicle body rates in roll, pitch and yaw, b is the lateral-directional reference length (span) of the vehicle, c is the longitudinal reference length (mean aerodynamic chord), C_{lp}, C_{lr} is the rolling moment coefficient of the basic vehicle with roll rate and yaw rate dynamic derivatives respectively, $C_{l\beta}$ is the rolling moment coefficient of the basic vehicle with side slip derivative, $C_{n\beta}$ is the yawing moment coefficient of the basic vehicle with side slip dynamic derivative, C_{mq} is the pitching moment coefficient of the basic vehicle with pitch rate dynamic derivative, C_{np} is the yawing moment coefficient of the basic vehicle with roll rate dynamic derivative and C_{nr} is the yawing moment coefficient of the basic vehicle with yaw rate dynamic derivative. $C_{l\delta_i}$, $C_{m\delta_i}$, $C_{n\delta_i}$ are the rolling, pitching, yawing moment increment coefficients of the corresponding control surfaces. The axial and normal force coefficients computed from the lift and drag coefficients are

$$\begin{bmatrix} C_A \\ C_N \end{bmatrix} = \begin{bmatrix} -\sin\alpha & \cos\alpha \\ \cos\alpha & \sin\alpha \end{bmatrix} \begin{bmatrix} C_L \\ C_D \end{bmatrix} \tag{2.12}$$

Aero force and moments about the centre of gravity of the vehicle are computed as

$$F_{Aero} = QS_{ref} \begin{bmatrix} -C_A \\ C_Y \\ -C_N \end{bmatrix} \tag{2.13}$$

$$M_{Aero} = QS_{ref} \begin{bmatrix} bC_n + X_{cg}C_Y \\ cC_m - X_{cg}C_N \\ bC_l \end{bmatrix} \tag{2.14}$$

where S_{ref} is the reference area and X_{cg} is the offset of centre of gravity in X-axis.

2.2.3 Vehicle Dynamics Model

The equations of motion of the vehicle in six dimensional space is described by translational and rotational dynamics. The force and moment equations in pitch, yaw and roll axis along with kinematic equations describe the dynamics of the vehicle. Different co-ordinate systems used to simplify guidance and control problem formulations are also discussed in this section.

2.2.3.1 Earth and Atmospheric Model

Oblate Earth model is used for the study and gravitational acceleration in ECI frame is computed considering the gravitational harmonics. Indian standard atmosphere is taken as the atmospheric model where the parameters pressure, density and temperature is stored as function of altitude. Speed of sound is computed by using the expression

$$C_s = \sqrt{1.4\frac{P}{\rho}} \tag{2.15}$$

where P is the engine pressure. The speed of sound is used for the computation of Mach number.

2.2.3.2 Translational Dynamics

Translational equations of motion describes the motion of the centre of gravity of the vehicle with respect to reference frame.The translational equations are derived with respect to ECI frame. Acceleration of the vehicle in ECI frame is computed from the total force acting on the vehicle as

$$\dot{\vec{V}}_I = \frac{1}{m}(IB)^{-1}\vec{F}_B + \vec{G}_0 \tag{2.16}$$

$$\dot{\vec{r}}_I = \vec{V}_I \tag{2.17}$$

where IB is the ECI frame to body frame conversion matrix and G_0 is the gravitational acceleration given by

$$G_0 = \begin{bmatrix} G_{xI} \\ G_{yI} \\ G_{zI} \end{bmatrix}$$

and the total force acting on the vehicle in body frame is the sum of thrust force, aero-force and control force which is given by

$$\vec{F}_B = \vec{F}_{TB} + \vec{F}_{AB} + \vec{F}_{CB} \tag{2.18}$$

The variation of center of mass due to the ejection of burning gas is minimal. The variation in c.g. is only 0.23 m, i.e. 7%. as shown in Figure 2.15. Hence, its effect on translational dynamics is not considered in the present work. The velocity and position vector in the ECI frame is computed by successive integration of acceleration using the Euler integration method.

$$V_I = \begin{bmatrix} u_I \\ v_I \\ w_I \end{bmatrix} \; r_I = \begin{bmatrix} x_I \\ y_I \\ z_I \end{bmatrix} \tag{2.19}$$

2.2.3.3 Rotational Dynamics

Rotational dynamics are described by motion of the vehicle about its center of gravity and is solved in body frame.

$$\dot{\vec{\omega}}_I = [I]^{-1}(\vec{M}_B - [\dot{I}]\vec{\omega} - \vec{\omega}[I]\vec{\omega}) \tag{2.20}$$

where the angular rate and inertia are given by

$$\bar{\omega} = \begin{bmatrix} r \\ q \\ p \end{bmatrix} \qquad I = \begin{bmatrix} I_{xx} & -I_{xy} & -I_{xz} \\ -I_{xy} & I_{yy} & -I_{yz} \\ -I_{zx} & -I_{yz} & I_{zz} \end{bmatrix}$$

The vehicle rotational motion has a loss of angular momentum w.r.t center of mass due to the velocity of the ejecting mass. This loss is called jet damping and is formulated as

$$F_e = -\dot{m}_e(\omega \times r_e) \tag{2.21}$$

$$M_e = r_e \times F_e \tag{2.22}$$

where r_e is the distance vector from c.g. to nozzle exit plane and $\dot{m}_e$ is the rate of flow of ejecting mass. Figure 2.15 shows the comparison of jet damping and $\dot{I}\omega$ terms along with the variation of moment of inertia and c.g. The effect of damping terms in closed-loop simulation is negligible.

The total moment in body frame is the sum of moments due to thrust, aero-force and control force.

$$\vec{M}_B = \begin{bmatrix} M_x \\ M_y \\ M_z \end{bmatrix} = \vec{M}_{TB} + \vec{M}_{AB} + \vec{M}_{CB} \tag{2.23}$$

2.2.3.4 Auxiliary Position and Velocity Computations

Relative velocity of the vehicle is computed in body frame and aerodynamic angles are calculated from its components. Similarly flight path angle and azimuth angle are computed from velocity components in geographic frame. The relative velocity in ECI frame is

$$V_{AI} = V_I - \Omega_e * t - V_{WI} \tag{2.24}$$

where Ω_e is the earth's angular rotation rate and the V_{WI} is the wind velocity in ECI frame. The relative velocity in body frame is given by

$$V_{AB} = \begin{bmatrix} u_A \\ v_A \\ w_A \end{bmatrix} = [IB] * V_{AI} \tag{2.25}$$

Pitch angle of attack and side slip angle is given by

$$\alpha = \tan^{-1}(\frac{u_A}{w_A}) \qquad \beta = \tan^{-1}(\frac{v_A}{w_A}) \tag{2.26}$$

Velocity in gravitational frame is computed by

$$V_{IG} = \begin{bmatrix} v_{XG} \\ v_{YG} \\ v_{ZG} \end{bmatrix} = [IG]V_I \tag{2.27}$$

where IG is the ECI frame to geographic frame conversion matrix. Flight path angle γ and Azimuth angle A_z are computed as

$$\gamma = \sin^{-1}(\frac{v_{XG}}{V_I}) \tag{2.28}$$

$$A_z = \tan^{-1}(\frac{v_{YG}}{v_{ZG}}) \tag{2.29}$$

The longitude and latitude [81] are calculated using position vector and velocity vector with respect to ECI frame.

$$r_I = \begin{bmatrix} x_I \\ y_I \\ z_I \end{bmatrix} \tag{2.30}$$

$$Latitude \quad \varphi = \sin^{-1}(\frac{z_I}{r_I}) \tag{2.31}$$

$$Longitude \quad \Theta = \tan^{-1}(\frac{y_I}{z_I}) \tag{2.32}$$

2.2.3.5 Kinematic Relations

Kinematic relations describe the instantaneous attitude of the system. Using Euler angles, the instantaneous rate of rotation in ECI frame about the pitch, yaw and roll axis are given by

$$\dot{\theta} = \frac{r\sin\phi + q\cos\phi}{\cos\psi} \tag{2.33}$$

$$\dot{\psi} = r\cos\phi - q\sin\phi \tag{2.34}$$

$$\dot{\phi} = p + \frac{\sin\psi(r\sin\phi + q\cos\phi)}{\cos\psi} \tag{2.35}$$

Using these angular rates pitch(θ), yaw(ψ) and roll(ϕ) angles are updated at each time interval.

2.2.3.6 Coordinate Systems Used

For describing the ascent trajectory, four different co-ordinate systems used in this study are:

1. The Earth-Centered Inertial Frame: This coordinate system in Figure 2.4 has the center of the Earth as the origin with the X axis pointing towards the Greenwich meridian in the equatorial plane at the time of launch t = 0, the Z axis pointing to the

north pole and the Y axis completing the triad. It is a non-rotating frame which is fixed at the time of launch.

2. The Guidance Frame: This coordinate system in Figure 2.4 has X-axis, pointing from the center of the earth towards the launch site while the Z-axis points downrange in the launch azimuth direction. The Y-axis completing the triad.

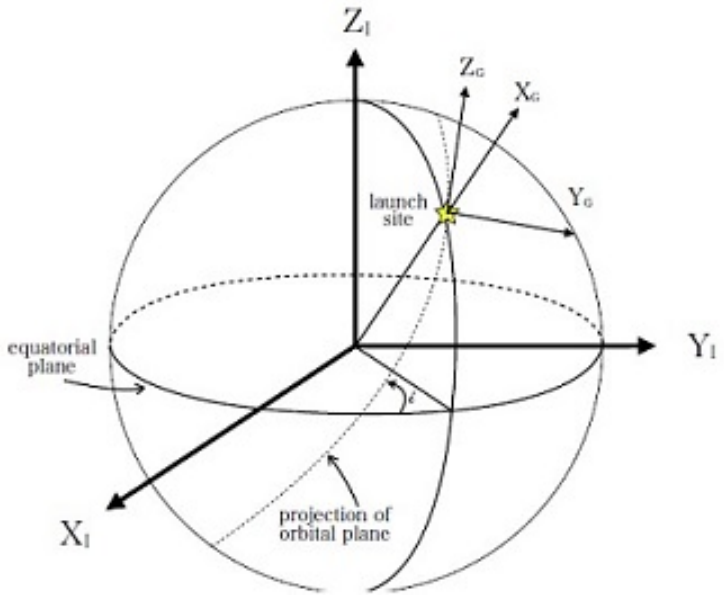

Figure 2.4: Earth centered and guidance co-ordinate systems [5].

3. Body-centered Co-ordinate System: This coordinate system in Figure 2.5 has the center of gravity of the vehicle as the origin, the X-axis points to the nose of the vehicle, the Y-axis points to the right wing, and the Z-axis completes the triad.

4. The Geographic Frame: This coordinate system in Figure 2.6 is located on the surface of the Earth at the current geocentric latitude and longitude of the vehicle. The Z axis points to the north in the local horizontal plane, the Y axis points to the east, and the X axis completes the triad.

2.2.3.7 Co-ordinate Transformations used

Transformation matrix to convert from ECI frame to guidance frame is given by

$$IEG = \begin{bmatrix} \cos\Theta\cos\Phi & \sin\Theta\cos\Phi & \sin\Phi \\ -\sin\Theta\cos A_z + \cos\Theta\sin\Phi\sin A_z & \cos\Theta\cos A_Z + \sin\Theta\sin\Phi\sin A_z & -\cos\Phi\sin A_z \\ -\sin\Theta\sin A_z - \cos\Theta\sin\Phi\cos A_z & \cos\Theta\sin A_Z - \sin\Theta\sin\Phi\cos A_z & \cos\Phi\cos A_z \end{bmatrix}$$

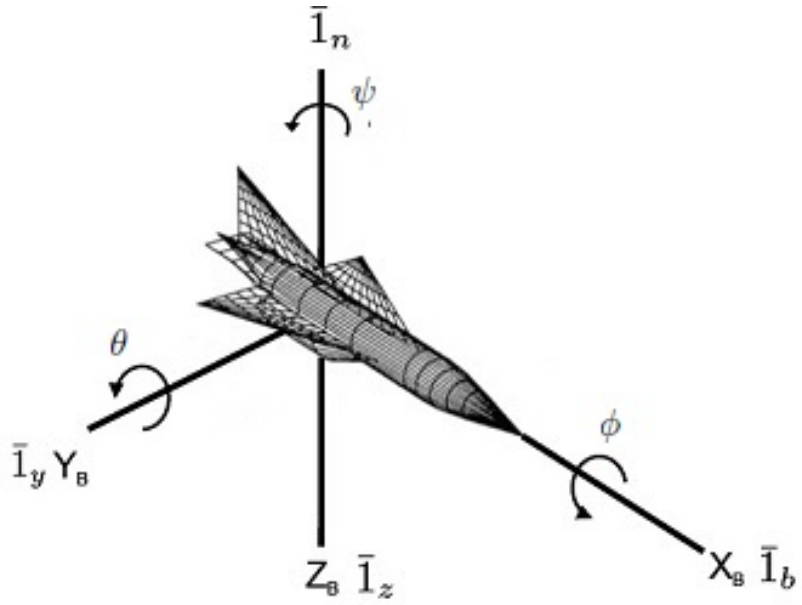

Figure 2.5: Body-centered co-ordinate system [5].

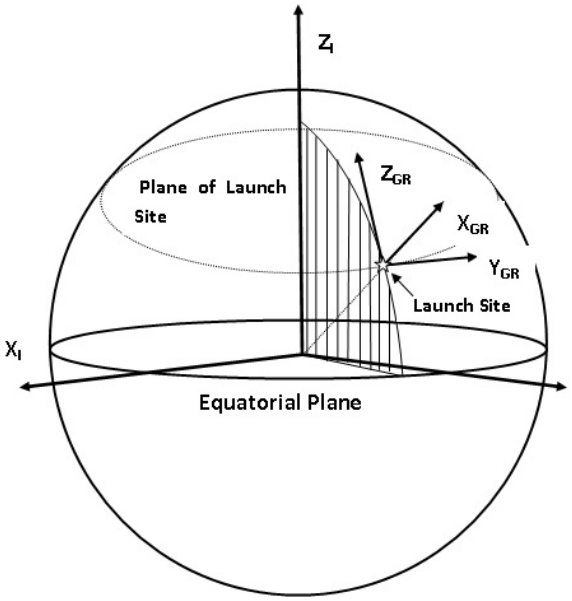

Figure 2.6: Geographic co-ordinate system

Transformation matrix to convert from body frame to guidance frame is given by

$$I_{BG} = \begin{bmatrix} \cos\theta\cos\psi & \sin\theta\sin\phi - \cos\theta\sin\psi\sin\phi & \sin\theta\cos\phi + \cos\theta\sin\psi\sin\phi \\ \sin\psi & \cos\psi\cos\phi & -\cos\psi\sin\phi \\ -\sin\theta\cos\psi & \cos\theta\sin\phi + \sin\theta\sin\psi\cos\phi & \cos\theta\cos\phi - \sin\psi\sin\theta\sin\phi \end{bmatrix}$$

The unit vector along body $x - axis$ in guidance frame is given by

$$\vec{I_b} = \begin{bmatrix} \cos\theta\cos\psi \\ \sin\psi \\ -\sin\theta\cos\psi \end{bmatrix}$$

The unit vector along body $y - axis$ and $z - axis$ in guidance frame are given by

$$\vec{I_y} = \begin{bmatrix} \sin\theta\sin\phi - \cos\theta\sin\psi\sin\phi \\ \cos\psi\cos\phi \\ \cos\theta\sin\phi + \sin\theta\sin\psi\cos\phi \end{bmatrix}$$

$$\vec{I_z} = \vec{I_b} \times \vec{I_y} = \begin{bmatrix} \sin\theta\cos\phi + \cos\theta\sin\psi\sin\phi \\ -\cos\psi\sin\phi \\ \cos\theta\cos\phi - \sin\psi\sin\theta\sin\phi \end{bmatrix}$$

and the body normal unit vector is $\vec{I_n} = -\vec{I_z}$.

2.3 Results and Discussions

Both the translational and rotational equations of motion of air-breathing vehicle solved from the initial conditions to propagate the open loop trajectory. A numerical simulation using Euler integration method in MATLAB environment, is done to demonstrate the performance of the vehicle. The initial conditions used for the simulation are given in Table 2.1.

Table 2.1: Initial conditions of the trajectory

Parameters	Initial condition	Unit
Altitude	2280	m
Velocity	1650	m/s
Flight path angle	0	deg
Weight	12700	kg
Mach	4.8	-

2.3.1 Verification and Validation

To validate the program, the open-loop results are compared with simulation results by Oscar J Murillo in [5]. Here the vehicle considered is winged cone configuration against the generic hypersonic aerodynamic model by Oscar J Murillo. The same initial conditions are assumed and trajectory simulation is carried out to achieve the same final conditions. The trend of the trajectory parameters fairly match with that of [5] as shown in Figure 2.7 and Figure 2.8.

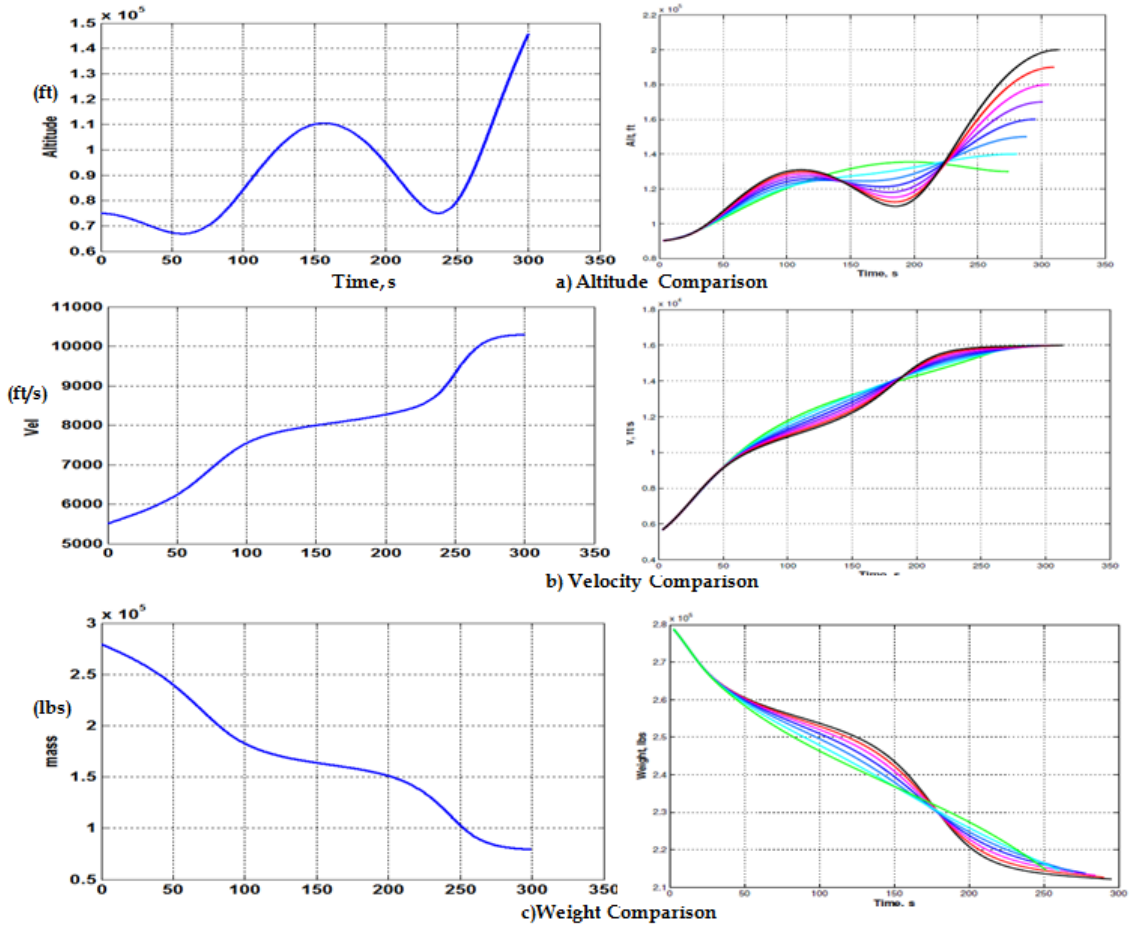

Figure 2.7: Comparison of trajectory parameters (altitude,velocity,weight) vs time-(column 1) with corresponding parameters in the reference [5]vs time-(column 2).

2.3.2 Open-loop Simulation Results

Open loop simulation results are shown Figure 2.9 and Figure 2.10. During the initial flight, there is a dip in the altitude upto 25s where the thrust build up is small as specific impulse

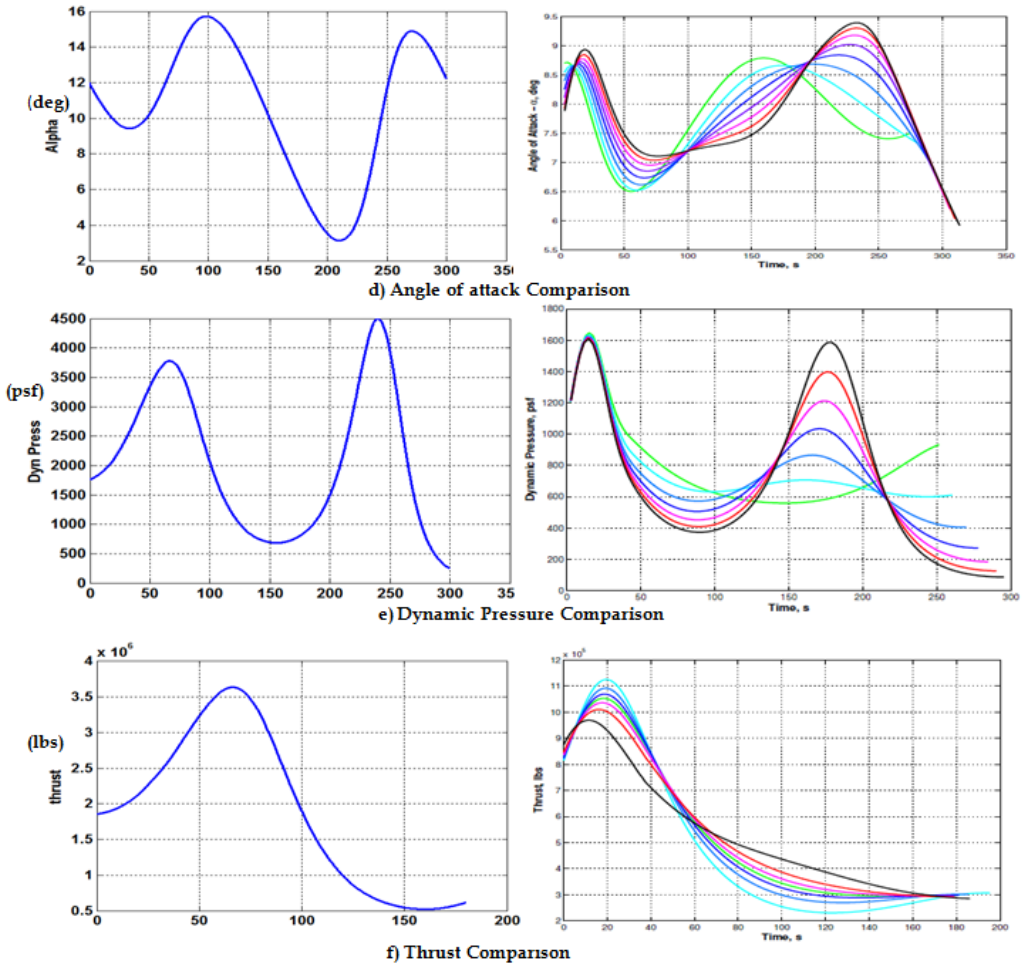

Figure 2.8: Comparison of trajectory parameters (Angle of attack,dynamic pressure and thrust) vs time-(column 1) with corresponding parameters in the reference [5]vs time-(column 2).

is Mach number dependent and the gravity effect is more. Further, as the thrust builds up it overcomes the gravity effect due to reduction in mass with fuel consumption. After 35s thrust starts falling as the vehicle attains high altitude and the density starts decreasing. Therefore, at lower altitudes vehicle has high accelerations. Because of this dynamic pressure also peaks around 40s after which it starts decreasing and the pattern continues as time progresses.

Simulation results with different initial altitudes keeping the same target conditions are shown in Figure 2.11 and Figure 2.12. As the initial altitude increases, the initial thrust build up is slow as the density is less at high altitudes. In order to attain more velocity, the vehicle dips, which causes the thrust to increase and the vehicle attains sufficient velocity

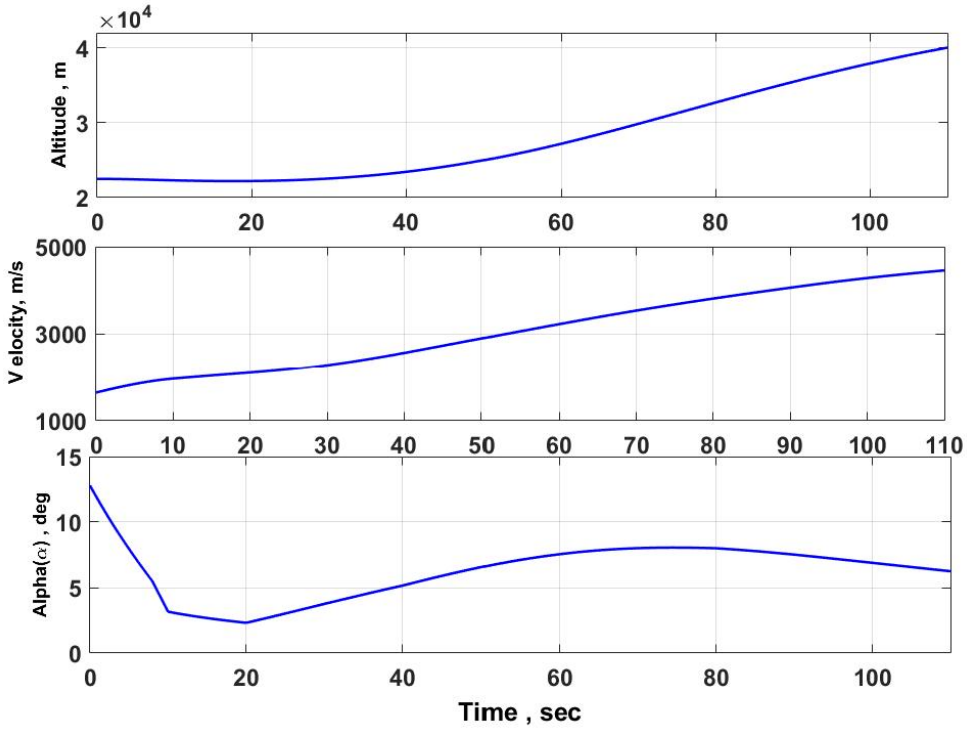

Figure 2.9: Open loop simulation results:Altitude,Velocity and Angle of attack

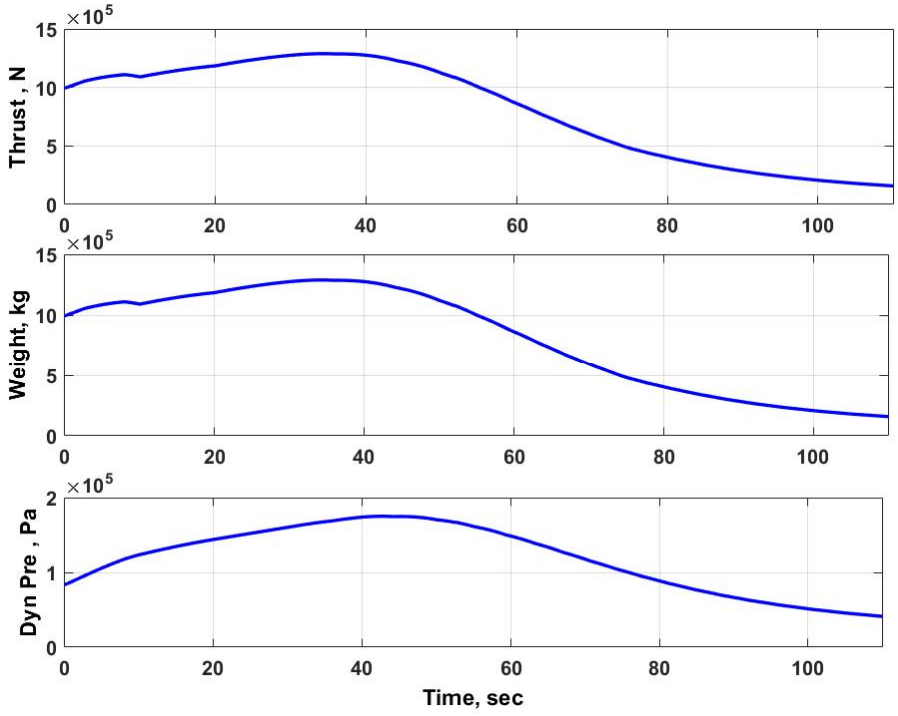

Figure 2.10: Open loop simulation results:Thrust,Weight and Dynamic Pressure

to reach the target conditions. Thus, the time taken to reach the target is more for high initial altitudes. There is decrease in final weight as initial altitude increases, as more propellant is used. But when the initial altitude is more than 25.5km, the vehicle dips much more to attain sufficient thrust and vehicle reaches the target condition faster. Thus the time to reach the target conditions decreases after 25.5km height of initial altitude. This shows that there is an optimum altitude at which scramjet can be powered so as to attain maximum propellant efficiency. Increasing the final altitude results in more time to reach to the target with more fuel consumption and the requirement of two peaks are seen in trajectory parameters.

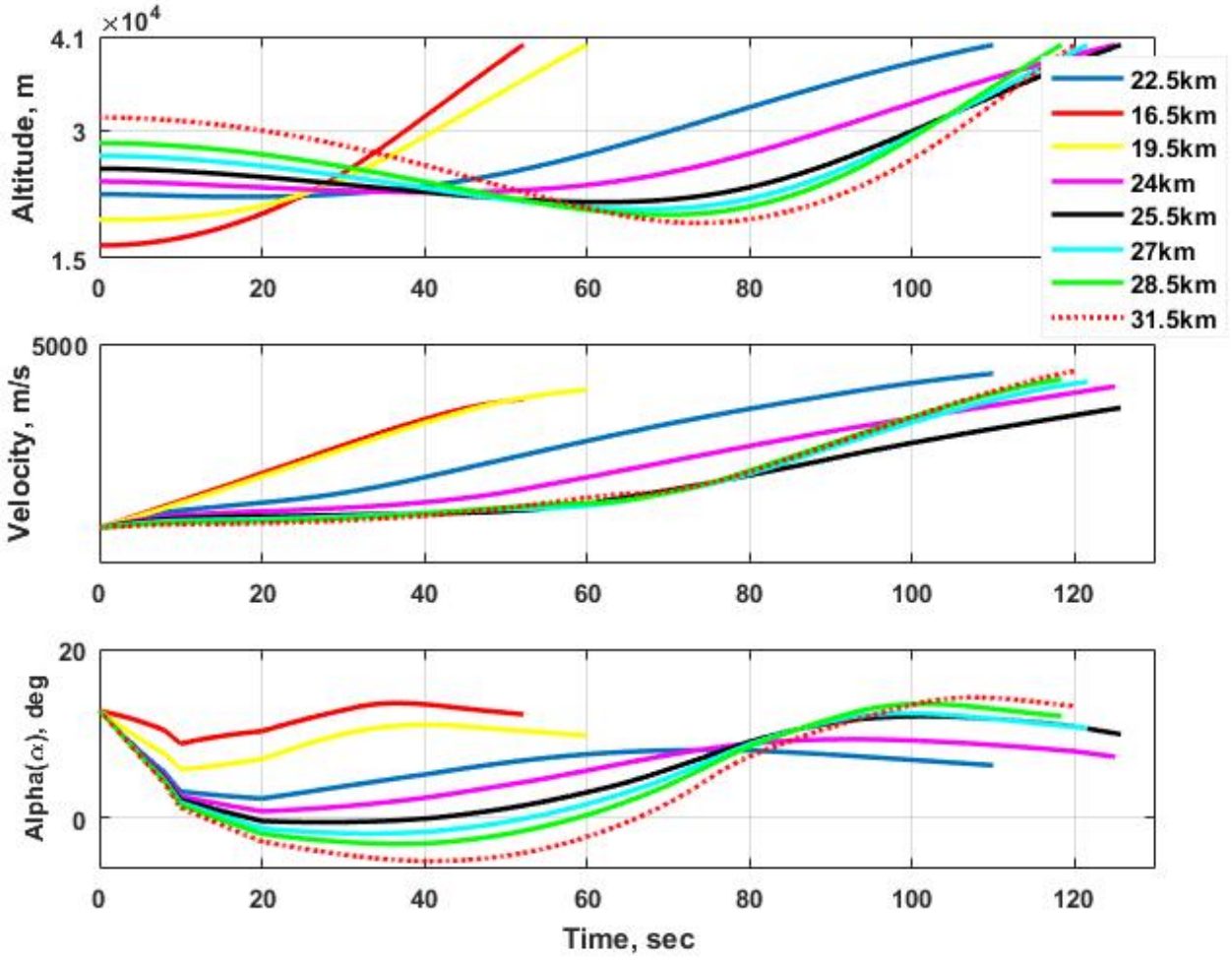

Figure 2.11: Open loop simulation results with different initial conditions: Altitude, Velocity and Angle of attack

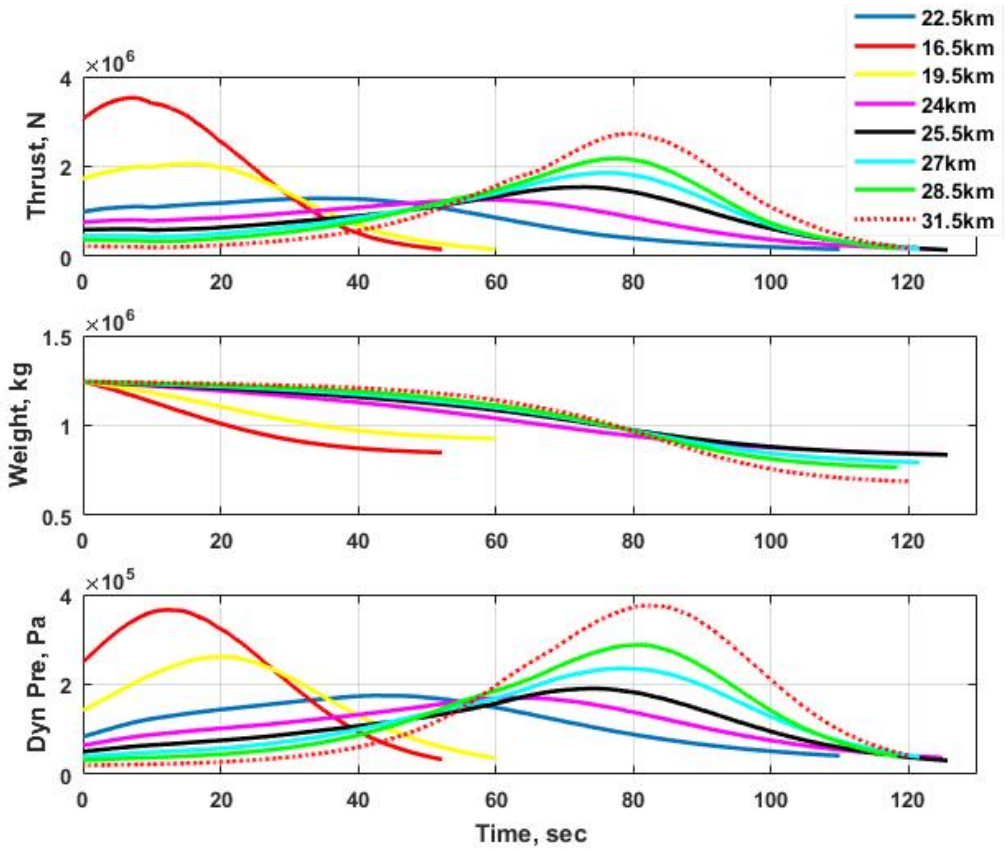

Figure 2.12: Open loop simulation results with different initial conditions: Thrust, Weight and Dynamic Pressure

2.3.2.1 Open-loop Simulation with Constraints on Angle of Attack and Dynamic Pressure

Open loop run with constraints on angle of attack and dynamic pressure is shown in Figure 2.13. Wherever dynamic pressure exceeds Q_{max}, throttle opening is reduced to limit the dynamic pressure. Variation of thrust with throttle opening is not linear as Isp is a function of throttle opening. Here the desired thrust is computed from the dynamic pressure constraint and then throttle opening for the desired thrust is computed in an iterative manner. Simulations shows that time required to achieve the target condition with constraints are 12s more compared to open loop run without constraint on dynamic pressure and angle of attack.

Comparison of open loop simulation with 6D and 3D models has been done in the present work and is shown in Figure 2.14. In 3D simulation, desired altitude is achieved with additional burning of the stage by 2sec with difference in terminal velocity of 245m/s.

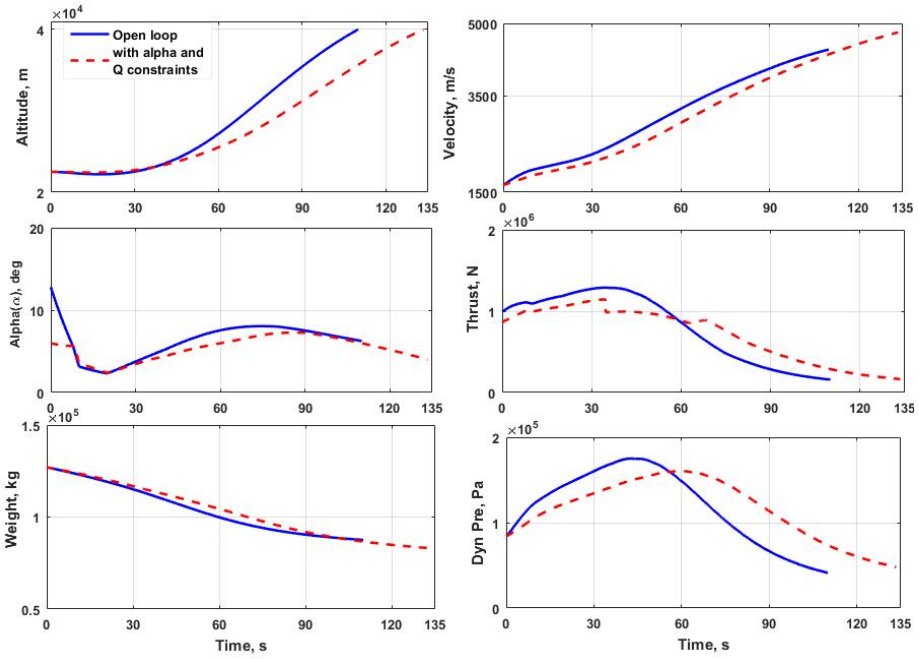

Figure 2.13: Open loop simulation results with constraints on angle of attack and dynamic pressure

Significant difference is seen in vehicle parameters like dynamic pressure, thrust, weight, and open-loop angle of attack. This difference in the vehicle parameters in open loop simulation will further affect the closed loop guidance command - optimal angle of attack generation with 3D model. In the present 6D model the force contribution from the control surface deflection is considered in addition to the force contribution from the basic vehicle in solving the co-state equations. In the controller design, also all coupling issues can be properly handled only by taking the translational and rotational states together. Thus, 6D trajectory simulation gave the actual dynamical behaviour of the vehicle under different flight environments.

2.4 Summary

In this chapter, 6D trajectory development of air breathing phase of ABSLV is studied. Modeling of different subsystems is presented, addressing the coupling between different systems. Open loop simulation results are validated with that of [5]. The sensitivity study of the trajectory parameters for different initial altitudes shows that there is an optimum altitude at which the scramjet can be powered in order to obtain maximum propulsive efficiency. The advantage of having a 6D trajectory over a 3D trajectory in handling the

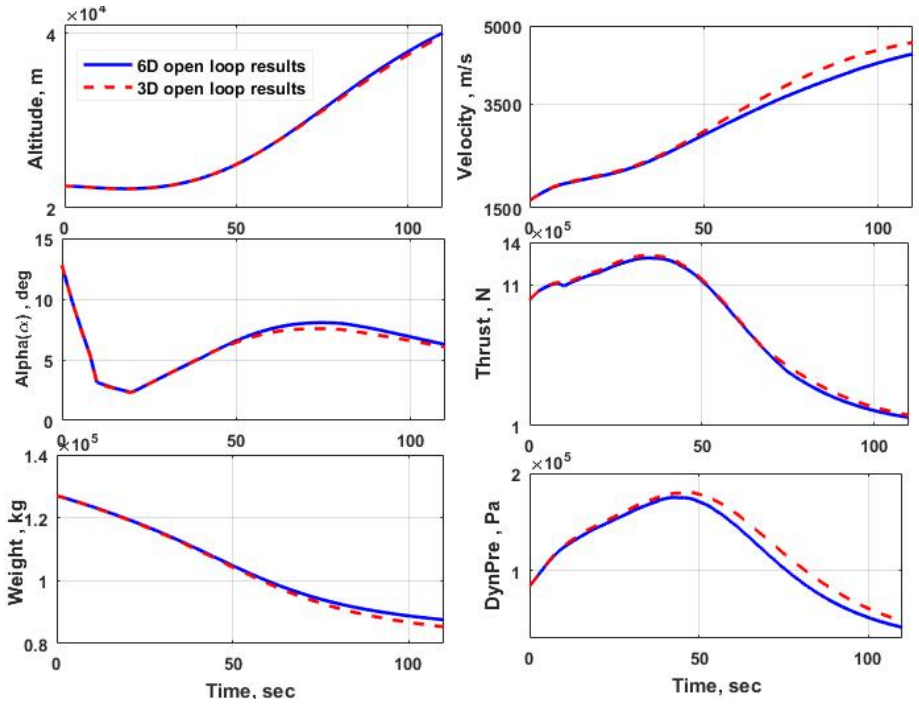

Figure 2.14: Comparison of vehicle parameters for 6D and 3D simulation

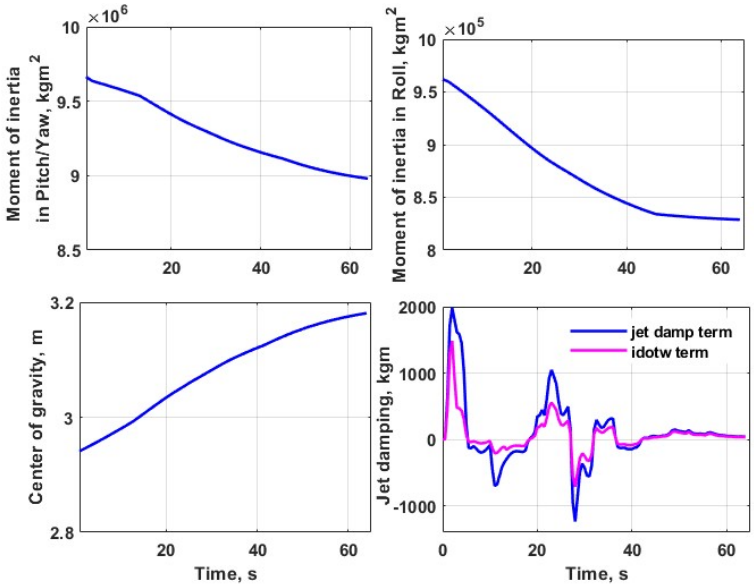

Figure 2.15: Variation of inertia, center of gravity and damping terms (jet damping and $\dot{I}\omega$) during air-breathing phase

coupling between translational and rotational dynamics through aerodynamics and propulsion is clearly brought out.

Chapter 3

Guidance Design

3.1 Introduction

Ascent phase guidance problem is formulated as optimal control problem to find the engine cut off time t_f and the desired body axis orientation to find direction of thrust and aerodynamic forces. The guidance formulation used here is similar to Oscar J. Murillo et al [5]. In this approach ascent guidance problem is solved as Hamiltonian two point boundary value problem derived from first order optimally conditions satisfying path constraints and terminal state conditions. To solve this TPBVP problem a numerical hybrid optimization methodology is followed.

3.2 Optimal Control Problem

The optimal problem is to find a control u*, which causes the system to follow the trajectory where the performance index will be minimized. Let the system be described as

$$\dot{x} = f(x, u, t) \tag{3.1}$$

where x is the state of the system, u is the control input and t is the time. The performance index

$$J = \Upsilon(x_f, t_f) + \int L(x(t), u(t), t)dt \tag{3.2}$$

where $\Upsilon(x_f, t_f)$ is a final weighting function that depends on the final states x_f and final time t_f, and $L(x(t), u(t), t)$ is the weighting function which depends on current states $x(t)$,$u(t)$,t. By adjoining the dynamic constraint to the integrand using Lagrange multiplier,

the augmented cost Function J_a is

$$J_a = \Upsilon(x_f, t_f) + \int L(x(t), u(t), t) + \lambda^T (f(x, u, t))dt \tag{3.3}$$

To minimize the cost function subject to constraints $\dot{x}(t) = f(x, u, t)$

$$J_a = \Upsilon(x_f, t_f) + \int L(x(t), u(t), t) + \lambda^T (f(x, u, t) - \dot{x})dt \tag{3.4}$$

Hamiltonian, a function of Lagrangian, adjoint vector and system dynamics is defined as

$$H(x, u, t) \stackrel{\triangle}{=} L(x, u, t) + \lambda^T f(x, u, t) \tag{3.5}$$

The terminal state constraint is given by

$$\Psi(x(t_f), t_f) = 0 \tag{3.6}$$

Now the augmented performance index can be written as

$$J_a = \Upsilon(x_f, t_f) + \upsilon^T \Psi(x(t_f), t_f) + \int (H(x, u, t) - \lambda^T \dot{x})dt \tag{3.7}$$

Now calculus of variation formulation is used to minimize the augmented cost function [22]. In the ascent phase the fuel has to be optimized at the terminal states, thus in guidance optimal formulation only the final weighing function Υ is used and no weight function, L based on current state is used. Hence it is a problem of Mayer i.e. function of system at terminal time t_f. The calculus of variation formulation is used to minimize the performance index, its derivative is set to zero at $t = t_f$. Since $x(t)$ is a continuous function of time, $dx(t)$ and dt are not independent. For the fixed final state problem $dx(t_f) = 0$ and terms with dt are considered. For fixed final time problem $dt_f = 0$ and terms associated with $dx(t_f)$ are considered. From this optimal conditions derived are

$$\text{State equation :} \quad \dot{x} = \frac{dH}{d\lambda} = f \quad t > t_0 \tag{3.8}$$

$$\text{Co-state equation :} \quad \dot{\lambda} = -\frac{dH}{dx} = \frac{df^T}{dx}\lambda \quad t < t_f \tag{3.9}$$

$$\text{Stationary equation :} \quad 0 = -\frac{dH}{du} = \frac{df^T}{du}\lambda \tag{3.10}$$

$$\begin{aligned} \text{Boundary condition :} \quad & x(t_0) \quad \text{given} \\ & (\Upsilon_x + \Psi_x^T \upsilon - \lambda)^T dx(t_f) = 0 \end{aligned} \tag{3.11}$$

3.3 Problem Definition

In the air-breathing phase of ABSLV, vehicle body axis frame is selected such that side slip angle is assumed to be zero. This is ensured through the controller by commanding the side slip angle to zero. Hence the vehicle will always be placed in a symmetrical plane, plane formed by the body axis $\vec{I_b}$ and the earth relative velocity vector V_r as in Figure 3.1.

$$\cos\alpha = I_b.I_{V_r} \quad \sin\alpha = \|I_{V_r} \times I_b\| \tag{3.12}$$

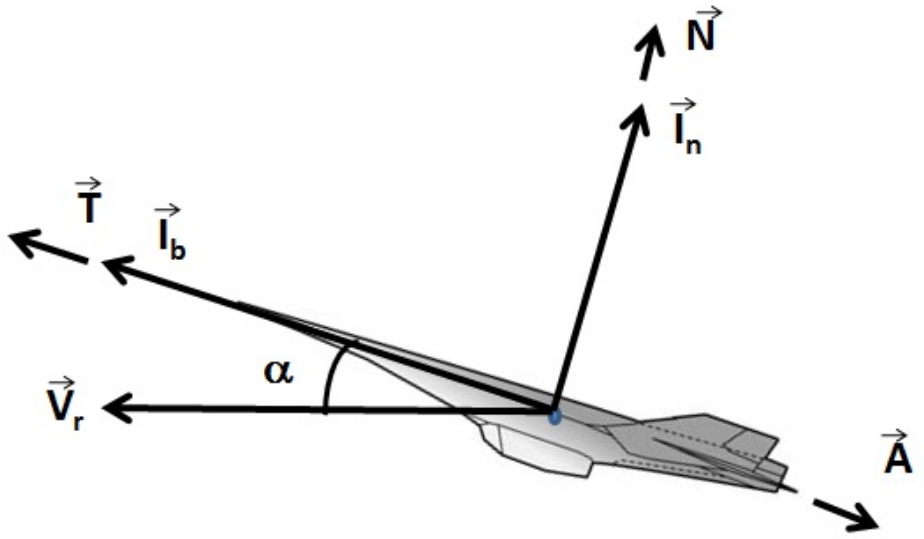

Figure 3.1: Direction of forces and relative velocity acting on the vehicle

Guidance problem for ascent phase is to find the body axis orientation $\vec{I_b}$ with time which determines the direction of aerodynamic forces and thrust optimally.

3.3.1 Optimal Formulation

For the ascent trajectories performance index is chosen in such a way to minimize the fuel consumption thus maximizing the payload.

$$J = -m(t_f) \tag{3.13}$$

The states considered are position, velocity and mass of the vehicle,the state equations in ECI frame system are given by

$$\dot{\vec{r_I}} = \vec{V_I} \tag{3.14}$$

$$\dot{\vec{V_I}} = \vec{g}(\vec{r_I}) + \frac{T\vec{I_b}}{m} + \frac{\vec{A}}{m} + \frac{\vec{N}}{m} \tag{3.15}$$

$$\dot{m} = \frac{T}{G_0 I_{sp}} \tag{3.16}$$

where $\vec{g}$ is acceleration due to gravity, $\vec{A}$ is the axial force, $\vec{N}$ is the normal force and $\vec{I_b}$ is the unit vector defining vehicle body axis. The Hamiltonian is defined as

$$H = \vec{P_r}\dot{\vec{r_I}} + \vec{P_v}\dot{\vec{V_I}} + P_m\dot{m} \tag{3.17}$$

$$\begin{aligned} H = \vec{P_r}^T\vec{V_I} + \vec{P_v}^T[-\frac{1}{r^3}\vec{r_I} \\ + (T-A)\vec{I_b} + N\vec{I_n}] - P_m\frac{T}{G_0 I_{sp}} \end{aligned} \tag{3.18}$$

where P_r and P_v are co-state vectors for position and velocity states and P_m is the co-state scalar for mass. From this co-state equations are

$$\begin{aligned} \dot{P_r} = \frac{\partial H}{\partial \vec{r_I}} = \frac{1}{r^3}P_v - \frac{3P_v\vec{r_I}}{r^5}\vec{r_I} \\ - \frac{P_v^T\vec{I_b}}{m}(\frac{\partial T}{\partial \vec{r_I}} - \frac{\partial A}{\partial \vec{r_I}}) - \frac{P_v^T\vec{I_n}}{m}\frac{\partial N}{\partial \vec{r_I}} \\ - \frac{N}{m}\frac{\partial \vec{I_b}}{\partial \vec{r_I}}P_v + \frac{P_m}{G_0}(\frac{\partial T}{\partial \vec{r_I} I_{sp}} + T\frac{\partial I_{sp}^{-1}}{\partial \vec{r_I}}) \end{aligned} \tag{3.19}$$

$$\begin{aligned}\dot{P}_v = \frac{\partial H}{\partial \vec{V}_I} = -P_r - \frac{P_v^T \vec{I}_b}{m}(\frac{\partial T}{\partial \vec{V}_I} - \frac{\partial A}{\partial \vec{V}_I}) \\ - \frac{P_v^T \vec{I}_n}{m}\frac{\partial N}{\partial \vec{V}_I} - \frac{N}{m}\frac{\partial \vec{I}_b}{\partial \vec{V}_I}P_v \\ + \frac{P_m}{G_0}(\frac{\partial T}{\partial \vec{V}_I I_{sp}} + T\frac{\partial I_{sp}^{-1}}{\partial \vec{V}_I})\end{aligned} \tag{3.20}$$

$$\begin{aligned}\dot{P}_m = \frac{\partial H}{\partial m} = -\frac{P_v^T \vec{I}_b}{m}(\frac{\partial T}{\partial m} - \frac{\partial A}{\partial m}) \\ - \frac{P_v^T \vec{I}_n}{m}\frac{\partial N}{\partial m} + \frac{P_m I_{sp}^{-1}}{G_0}(\frac{\partial T}{\partial m})\end{aligned} \tag{3.21}$$

Applying maximum principle to Hamiltonian

$$\frac{\partial H}{\partial \vec{I}_b} = 0 \tag{3.22}$$

The optimal control $\vec{I}_b^*$ lies in the symmetric plane where P_v and V_r lies as slide slip angle is zero as shown in Figure 3.2 . Let

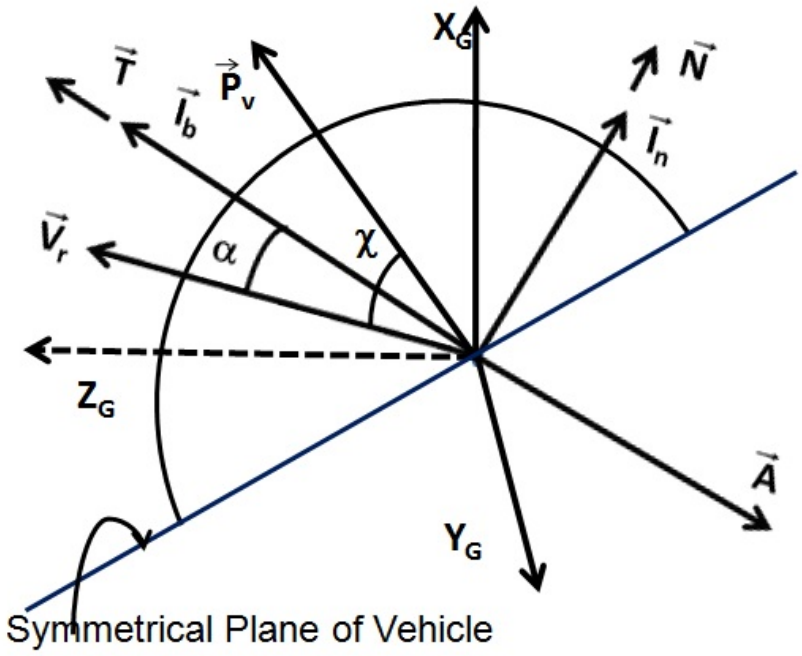

Figure 3.2: Plane containing relative velocity and velcoty co-state vector

$$\cos\chi = \vec{I}_{P_v}^T \vec{I}_{V_r} \tag{3.23}$$

where I_{P_v} and I_{V_r} are the unit vectors in the direction of P_v and V_r and χ is the angle between P_v and V_r. The following relationship can be made from the above figure

$$\vec{I}_b^T \vec{P}_v = P_v \cos(\chi - \alpha) \tag{3.24}$$

$$\vec{I}_n^T \vec{P}_v = P_v \sin(\chi - \alpha) \tag{3.25}$$

Using these relations Hamiltonian can be written as

$$\begin{aligned} H &= \vec{P}_r^T \vec{V} - \frac{1}{r^3}\vec{P}_v^T \vec{r} + (T - A)\vec{P}_v^T \vec{I}_b + N\vec{P}_v^T \vec{I}_n - P_m \frac{T}{G_0 I_{sp}} \\ &= \vec{P}_r^T \vec{V} - \frac{1}{r^3}\vec{P}_v^T \vec{r} + (T - A)P_v \cos(\chi - \alpha) \\ &+ NP_v \sin(\chi - \alpha) - P_m \frac{T}{G_0 I_{sp}} \end{aligned} \tag{3.26}$$

Maximizing the Hamiltonian with respect to $\vec{I}_b$ is equivalent to maximizing with respect to alpha.

$$\frac{\partial H}{\partial \alpha} = 0 \tag{3.27}$$

gives

$$\begin{aligned} \tan(\chi - \alpha)(T - A + N_\alpha) - (A_\alpha - T_\alpha + N) \\ - \frac{P_m}{P_v G_0 I_{sp}} T_\alpha \sec(\chi - \alpha) = 0 \end{aligned} \tag{3.28}$$

With the known values of co-states, the above equation is solved numerically using iterative algorithm for the optimum alpha satisfying the path constraints on angle of attack and dynamic pressure.

3.3.2 Path Constraints

In order to fly the vehicle in a safe corridor , the following path constrains are considered.

- Dynamic pressure constraint $Q = \frac{1}{2}\rho V_r^2$: To avoid excessive structural loading and heating of the vehicle

- angle of attack α

- the product of dynamic pressure and angle of attack $Q\alpha$

Usually the product of dynamic pressure and angle of attack can sufficiently represent all the above path constrains. Let $Q\alpha_{max}$ represent the upper limit on the product of dynamic pressure and angle of attack, then the constraint can be represented as

$$S = Q\alpha - Q\alpha_{max} \leq 0 \tag{3.29}$$

3.3.3 Terminal Constraints

The final conditions at the end of scramjet engine shut off are the states - altitude, velocity, flight path angle $x(t_f) = [r_f^*, v_f^*, \gamma_f^*]$ and the inclination i^* for representing the sub orbit that can be achieved. The final conditions can be represented as

$$\begin{aligned}
\Psi_1 &= \frac{1}{2}\vec{r}_f^T\vec{r}_f - \frac{1}{2}r_f^{*2} = 0 \\
\Psi_2 &= \frac{1}{2}\vec{V}_f^T\vec{V}_f - \frac{1}{2}V_f^{*2} = 0 \\
\Psi_3 &= \vec{I}_n^T(\vec{r}_f \times \vec{V}_f - \|\vec{r}_f \times \vec{V}_f\| \cos i^* = 0 \\
\Psi_4 &= \vec{r}_f\vec{V}_f - r_f^* V_f^* \sin\gamma_f^* = 0
\end{aligned} \tag{3.30}$$

3.3.4 Transversality Conditions

The optimal solution must meet the following transversality conditions.

$$\vec{P}_r(t_f) = -\frac{\partial\Upsilon(\vec{r}_f, \vec{V}_f, m_f, t_f)}{\partial\vec{r}_f} + \left(\frac{\partial\vec{\Psi}}{\partial\vec{r}_f}\right)^T\vec{v} \tag{3.31}$$

$$\vec{P}_V(t_f) = -\frac{\partial\Upsilon(\vec{r}_f, \vec{V}_f, m_f, t_f)}{\partial\vec{V}_f} + \left(\frac{\partial\vec{\Psi}}{\partial\vec{V}_f}\right)^T\vec{v} \tag{3.32}$$

$$\vec{P}_m(t_f) = -\frac{\partial\Upsilon(\vec{r}_f, \vec{V}_f, m_f, t_f)}{\partial\vec{m}_f} + \left(\frac{\partial\vec{\Psi}}{\partial\vec{m}_f}\right)^T\vec{v} \tag{3.33}$$

$$H(\vec{P}_r, \vec{P}_V, P_m, \vec{r}^*, \vec{V}^*, m^*, \vec{I}_b^*, t) \mid_{t_f} = \frac{\partial \Upsilon}{\partial t_f} \tag{3.34}$$

where $\vec{v} \in \mathrm{Re}^k$ is a constant multiplier and the final condition (3.11) is used for problems where final time is not specified. Substituting the equations for Υ and Ψ from (3.13) and (3.30) we get co-state values at terminal point as

$$\vec{P}_r(t_f) = \upsilon_1 \vec{r}_f + \upsilon_3 [\vec{V}_f \times \vec{I}_n - \frac{\vec{V}_f \times \vec{h}_f}{\parallel \vec{r}_f \times \vec{V}_f \parallel} \cos i^*] + \upsilon_4 \vec{V}_f \tag{3.35}$$

$$\vec{P}_V(t_f) = \upsilon_2 \vec{V}_f + \upsilon_3 [\vec{I}_n \times \vec{r}_f - \frac{\vec{r}_f \times \vec{h} r_f}{\parallel \vec{r}_f \times \vec{V}_f \parallel} \cos i^*] + \upsilon_4 \vec{r}_f \tag{3.36}$$

$$P_m(t_f) = 1 \tag{3.37}$$

The unknown constant vector υ can be eliminated using the terminal constraints and transversality conditions. Defining $\vec{h}_f = \vec{r}_f \times \vec{V}_f$, the following conditions we get

$$(\vec{V}_f^T \vec{V}_f)(\vec{r}_f^T \vec{P}_{V_f}) - (\vec{r}_f^T \vec{r}_f)(\vec{V}_f^T \vec{P}_{r_f}) - (\vec{V}_f^T \vec{r}_f)[\vec{r}_f^T \vec{P}_{r_f} - \vec{V}_f^T \vec{P}_{V_f}] = 0 \tag{3.38}$$

$$-\vec{h}_f^T \vec{P}_{r_f} [\vec{h}_f^T (\vec{I}_n \times \vec{r}_f)] + \vec{h}_f^T \vec{P}_{V_f} [\vec{h}_f^T (\vec{V}_f \times \vec{I}_n)] = 0 \tag{3.39}$$

$$P_m(t_f) - 1 = 0 \tag{3.40}$$

Above three conditions combined with four terminal constraints forms the seven terminal boundary conditions. Thus the ascent phase optimal control problem with path and terminal constraints is transformed to TPBVP with state , co-state variables, initial conditions and final terminal boundary conditions. Define $x = [r^T, V^T, m^T]^T$ as states, $P = [P_r^T, P_V^T, P_m]^T$ as co-states, $y = [x^T, P^T]^T \in \mathrm{Re}^{14}$ the TPBVP equations can be represented as

$$\begin{aligned} \dot{y} &= f(t, y) \\ B_0(y_0) &= 0 \\ B_f(y_f) &= 0 \end{aligned} \tag{3.41}$$

where $B_0 = 0$ is the initial conditions at $t = t_0$ and $B_f = 0$ are the seven terminal conditions.

3.3.5 Gauss Pseudo-spectral Method

The ascent phase TPBVP is non linear and complicated and cannot be solved using analytical method. Gauss pseudo-spectral method [82], [83], [84], [85] is one of the best method available in literature to solve this problem without compromising for accuracy and efficiency. This method consists of

1. First the unknown state variables $y = [x^T, P^T]^T$ is discretized at required grid points called Legendre-Gauss points,

2. State time history is then approximated by global Lagrange interpolation polynomials structured by discrete states $y(t) = \sum_{i=0}^{N} Y(t)L(t)$,

3. Discretize the differential equations using finite difference method and are solved using efficient numerical method.

3.3.5.1 Time Domain Transformation

The grid points are shifted to Legendre-Gauss points by mapping the physical domain $t \in [t_0, t_f]$ to computational domain $\tau \in [1, -1]$ using the following affine transformation

$$\tau = \frac{2t - (t_f + t_0)}{t_f - t_0} \tag{3.42}$$

After transformation τ becomes independent variable with $\tau = -1$ corresponds to t_0 and $\tau = 1$ corresponds to t_f. The differential equation(3.41) transforms to

$$\begin{aligned} \frac{dy(\tau)}{d\tau} &= \frac{(t_f - t_0)}{2} f(\tau, y(\tau)) \\ B_0(y(-1)) &= 0 \\ B_f(y(1)) &= 0 \end{aligned} \tag{3.43}$$

3.3.5.2 Approximation of Differential Equation Using Lagrange Interpolation Polynomials

State variables are approximated by interpolating Lagrange basis function with the states of N Legendre-Gauss points.

$$y(\tau) \approx Y(\tau) = \sum_{i=0}^{N} Y(\tau_i) L_i(\tau) \tag{3.44}$$

where the Lagrange polynomial is given by

$$L_i(\tau) = \prod_{\substack{j=0 \\ j \neq i}}^{N} \frac{(\tau - \tau_j)}{(\tau_i - \tau_j)} \quad i = 0, 1, ..., N \tag{3.45}$$

We can approximate the derivative of state variables by derivative of its polynomial approximation. Differentiating (3.44) gives $12N$ algebraic equations

$$\dot{y(\tau)} \approx \dot{Y(\tau)} = \sum_{i=0}^{N} Y(\tau_i) \dot{L_i(\tau)} = \frac{(\tau_f - \tau_0)}{2} f(\tau_k, Y_k)$$

$$E_k = \sum_{i=0}^{N} D_{ki} Y_i - \frac{(\tau_f - \tau_0)}{2} f(\tau_k, Y_k) = 0, \quad k = 1, ..., N \tag{3.46}$$

where D_{ki} is a constant matrix given by

$$D_{ki} = \dot{L_i(\tau_k)} = \sum_{i=0}^{N} \frac{\prod_{\substack{j=0 \\ j \neq i,l}}^{N} (\tau_k - \tau_j)}{\prod_{\substack{j=0 \\ j \neq i,l}}^{N} (\tau_i - \tau_j)} \tag{3.47}$$

The initial boundary condition is B_0 and the final boundary condition B_f can be approximated by Gauss quadrature formula

$$Y_f = Y_0 + \frac{(\tau_f - \tau_0)}{2} \sum_{k=1}^{N} w_k f(\tau_k, Y_k) \tag{3.48}$$

Using Equation (3.46), $f(\tau_k, Y_k)$ is substituted by $D_{ki} Y_{ki}$ to get

$$Y_f = Y_0 + \sum_{k=1}^{N} \sum_{i=0}^{N} w_k D_{ki} Y_i \tag{3.49}$$

Using Y_f the terminal boundary conditions $B_f = 0$ can be computed. Define $E_0 = [B_0, B_f]$ and using Equation (3.46), the TPBVP is transformed to algebraic equations

$$E(Y_i) = 0, \quad i = 0, 1..., N \tag{3.50}$$

with roots $(Y_0^T, Y_1^T, ...Y_N^T)^T \in \mathrm{Re}^{12(N+1)}$.

3.3.5.3 Numerical Method

The transformed TPBVP equations are solved using Modified Newton method which converges fast and has got quadratic order of convergence. However convergence to the solution cannot be guaranteed from arbitrary initial point and has to be sufficiently close to the solution. Initial guess for altitude and velocity co-state vectors are made from the vacuum solution of the rocket equation using constant thrust as mentioned in Appendix C. From the transversality condition $P_m(t_f) = -1$ initial value of P_m is computed by back propagation of $\dot{P_m}$ equation with time. Starting from the initial guess X_0 the search direction d_j in the j^{th} can be given by

$$d_j = -\left(\frac{\partial E(Y)}{\partial Y}\bigg|_{Y=Y_{j-1}}\right)^{-1} E(Y_{j-1}), \quad j = 1, 2.... \tag{3.51}$$

where j denotes the jth iteration and the update on Y_j is given by

$$Y_j = Y_{j-1} + \sigma_j d_j, \quad 0 < \sigma_j \leq 1 \tag{3.52}$$

the step size parameter σ_j begins with 1 and is halved till the following condition is met.

$$\sigma_j = \max_{0 \leq i} \left\{ \frac{1}{2^i} \bigg| E^T(Y_{j-1}) + \frac{\Delta Y_j}{2^i}) E^T(Y_{j-1}) + \frac{\Delta Y_j}{2^i}) < E^T(Y_{j-1}) E(Yj-1) \right\} \tag{3.53}$$

Here $\|E(Y_j)\|$ is monotonically converging and is achieved when $\|E(Y_j)\|$ is less than specified tolerance band. The Jacobian matrix $(\frac{\partial E}{\partial Y})$ is computed using finite difference approach. In finite difference approach functions can be evaluated by algebraic equation otherwise the analytical computation of Jacobian matrix is complex as it involves second order partial derivatives. For the boundary condition Jacobian can be determined analytically. For the initial boundary condition $E_0(Y_0) = B_0(Y_0) = 0$, the Jacobian matrices

are

$$\frac{\partial E}{\partial X_0} = \text{is } 7 \times 7 \text{ identity matrix} \tag{3.54}$$

$$\frac{\partial E}{\partial P_0} = = \text{is } 7 \times 7 \text{ zero matrix} \tag{3.55}$$

and the final boundary condition is $E_0(Y_f) = B_0(Y_f) = 0$, the Jacobian matrices are

$$\frac{\partial E}{\partial X_f} = \begin{bmatrix} \vec{r}_f & 0 & 0 \\ 0 & \vec{V}_f & 0 \\ \vec{V}_f \times \vec{I}_n - \frac{\vec{V}_f \times \vec{h}_f}{\vec{h}_f} \cos(i) & -\vec{r}_f \times \vec{I}_n + \frac{\vec{r}_f \times \vec{h}_f}{\vec{h}_f} \cos(i) & 0 \\ \vec{V}_f & \vec{r}_f & 0 \\ \vec{V}_f^2 \vec{P}_{vf} + \vec{V}_f(\vec{r}_f^T \vec{P}_{rf}) + & \vec{r}_f^2 \vec{P}_{rf} + \vec{r}_f(\vec{r}_f^T \vec{P}_{rf}) - & \\ \vec{P}_{rf}(\vec{V}_f^T \vec{r}_f) - \vec{V}_f(\vec{V}_f^T \vec{P}_{vf}) & \vec{r}_f(\vec{V}_f^T \vec{P}_{vf}) - \vec{P}_{vf}(\vec{V}_f^T \vec{r}_f) & 0 \\ \vec{C}_1 & \vec{C}_2 & 0 \\ 0 & 0 & 0 \end{bmatrix} \tag{3.56}$$

$$\frac{\partial E}{\partial P_f} = \begin{bmatrix} 0 & 0 & 0 \\ 0 & 0 & 0 \\ 0 & 0 & 0 \\ 0 & 0 & 0 \\ -\vec{r}_f^2 \vec{V}_f + \vec{r}_f(\vec{V}_f^T \vec{r}_f) & \vec{V}_f^2 \vec{r}_f - \vec{V}_f(\vec{V}_f^T \vec{r}_f) & 0 \\ (\vec{h}_f(\vec{r}_f \times \vec{I}_n))\vec{h}_f & (\vec{h}_f^T(\vec{V}_f \times \vec{I}_n))\vec{h}_f & 0 \\ 0 & 0 & 1 \end{bmatrix} \tag{3.57}$$

where $\vec{C}_1$ and $\vec{C}_2$ is given as

$$\begin{aligned} \vec{C}_1 = {} & (\vec{h}_f^T \vec{P}_{r_f})(\vec{I}_n \times \vec{h}_f + \vec{V}_f \times (\vec{r}_f \times \vec{I}_n)) + (\vec{h}_f^T(\vec{r}_f \times \vec{I}_n))(\vec{V}_f \times \vec{P}_{rf}) \\ & + (\vec{h}_f^T \vec{P}_{vf})(\vec{V}_f \times (\vec{V}_f \times \vec{I}_n)) + (\vec{h}_f^T(\vec{V}_f \times \vec{I}_n))(\vec{V}_f \times \vec{P}_{vf}) \end{aligned} \tag{3.58}$$

$$\begin{aligned} \vec{C}_2 = {} & (\vec{h}_f^T \vec{P}_{v_f})(\vec{I}_n \times \vec{h}_f + (\vec{V}_f \times \vec{I}_n) \times \vec{r}_f) + (\vec{h}_f^T(\vec{V}_f \times \vec{I}_n))(\vec{P}_{vf} \times \vec{r}_f) \\ & + (\vec{h}_f^T \vec{P}_{rf})((\vec{r}_f \times \vec{I}_n) \times \vec{r}_f) + (\vec{h}_f^T(\vec{r}_f \times \vec{I}_n))(\vec{P}_{vf} \times \vec{r}_f) \end{aligned} \tag{3.59}$$

The TPBVP is solved as a fixed final time problem but the actual ascent guidance is free final time problem. To tackle this here initially trajectory is solved for a fixed final time t_{f_1} and Hamiltonian $H(t_{f_1})$ is computed at this time. Then the time is perturbed by a value δ and trajectory is solved for the fixed time $t_{f_2} = t_{f_1} + \delta$ and the new Hamiltonian $H(t_{f_2})$ is computed. Now the final time t_f which satisfies the tranversality conditions is computed using the secant method.

$$t_{f_{k+1}} = t_{f_k} + \frac{t_{f_k} - t_{f_{k-1}}}{H(t_{f_k}) - H(t_{f_{k-1}})} H(t_{f_k}) \quad k = 1, 2, ...n \tag{3.60}$$

where n is such that $|H(t_{f_n})| < \epsilon$ The number of nodes are selected in such way to get sufficient level of accuracy with minor number of nodes.

3.4 Results and Discussions

Guidance equations are solved to compute the commanded angle of attack to steer the vehicle in the optimal path to minimize the fuel. Guidance commands are computed in every 100ms and the controller is solved in every 20ms. The specified terminal conditions at the engine cut off of air-breathing phase are summarized in Table 3.1. The path constraint of $Q\alpha$ is considered and the initial conditions corresponding to initial vertical ascent are given in Table 2.1.

Table 3.1: The terminal conditions of the air-breathing phase

Parameters	Terminal condition	Unit
Altitude	40000	m
Velocity	3085	m/s
Flight path angle	6.2	deg
Mach	9.0	-

Comparison of the closed loop results with that of open loop results are shown Figure 3.3 and Figure 3.4. Simulation results shows that time required to achieve the target conditions in closed loop run is 64s. Twenty five nodes are used in Gauss pseudo-spectral method. Optimal alpha profile demanded by the closed loop guidance generates more thrust so that the terminal pill box conditions are achieved at the computed time to go t_f. The maximum rate of commanded angle of attack less than 1.75deg/s against the design limit of 2deg/s. The initial angle of attack demanded is high upto 20s, correspondingly thrust is

maximum as I_{sp} is a function of angle of attack. The initial dip in altitude is not seen as the thrust is sufficient to overcome the gravity effect. The dynamic pressure builds to maximum during this zone, not touching maximum limit of Q_{max}. As the altitude increases, density decreases and the optimal angle of attack reduces. Hence thrust is gradually reduced, as result the dynamic pressure also decreases. Afterwards optimal angle of attack gradually increased and maintained around 9deg to achieve the terminal pill box conditions.

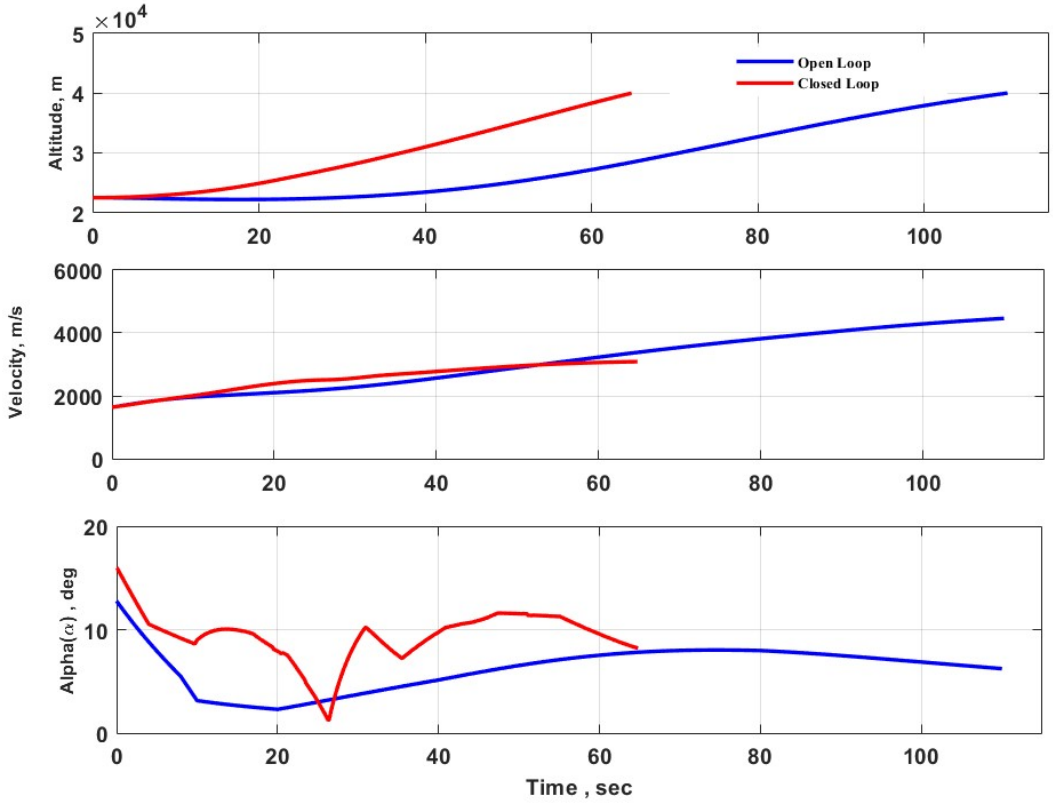

Figure 3.3: Closed loop simulation results with ideal control: Altitude, Velocity and Angle of attack

3.5 Summary

In this chapter, ascent guidance algorithm is developed for air-breathing phase of hypersonic launch vehicle using mass as one of the varying states along with altitude and velocity. This handles the thrust variation during the air sucking phase along with aerodynamic forces in generating an optimal trajectory with angle of attack as the control variable. The complex TPBVP is solved using Gauss pseudo-spectral approach by which the differential

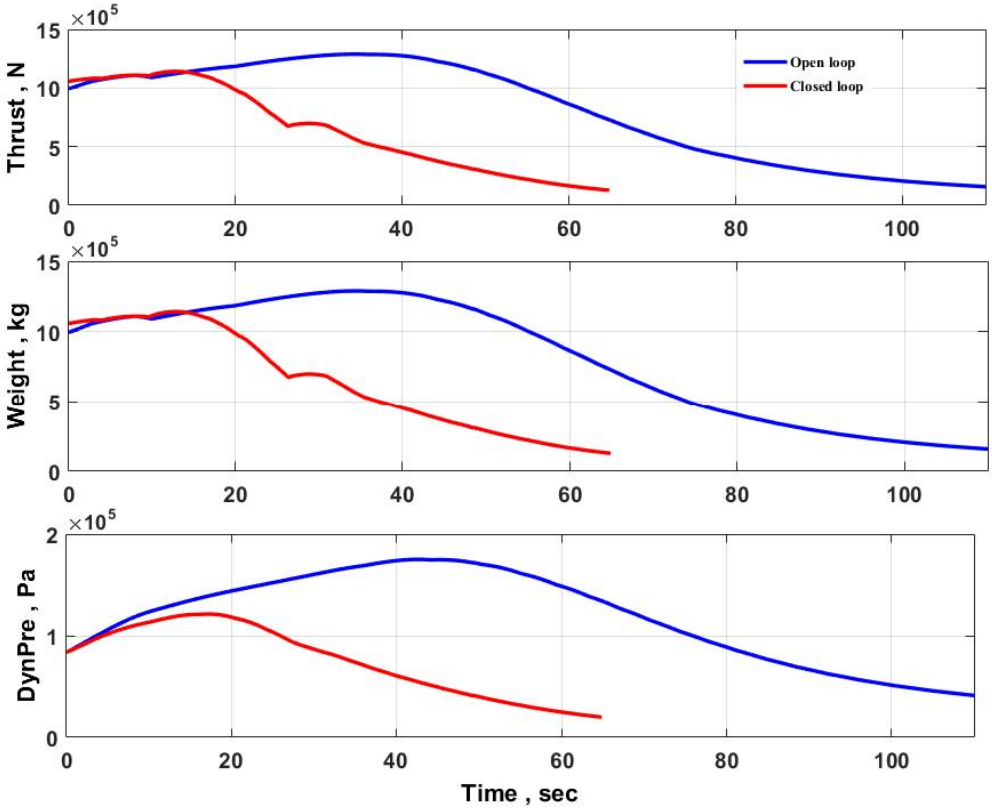

Figure 3.4: Closed loop simulation results with ideal controller :Thrust,Weight and Dynamic Pressure

equations are discretized at the required nodal points without compromising for accuracy and efficiency. The transformed TPBVP is solved using Modified Newton method which has got second order convergence rate. In this approach 6D trajectory is used for guidance design, thus the effect of aerodynamic forces due to trim control deflection is considered for optimal control command computation.

Chapter 4

Integrated Controller Design

4.1 Introduction

The control design for ABSLV is highly challenging due to highly coupled dynamics between different subsystems. Temperature induced stiffness vibration impact on structural dynamics which in turn affects aerodynamic properties. The vibration of the fuselage causes difference in the pressure distribution over the foreward body which in turn manifest as thrust, lift, drag and pitching moment perturbations. Compensating for these structural, aerodynamics and propulsion effects high fidelity modeling and accurate control laws are warranted. Controller for the highly interacting dynamics of ABSLV should handle the coupling aspects of various dynamics and should provide stability and robustness for parameter uncertainties.

4.2 Control Design Model

For the controller design, a simplified control design model model has been developed by substituting the aerodynamic forces, moments and thrust with curve fitted equations []. Scramjet engine model produces the thrust which depends on the vehicle states h, V, α and the control input-equivalence ratio Φ. The thrust in the control design model is approximated as,

$$T \approx QS(C_{T,\Phi}(\alpha)\Phi + C_{T,A_d}(\alpha)A_d + C_{T,0}(\alpha) + C_{T,\eta}(\alpha)\eta) \tag{4.1}$$

where η is the flexibility states and is neglected. Since the diffuser area ratio-A_d is not an independent control variable, its value is set at $A_d = 1$. Now the thrust mapping polynomial is approximately cubic in α and each coefficient of the polynomial is linear function of Φ.

Thus thrust is approximated as

$$\begin{aligned} T &\approx QS[C_T^{\alpha^3}\alpha^3 + C_T^{\alpha^2}\alpha^2 + C_T^{\alpha}\alpha + C_T^0] \\ &\approx T_\alpha(\alpha) + T_\Phi\Phi \end{aligned} \tag{4.2}$$

where

$$C_T^{\alpha^3} = \kappa_1\Phi + \kappa_2, \qquad C_T^{\alpha^2} = \kappa_3\Phi + \kappa_4,$$

$$C_T^{\alpha} = \kappa_5\Phi + \kappa_6, \qquad C_T^0 = \kappa_7\Phi + \kappa_8$$

The coefficients κ_i vary with dynamic pressure Q and altitude h, but their variation is vey slow compared to changes in Φ and α and are assumed to be constant for control design. These constants are fine tuned by matching with thrust-time profile used for simulation as shown in Figure 4.1.

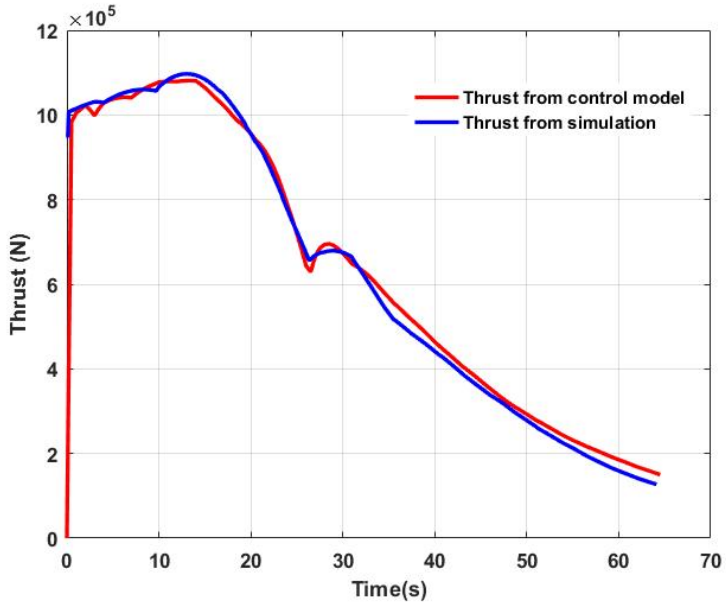

Figure 4.1: Thrust from simulation Vs Thrust from control model

The expression for lift and drag forces and moments are computed similarly.

$$\begin{aligned} L &= QSC_L(\alpha, \delta_e, \delta_{ru}, \delta_c) \\ D &= QSC_D(\alpha, \delta_e, \delta_{ru}, \delta_c) \\ M &= z_T T(\alpha, \Phi) + QSC_M(\alpha, \delta_a, \delta_{ru}, \delta_e, \delta_c) \end{aligned} \tag{4.3}$$

The integration of the scramjet engine and air-frame makes the thrust to directly affect the pitching moment. The pitching moment M contains the term $z_T T$ to account for the pitching moment generated by the under slung scramjet engine. z_T is the thrust to moment coupling constant shown in Figure 1.2 and

$$\begin{aligned} C_M &= C_M^{\alpha^2}\alpha^2 + C_M^{\alpha}\alpha + C_M^{\delta_e}\delta_e + C_M^{\delta_{ru}}\delta_{ru} + C_M^{\delta_c}\delta_c + C_M^0 \\ C_D &= C_D^{\alpha^2}\alpha^2 + C_D^{\alpha}\alpha + C_D^{\delta_e}\delta_e + C_D^{\delta_{ru}}\delta_{ru} + C_D^{\delta_c}\delta_c + C_D^0 \\ C_L &= C_L^{\alpha}\alpha + C_L^{\delta_e}\delta_e + C_L^{\delta_{ru}}\delta_{ru} + C_L^{\delta_c}\delta_c + C_L^0 \end{aligned} \tag{4.4}$$

The above aero-coefficients are functions of Mach, angle of attack and deflection of control surfaces. They are computed from the aerodynamic data base of the winged cone model (as shown in Appendix B) used for the study. Similarly lateral dynamics moment coefficients are also computed.

4.3 Control Philosophy

The integrated controller designed in this work considers both the rotational states (angle of attack, side slip angle, pitch/roll angles and body rates in pitch/yaw/roll) and translational states (velocity as horizontal translational state and flight path angle as vertical translational state). The controller is a combination of a) an attitude controller with longitudinal and lateral states which controls the aerodynamic angles and rates through aerodynamic control surfaces b) a velocity controller for tracking the optimal velocity profile by modulating the thrust of the vehicle through fuel equivalence ratio and c) an altitude-flight path angle controller for tracking the flight path angle command required for the altitude dynamics through canard. Thus the Integrated Controller consists of

1. **Attitude controller**: The attitude dynamics of launch vehicles consists of longitudinal and lateral dynamics [86]. The yaw and roll is highly coupled in the vehicle through aero dynamic coefficients both for the basic vehicle and aerodynamic control surface [87]. Kinematic coupling exists between longitudinal and lateral dynamics. The trajectory of the vehicle demands high dynamic pressure and angle of attack during the ascent phase which causes significant coupling between lateral and longitudinal dynamics [88] [8]. The attitude dynamics are

$$\dot{q} = \frac{M_y}{I_{yy}} \tag{4.5}$$

$$\dot{\theta} = q\cos\phi - r\sin\phi \tag{4.6}$$

$$\dot{\alpha} = -\frac{L + T\sin\alpha}{mV} + q + \frac{g}{V}\cos\gamma \tag{4.7}$$

$$\dot{r} = \frac{M_x}{I_{zz}} \tag{4.8}$$

$$\dot{\beta} = \frac{Y\sin\beta}{mV} + p\sin\alpha + r\cos\alpha + \frac{g}{V}\sin\phi\cos\theta \tag{4.9}$$

$$\dot{p} = \frac{M_z}{I_{xx}} \tag{4.10}$$

$$\dot{\phi} = p + q\tan\theta\sin\phi + r\tan\theta\cos\phi \tag{4.11}$$

The above vehicle states are grouped into longitudinal states with angle of attack, pitch angle, pitch rate, lateral states with side slip angle, yaw rate, roll angle, roll rate, vertical translational states with velocity and horizontal translational states with altitude, flight path angle. These states are simultaneously controlled so that all coupling issues can be properly addressed.

2. **Velocity Controller** : In the horizontal translational dynamics, the reference velocity is achieved by controlling the vehicle's thrust through equivalence ratio Φ. The velocity of the vehicle is given by

$$\dot{V} = \frac{(T_\alpha(\alpha) + T_\Phi\Phi)\cos\alpha - D}{m} - g\sin\gamma \tag{4.12}$$

Velocity is commanded to follow the optimal trajectory adjusting Φ.

3. **Altitude-flight Path Angle Controller**: In the vertical translational motion, the reference altitude profile is achieved by controlling the flight path angle through canard. For the altitude to perfectly track the reference trajectory, a flight path angle reference

command is generated from altitude-flight path angle dynamics.

$$\dot{h} = V \sin\gamma \tag{4.13}$$

$$\dot{\gamma} = \frac{L + T\sin\alpha}{mV} - \frac{g}{V}\cos\gamma \tag{4.14}$$

The tracking error in altitude dynamics is given by

$$\dot{\tilde{h}} = V\sin\gamma - \dot{h}_c \approx V\gamma - \dot{h}_c \tag{4.15}$$

where h_c is the commanded altitude. Using small angle approximation $\sin\gamma \approx \gamma$, which is valid for the entire trajectory, the flight path angle command is generated as

$$\gamma_c = -k_\gamma \tilde{h} + \dot{h}_c/V \tag{4.16}$$

where $k_\gamma > 0$ is the gain parameter

The entire control design model [89] is described by the following equations

$$\begin{aligned}
\dot{p} &= l_p p + l_q q + l_r r + l_\beta \beta + l_{\delta_a}\delta_a + l_{\delta_r}\delta_r \\
\dot{q} &= m_q q + m_\alpha \alpha + \frac{z_T T_\alpha(\alpha)}{I_{yy}}\alpha + m_{\delta_e}\delta_e + \frac{z_T T_\Phi(\alpha)}{I_{yy}}\Phi \\
\dot{r} &= n_p p + n_q q + n_r r + n_\beta \beta + n_{\delta_a}\delta_a + n_{\delta_r}\delta_r + n_{\delta_e}\delta_e \\
\dot{\alpha} &= q - z_\alpha \alpha - \frac{T_\alpha(\alpha)}{mV}\alpha - z_{\delta_e}\delta_e - \frac{T_\Phi(\alpha)}{mV}\Phi \\
\dot{\beta} &= y_\beta \beta + p\sin\alpha_0 - r\cos\alpha_0 + y_{\delta_r}\delta_r \\
\dot{\phi} &= p + r\tan\theta_0 \\
\dot{\theta} &= q \\
\dot{\gamma} &= z_\alpha \alpha + \frac{T_\alpha(\alpha)}{mV}\alpha + z_{\delta_c}\delta_c + \frac{T_\Phi(\alpha)}{mV}\Phi \\
\dot{V} &= \frac{T_\alpha(\alpha)}{m} - x_\alpha \alpha - g\gamma + x_{\delta_e}\delta_e + \frac{T_\Phi(\alpha)}{m}\Phi \\
\dot{h} &= V\sin\gamma
\end{aligned} \tag{4.17}$$

where l_i, m_i and n_i are the moment coefficients in pitch, yaw and roll ie $l_i = \frac{\partial l/\partial i}{I_{xx}}$, i can take the values $p, q, r, \alpha, \beta, \delta_a, \delta_e, \delta_r, \delta_c$ and $l = M_z$ is the total moment in roll. Similarly, x_i, y_i and z_i are the force coefficients in x, y and z axis ie $y_i = \frac{\partial Y/\partial i}{mV}$, i can take the values

$\alpha, \beta, \delta_e, \delta_r, \delta_c$ and Y is the total force in y-axis. The δ_a, δ_r, δ_e, and δ_c are the control inputs to ailerons, rudder, elevons and canard respectively. Here $l_{\delta_a} = (l_{\delta_{eL}} - l_{\delta_{eR}})/2$ is the rolling moment coefficient of aileron and $n_{\delta_a} = (n_{\delta_{eL}} - n_{\delta_{eR})/2}$ is the yawing moment coefficient of aileron by the differential deflection of right and left elevons. Similarly $m_{\delta_e} = (m_{\delta_{eL}} + m_{\delta_{eR}})/2$ is the pitching moment increment coefficient of elevon and V is the velocity of free stream. The five control inputs $u(t) = [\delta_a \ \delta_r \ \delta_e \ \delta_c \ \Phi]$ - deflection angle of aileron, rudder, elevon, canard, and fuel equivalence ratio respectively - affect the states through aerodynamic and propulsive forces. The design approach uses state feedback to achieve decoupling augmented with classical controller in each channel to meet desired tracking performance and stability margins.

4.3.1 Control Objective

The control philosophy is to simultaneously control the longitudinal, lateral and translational states to follow the reference trajectory without defining any authority to a particular state. The attitude controller has to track the angle of attack through elevons by controlling the pitching moment and to regulate the side slip angle and roll angle to zero by differential deflection of elevons. The velocity controller force the vehicle velocity to the reference velocity profile through the fuel equivalence ratio by modulating the thrust. Altitude dynamics is controlled through flight path angle by suitably generating the γ_c from the reference altitude profile. The role of the canard is to decouple lifting force from pitching moment thus making the system minimum phase w.r.t γ, enforce equilibrium through trim profile and also provides a partial stabilizing action. Control limitations are not included explicitly in the design but are honored in the control law implementation by limiting the control effort. The control limitations considered in this study are

- aerodynamic control surface defections - $\delta_e, \delta_{ru}, \delta_c \in [60deg \quad -60deg]$
- fuel equivalence ratio - $\Phi \in [0.5 \quad 4]$.

To achieve the above objectives a hybrid controller is designed which blends the state feedback and classical controller philosophy to handle the coupling between longitudinal and lateral dynamics as well as translational and rotational dynamics of air breathing vehicle.

4.4 Control Law development - Hybrid Control Law

Strong coupling exists between lateral and longitudinal dynamics through aerodynamic control surfaces and between longitudinal and translational states through propulsion and aerodynamics. All the control surfaces work together to handle the aero-propulsive couplings and parameter uncertainties. In this study an integrated multi input multi output control law is developed using input/output decoupling with state feedback augmented with classical controller. Thus the hybrid controller, which is a combination of decoupling and classical controllers addresses the above coupling issues and provides the required stability margins. Decoupling controller consists of forward and feedback gains to decouple the states. Then classical controller developed in each channel (angle of attack, velocity, flight path angle, side slip angle and roll angle), is the Proportional Integral Derivative(PID) controller with compensator to improve tracking performance and stability margins. The hybrid controller structure is shown in Figure. 4.2.

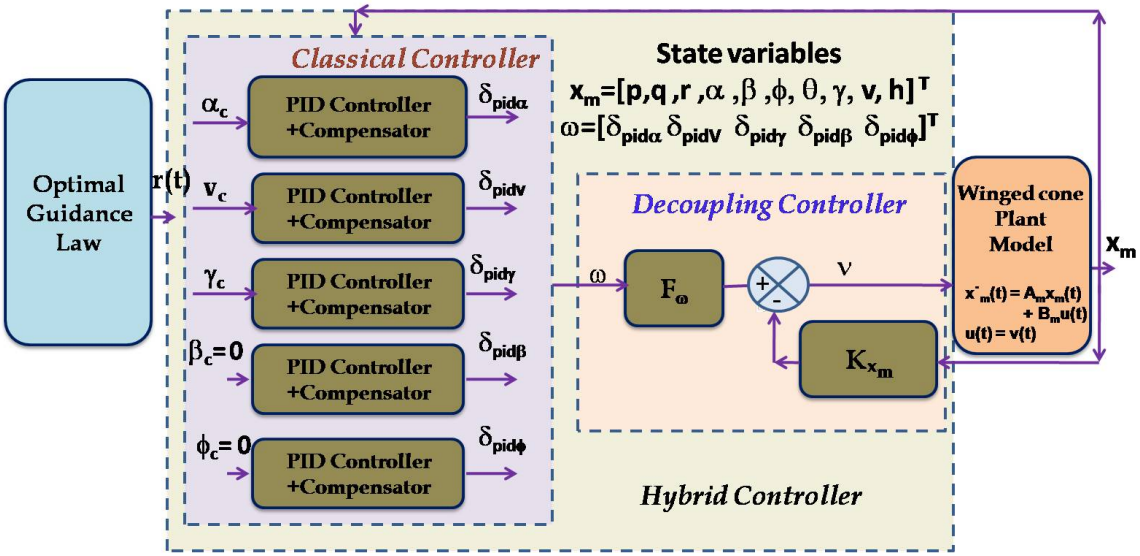

Figure 4.2: Integrated controller architecture

4.4.1 Decoupling Controller Design

Decoupling [90] is primarily used to control the desired output variables using separate command inputs [91] [92]. The class of non linear time variant plant is defined by

$$\dot{x} = A(t)x(t) + B(t)\nu(t)$$

$$y = C(t)x(t) \tag{4.18}$$

where $x(t) \in R^n$ is the state vector, $\nu(t) \in R^m$ is the control vector and $y(t) \in R^p$ is the output vector. $A \in R^{nXn}$, $B \in R^{nXm}$, $C \in R^{pXn}$ are assumed to be continuous with time and have partial derivatives everywhere in x. Complete input-output decoupling is achieved through a state feed back control law

$$\nu(t) = K(t)x(t) + F(t)\omega(t) \tag{4.19}$$

where $K(t) \in R^{mXn}$ and $F(t) \in R^{mXm}$ and $\omega(t)$ is the new control vector. The closed loop system $C_{L(x)}(A, B, C, K, F)$

$$\dot{x} = (A + BK)x(t) + BG\omega(t)$$

$$y(t) = Cx(t) \tag{4.20}$$

is said to be decoupled if

1. there exists i^{th} output vector to be controlled by i^{th} input vector $i \in (1..m)$

2. any j^{th} output is not influenced by any i^{th} input for $i, j \in (1..m) j \neq i$

Define

$$AC_i(x) = \frac{\partial C_i(x)}{\partial x} A(x) \tag{4.21}$$

$$BA^j C_i(x) = (\frac{\partial A^j C_i(x)}{\partial x}) B(x) \tag{4.22}$$

To achieve input-output decoupling and linearization, take the successive derivative of $y_i(t)$ until input appear in the resulting derivative.

$$y_i^j = \begin{cases} A^j C_i(x) = AA^{j-1} C_i(x) & j = 0, 1...d_i \\ A^j C_i(x) + BA^{j-1} C_i(x) & j = d_i + 1 \end{cases} \tag{4.23}$$

There exists a non negative integer d_i

$$d_i = \begin{cases} \min k, BA^k C_i(x) \neq 0 & k \in (0, 1...n-1) \\ n-1, BA^k C_i(x) = 0 & i \in (1..n) \end{cases} \tag{4.24}$$

The necessary and sufficient condition for the a state feedback control law to achieve input output decoupling is that there exist

$$D = \begin{bmatrix} BA^{d_i} C_1(x) \\ . \\ . \\ BA^{d_m} C_m(x) \end{bmatrix} \tag{4.25}$$

such that D is non singular for the control to be bounded. Define

$$A^* = \begin{bmatrix} A^{d_i+1} C_1(x), & . & . & A^{d_m+1} C_m(x) \end{bmatrix} \tag{4.26}$$

The decoupling control law is given by

$$\nu = D^{-1}(x)(-A^*(x) + \omega) \tag{4.27}$$

where $K = D^{-1}(x)(-A^*(x)$ is the feed back gain and $F = D^{-1}(x)$ is the feed forward gain used to decouple the system in pitch/yaw/roll channel.

4.4.2 Classical Controller Design

Trim profile for the static equilibrium is generated for the aerodynamic data of the winged cone vehicle model. For the trim deflection of the control surface, aerodynamic moment and force increment coefficients for the control surfaces and aero-coefficients for basic vehicle are generated along trajectory. With these aero-coeffcients and vehicle parameters, controller is solved at 20ms periodicity to compute decoupling gains through state feed back. Then PID controller and compensator are designed in each input-output channel to improve tracking performance and stability. The design specifications taken in each channel for classical controller design are given in Table 4.1.

Second order actuators(6Hz with 0.7damping) and sensors(12Hz with 0.7damping) are considered for the design. Then classical PID controller with compensator designed to get the tracking performance and stability margins. Roll off filters are used to suppress the high

Table 4.1: Design specifications of the controller

Channel	Bandwidth(rad/s)	Damping
Alpha	4	0.7
Beta	3	0.7
Roll	3	0.7
Velocity	1	1
Flight path angle	1	1

frequency components and lag lead filters are used to improve the stability margins. The frequency response and step response plots of the controller in each channel are given in Figure 4.3 and Figure 4.4. For the attitude controller, step command is given to α channel and β and ϕ are commanded to zero. To decouple the system rudder is demanded to 0.2deg.

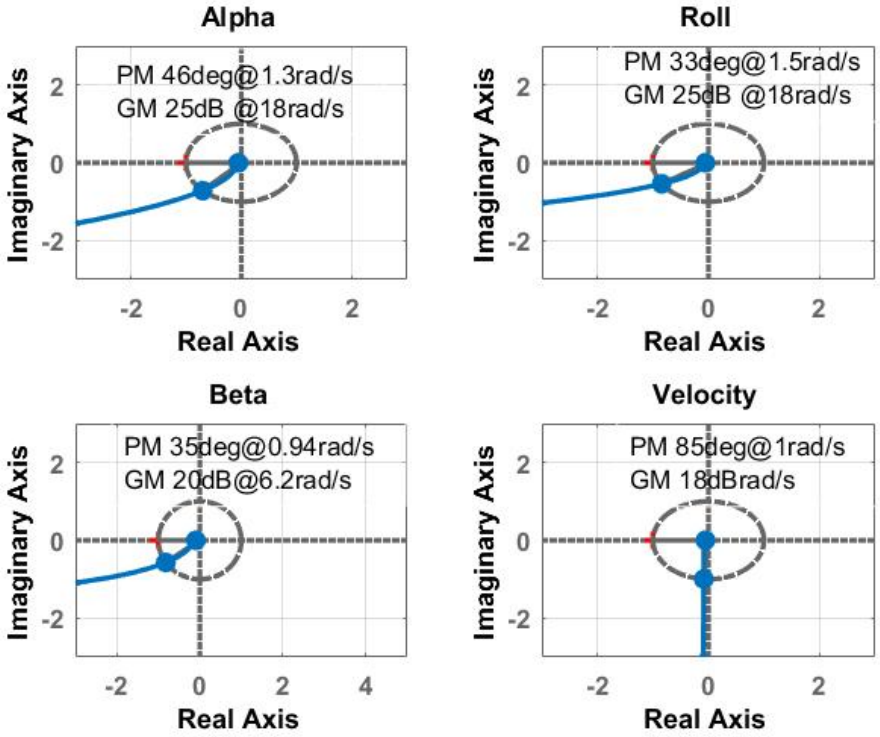

Figure 4.3: Nyquist plot of the controller in Pitch/Yaw/Roll channel at 60s

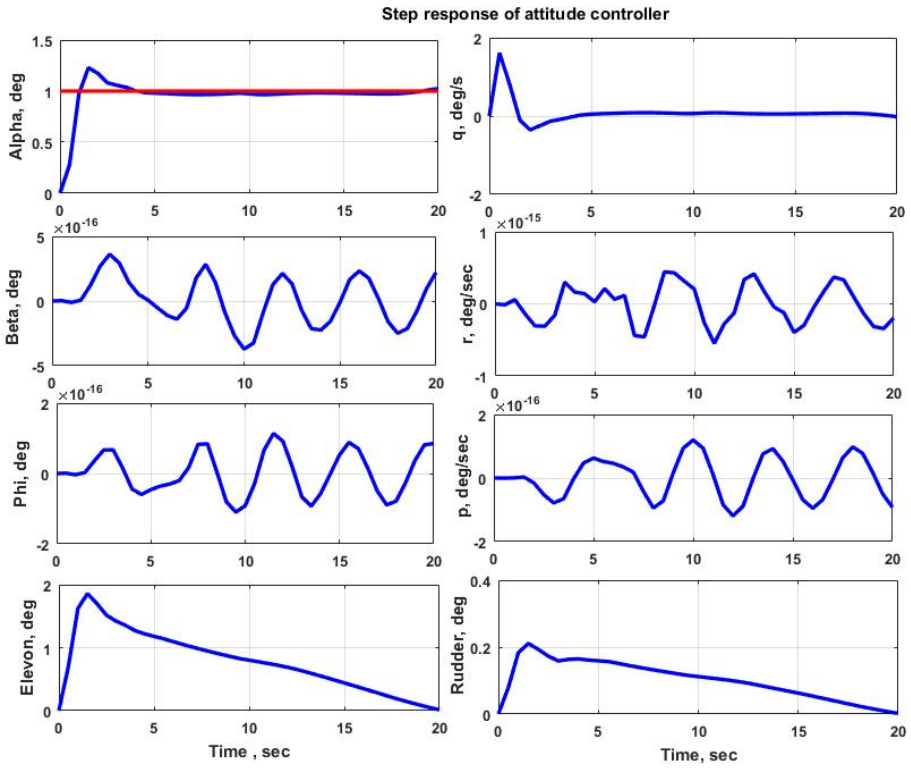

Figure 4.4: Step response of attitude controller in Pitch/Yaw/Roll channel

4.5 Results and Discussions

For the actual control trajectory simulations, the hybrid controller is integrated in 6D simulator and response of the vehicle to the commanded angle of attack, velocity and flight path angle from reference trajectory is assessed. The response of the longitudinal states of the vehicle is shown in Figure 4.6 and that of lateral dynamics is shown in Figure 4.7. The altitude,velocity and angle of attack are tracking perfectly. The yaw and roll rate build up in response to alpha command tracking is negligible as decoupling gains nullifies the effect of coupling terms. Design robustness against parametric perturbations is demonstrated in Figure 4.8. The following cases are simulated

- Case 1 : Aerodynamic disturbance coefficient m_α is perturbed up by 20%
- Case 2 : Control effectiveness of aerodynamic control surfaces are reduced by 20%
- Case 3 : Both aero-disturbance coefficient is perturbed up by 20% and control effectiveness perturbed down by 20%.

In all the three cases the decoupling and classical controllers' parameters are not changed

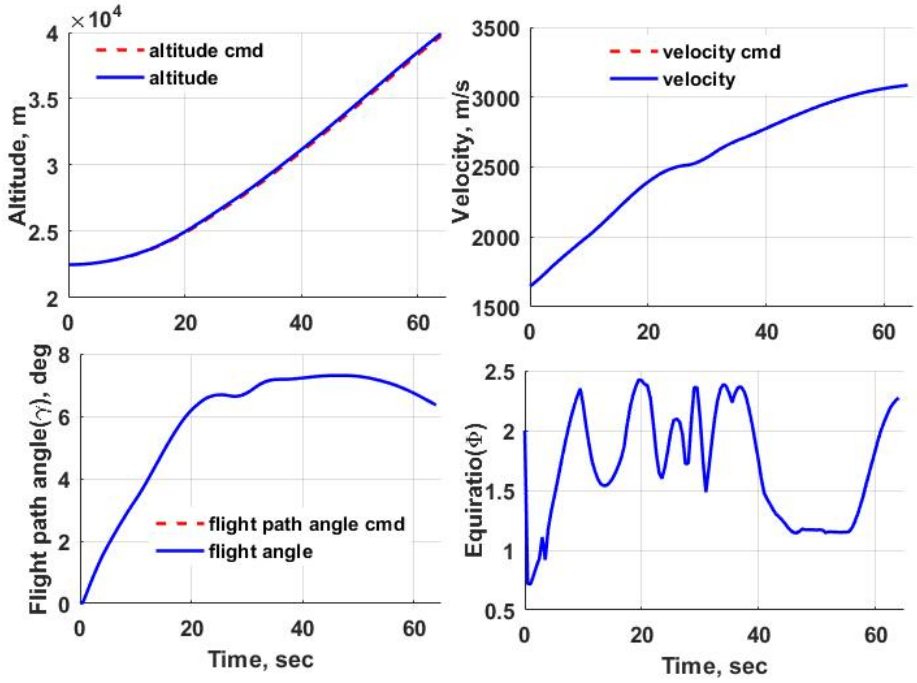

Figure 4.5: Trajectory simulation results with controller:Longitudinal dynamics

and the plant parameters are perturbed to get reduced control effectiveness and aero disturbance. The tracking error in α is building in the three cases (upto 7deg in case 3) around 48s and is controlled to less than 2deg at the terminal state. The end conditions are met with error in altitude less than 400m , in velocity less than 186m/s and in flight path angle of the order of 0.37deg for case 3, maintaining the stability of the vehicle. Limiting parametric perturbation study shows that the vehicle can tolerate a combined perturbation of m_α up by 40% and control effectiveness of aero surface down by 20% ensuring the stability of the vehicle.

4.6 Summary

In this chapter, hybrid controller is developed for air breathing phase of hypersonic launch vehicle using input-output decoupling based on state feedback augmented with classical controller for improved robustness. Control model considers rotational (both longitudinal and lateral dynamics) and translational states simultaneously so that all the couplings between the states are properly addressed in the control law. It has been demonstrated through simulation that integrated control law tracks the reference trajectory with precise tracking performance and the limit of perturbation that the controller can handle.

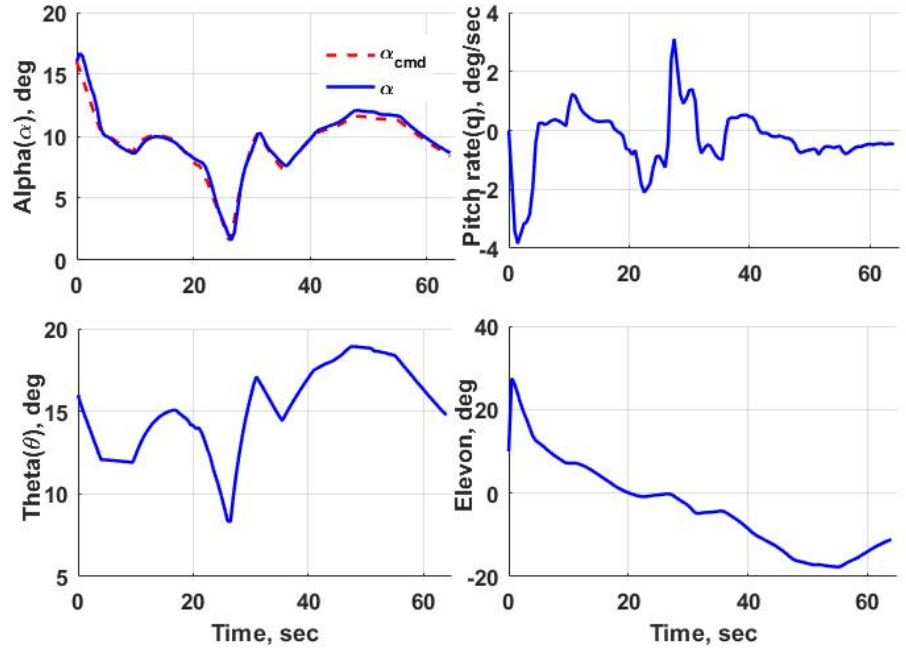

Figure 4.6: Trajectory simulation results with controller:Longitudinal dynamics

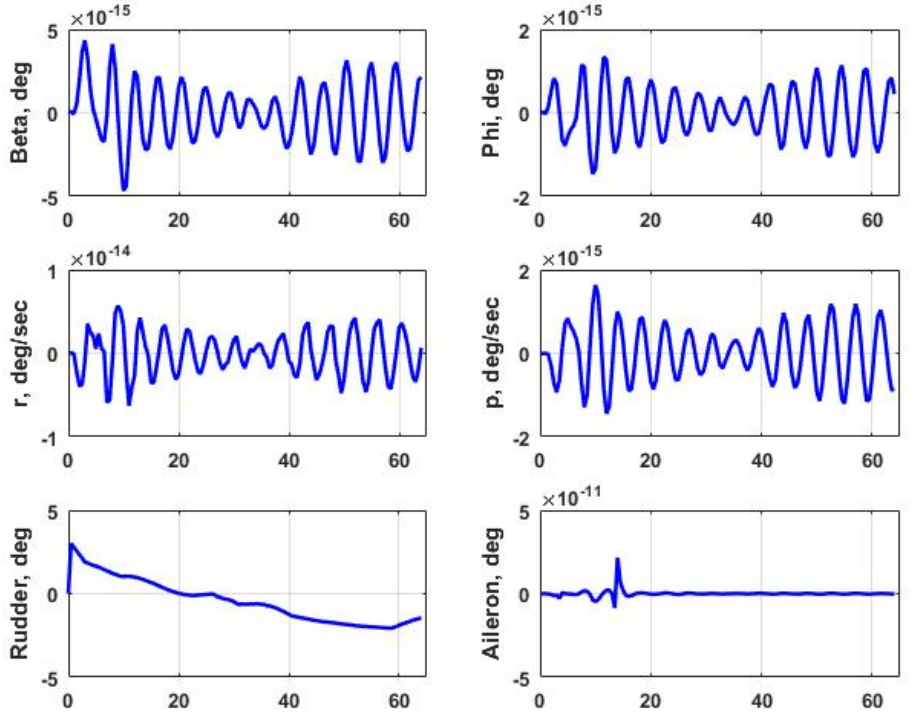

Figure 4.7: Trajectory simulation results with controller:Lateral Dynamics

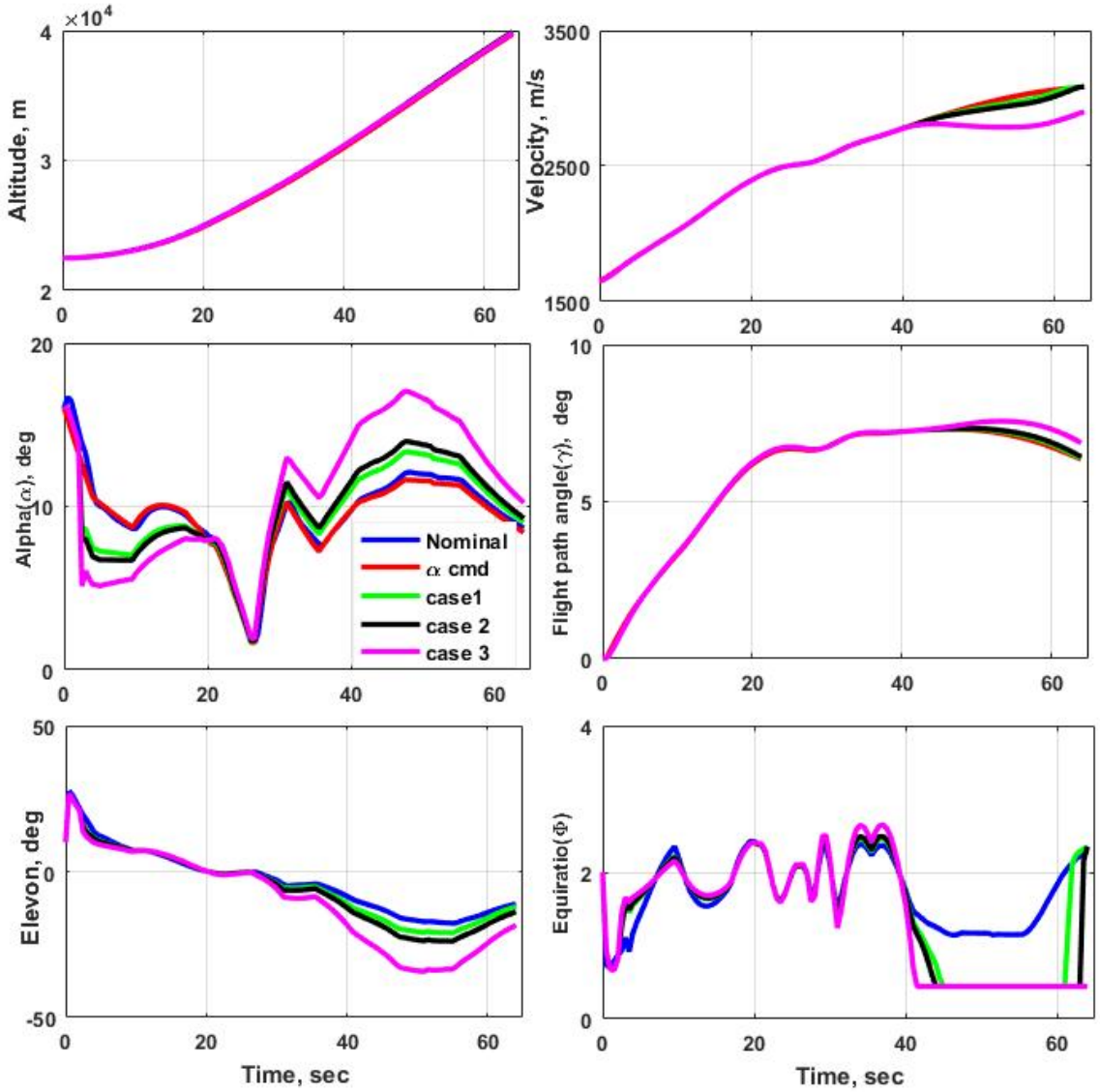

Figure 4.8: Simulation results with parameter perturbations against nominal flight; Case 1 : Aerodynamic disturbance coefficient m_α is perturbed up by 20%; Case 2 : Control effectiveness of aerodynamic control surfaces are reduced by 20% ; Case 3 : Both aero-disturbance coefficient is perturbed up by 20% and control effectiveness perturbed down by 20%

Chapter 5

Adaptive Guidance and Control Law Augmentation to Integrated Controller

5.1 Introduction

Design of the adaptive control and guidance for an air breathing vehicle in ascent phase is different from conventional control problems due to strong coupling between different subsystems and the possible presence of unmodeled dynamics during scram-jet operation. Usually the adaptive control laws [93] are applied to systems having time-invariant or slowly time-varying disturbance and dynamics, but in air breathing vehicle the uncertainties associated with are state and time dependent as the system undergo sudden changes in dynamics. Unmodeled dynamics is also time varying with respect to plant dynamics. To handle highly time varying dynamics and disturbance, adaptive control without derivative based update or modification terms are preferable. In derivative free update laws the designer has the freedom to increase the adaptive gain for fast adaptation without affecting the stability of the overall system. While increasing the adaptive gain the fact to be considered is that increased control effort demands the deflection of control surfaces. This can increase the angle of attack at the air intake zone resulting in the dynamic interaction between aerodynamics and propulsion.

Considering the ascent phase guidance design, due to strong interaction between different subsystems and the slender geometry, a narrow vehicle trajectory corridor only exists in the air breathing phase to meet the high propulsive efficiency, different structural and thermal constraints and stability. Other than the parameter uncertainties and unmodeled dynamics, ascent phase flight is susceptible to large initial state errors. Added to this is the possibility of failure of control power plant or the degraded propulsive performance. Hence along with adaptive control law, an all-coefficient adaptive predictor-corrector guid-

ance algorithm is also proposed to reshape the trajectory to meet the terminal conditions at air breathing phase. Stability analysis of the derivative free adaptive law and predictor-corrector guidance law is also discussed. The new adaptive control and guidance algorithm is validated through various parameter perturbations for aerodynamic parameters, control effectiveness and propulsive parameters and also evaluated the limit of perturbation that the overall system can handle. Finally, the new scheme's robustness is demonstrated via Monte Carlo simulations.

5.2 Adaptive Control Law Augmentation

In the hybrid controller architecture detailed in the previous chapter, the longitudinal rotational state - angle of attack (α), horizontal translational state-velocity and the vertical translational state - flight path angle are tracked to follow the optimal trajectory. The other rotational states-side slip angle (β) and roll angle (ϕ) are regulated to zero. Control law is a hybrid control law where input-output decoupling is achieved using state feedback and then proportional integral derivative (PID) control is used in each channel to improve the robustness.

An adaptive control law based on derivative free update law is augmented to the existing controller to handle wide range of parametric uncertainties by tuning the adaption gain without compromising the stability of the overall system.

The overall system is linearized and considering a second order unmodeled dynamics, the system is represented as

$$\dot{x}_m(t) = A_m x_m(t) + B_m u(t) + H_g x_g(t) \tag{5.1}$$

$$\dot{x}_g(t) = A_g x_g(t) + H_m x_m(t) \tag{5.2}$$

where

$x_m(t) = \begin{bmatrix} p & q & r & \alpha & \beta & \phi & \theta & \gamma & V & h \end{bmatrix}^T$ is the modelled state vector

$u(t) = \begin{bmatrix} \delta_a & \delta_r & \delta_e & \delta_c & \Phi \end{bmatrix}^T$ is the control input vector

$x_g(t) =$ is 2×1 unmodelled state vector

$$A_m(t) = \begin{bmatrix} l_p & 0 & 0 & 0 & l_\beta & 0 & 0 & 0 & 0 & 0 \\ 0 & m_q & 0 & m_\alpha & 0 & 0 & 0 & 0 & 0 & 0 \\ n_p & n_q & n_r & 0 & n_\beta & 0 & 0 & 0 & 0 & 0 \\ 0 & 1 & 0 & -(z_\alpha + \frac{T_\alpha(\alpha)}{mV}) & 0 & 0 & 0 & 0 & 0 & 0 \\ \sin\alpha_0 & 0 & -\cos\alpha_0 & 0 & y_\beta & 0 & 0 & 0 & 0 & 0 \\ 1 & 0 & \tan\theta_0 & 0 & 0 & 0 & 0 & 0 & 0 & 0 \\ 0 & 1 & 0 & 0 & 0 & 0 & 0 & 0 & 0 & 0 \\ 0 & 0 & 0 & z_\alpha + \frac{T_\alpha(\alpha)}{mV} & 0 & 0 & 0 & 0 & 0 & 0 \\ 0 & 0 & 0 & \frac{T_{\alpha\alpha}(\alpha)}{m} - x_\alpha\alpha & 0 & 0 & 0 & -g & 0 & 0 \\ 0 & 0 & 0 & 0 & 0 & 0 & 0 & V_{i-1} & 0 & 0 \end{bmatrix}$$

$$B_m(t) = \begin{bmatrix} l_{\delta a} & l_{\delta r} & 0 & 0 & 0 \\ 0 & 0 & m_{\delta e} & 0 & 0 \\ n_{\delta a} & n_{\delta r} & n_{\delta e} & 0 & 0 \\ 0 & 0 & -z_{\delta e} & 0 & -\frac{T_\Phi(\alpha)}{mV} \\ 0 & y_{\delta r} & 0 & 0 & 0 \\ 0 & 0 & 0 & 0 & 0 \\ 0 & 0 & 0 & 0 & 0 \\ 0 & 0 & 0 & z_{\delta c} & \frac{T_\Phi(\alpha)}{mV} \\ 0 & 0 & x_{\delta e} & 0 & \frac{T_\Phi(\alpha)}{m} \\ 0 & 0 & 0 & 0 & 0 \end{bmatrix}$$

and $H_g^{10\times2}$, $H_m^{2\times10}$ and $A_g^{2\times2}$ are unknown parameters. The following sections describe the design methods adopted to improve the robustness for time varying plant parameters and uncertainties.

5.2.1 Scheduling of Gains

Time slice approach is adopted for the controller design. Linearization approach is extended to a range of operating points, decoupling gains, proportional and rate gains are designed at these points during the air breathing phase. The gains are then scheduled with respect to angle of attack and dynamic pressure to handle the time varying nature of the parameters during the entire air breathing phase. Decoupling gains which are significant only are identified and scheduled. The resulting family of linear controllers are implemented as a single controller whose parameters are changed by monitoring the scheduling variables. Under ideal conditions when no uncertainties or unmodeled dynamics are present

the control input $\nu(t)$ is given by

$$\nu(t) = -K_{x_m}(\alpha, Q)(x_m(t)) + F_\omega(\alpha, Q)(\omega(t)) \tag{5.3}$$

where $K_{x_m}(\alpha, Q)$ is the nominal gain-scheduled feedback gain, $F_\omega(\alpha, Q)$ is the feed forward gain and $\omega(t)$ is the classical controller output. Similarly, the classical proportional and rate path gains are also scheduled to increase the robustness of the design.

The difference in the closed loop model of family of parameterized linear model used in design and actual closed loop non-linear plant about the operating point results in a different zero location in the closed loop transfer function. The closed loop tracking performance are already met as the poles of both closed loop systems are same. The transient part of the step response will be affected by zero location which is thoroughly studied through exhaustive simulations.

5.2.2 Derivative-free Adaptive Controller

In air-breathing phase of hypersonic vehicle unmodeled dynamics and plant uncertainties are subjected to fast variation, as system undergo sudden changes in dynamics. Under such situation usual derivative based adaptive laws (detailed in Appendix D) where constant weight functions are used to parameterize the uncertainties are not advisable, which may lead to poor transient response and instability. In this work, along with gain scheduling a derivative- free adaptive law having time varying weight functions is designed to handle the unmodeled dynamics and parameter uncertainties.

Consider the gain scheduled plant parameter model for command tracking described by a set of equation.

$$\dot{x}_t(t) = A_t(\alpha, Q)x_t(t) + B_t(\alpha, Q)c(t) \tag{5.4}$$

with $A_t > 0$, $x_t(t)$ is the commanded state and $c(t)$ is uniformly bounded continuous command.

$$\begin{aligned} A_t(\alpha, Q) &= A_m(\alpha, Q) - B_m(\alpha, Q)K_{x_m}(\alpha, Q) \\ B_t(\alpha, Q) &= -B_m(\alpha, Q)F_\omega(\alpha, Q) \end{aligned} \tag{5.5}$$

where $A_m(\alpha, Q)$ and $B_m(\alpha, Q)$ are the gain scheduled system matrix and input matrix given by Equation 5.1 at scheduled interval. The control input to the plant is modified continuously to track the reference system in presence of parameter and model uncertainties

as

$$u(t) = \nu(t) + u_{ada}(t) \tag{5.6}$$

where the adaptive part $u_{ada}(t)$ is given by

$$u_{ada} = -\hat{w}_m^T(t)\mu_m(x_m(t)) \tag{5.7}$$

After putting the revised control $u(t)$, the Equation 5.1 becomes

$$\begin{aligned}\dot{x}_m(t) = A_m(\alpha, Q)x_m(t) + B_m(\nu(t) + u_{ada}(t) \\ + {w_m}^T(t)\mu_m(x_m(t))) + H_g x_g(t)\end{aligned} \tag{5.8}$$

Further, consider the command tracking plant reference system as per Equation 5.5

$$\begin{aligned}\dot{x}_m(t) = A_t(\alpha, Q)x_m(t) + B_t(\alpha, Q)c(t) \\ + B_m(u_{ada}(t) + {w_m}^T(t)\mu_m(x_m(t))) + H_g x_g(t)\end{aligned} \tag{5.9}$$

where

$$w_m = [0, {B_m}^{-1}(A_t - A_m), -{B_m}^{-1}B_t]^T \tag{5.10}$$

is the unknown weight function to estimate the parameter uncertainty and $\mu_m(x_m(t))$ is the basis function of the form

$$\mu_m(x_m(t)) \stackrel{\triangle}{=} [\mu_{m_1}(x_{m_1}(t)), \mu_{m_2}(x_{m_2}(t))..\mu_{m_n}(x_{m_n}(t))]^T \tag{5.11}$$

Instead of using the derivative of weight function, here a time delayed weight function is used in the update law. Let $\hat{w}_m^T(t)$ be the estimate of w_m is given by

$$\hat{w}_m^T(t) = \Gamma_1 \hat{w}_m^T(t - \xi) + \Gamma_2 \mu_m(x_m(t))\varepsilon^T(t)PB_m(\alpha, Q) \tag{5.12}$$

where ξ is a time interval to update the weight function which is independent of the control law interval. P is the positive definite solution of Lyapunov equation given by $0 = A_t^T P + PA_t + Q$ for $Q = Q^T > 0$. Γ_1, Γ_2 are the adaption gains such that $0 <| \Gamma_1 |< 1$. It is proved in [55] that derivative free adaptive law has the freedom to tune ξ and increase Γ_2 which improve robustness to unmodelled dynamics without affecting the closed loop

performance of the system. Now the derivative of error function becomes

$$\dot{\varepsilon}(t) = \dot{x_t}(t) - \dot{x_m}(t) \tag{5.13}$$

$$\begin{aligned}\dot{\varepsilon(t)} &= A_t(\alpha, Q)\varepsilon(t) \\ &+ (A_t(\alpha, Q) - A_m(\alpha, Q) - B_m(\alpha, Q)K(\alpha, Q))x_m(t) \\ &+ (B_t(\alpha, Q) - B_m(\alpha, Q)F(\alpha, Q))c(t) + B_m(\alpha, Q)(u_{ada}(t) \\ &+ \tilde{w}_m^T(t)\mu_m(x_m(t))) + H_g x_g(t)\end{aligned} \tag{5.14}$$

where $\tilde{w}_m = w_m - \hat{w}_m$ is the weight estimation error.

5.2.3 Stability Analysis

Using the Lyapunov Krasovskii functional as proposed in [55]

$$\begin{aligned}\mathcal{V}[\varepsilon(t),\tilde{w}_m(t), x_g(t)] &= \frac{1}{2}\varepsilon(t)^2 + \frac{1}{2}{x_g}^2(t) \\ &+ \frac{\chi\|B_m(\alpha, Q)\|}{2}\int_{t-\xi}^{t}\tilde{w}_m(s)\tilde{w}_m^T(s)ds, \quad \chi \triangleq \frac{1}{\Gamma_2\varrho}, \quad \varrho > 1\end{aligned} \tag{5.15}$$

Differentiating the above equation gives

$$\begin{aligned}\dot{\mathcal{V}}[\varepsilon(t),\tilde{w}_m(t), x_g(t)] &= \varepsilon(t)\dot{\varepsilon}(t) + x_g(t)\dot{x}_g(t) \\ &+ \frac{\chi\|B_m(\alpha, Q)\|}{2}[\tilde{w}_m^T(t)\tilde{w}_m(t) - \tilde{w}_m^T(t-\xi)\tilde{w}_m(t-\xi)]\end{aligned} \tag{5.16}$$

Rearranging the above equation gives

$$\begin{aligned}\dot{\mathcal{V}}[\varepsilon(t),\tilde{w}_m(t), x_g(t)] &= \varepsilon(t)\dot{\varepsilon}(t) + x_g(t)\dot{x}_g(t) \\ &+ \frac{\chi\|B_m(\alpha, Q)\|}{2}[-\varsigma\tilde{w}_m^T(t)\tilde{w}_m(t) \\ &+ \varrho\tilde{w}_m^T(t)\tilde{w}_m(t) - \tilde{w}_m^T(t-\xi)\tilde{w}_m(t-\xi)]\end{aligned} \tag{5.17}$$

where $\varrho = 1 + \varsigma, \varsigma > 0$. Now from the update law

$$\hat{w}_m^T(t) = \Gamma_1\hat{w}_m^T(t-\xi) + \Gamma_2\mu_m(x_m(t))\varepsilon(t)^T PB_m(\alpha, Q) \tag{5.18}$$

Let

$$\Omega = (1 - \Gamma_1)w_m \tag{5.19}$$

Now the Equation.5.16 becomes

$$\begin{aligned}\dot{\mathcal{V}}[\varepsilon(t),\tilde{w}_m(t),x_g(t)] \leq & -\begin{bmatrix} \mid \varepsilon(t) \mid \\ \mid x_g(t) \mid \end{bmatrix}^T \\ & \begin{bmatrix} A_t + \frac{1}{2}\Gamma_2 \mid B_m \mid & -\frac{1}{2}(\mid H_m \mid + \mid H_g \mid) \\ -\frac{1}{2}(\mid H_m \mid + \mid H_g \mid) & A_g \end{bmatrix} \begin{bmatrix} \mid \varepsilon(t) \mid \\ \mid x_g(t) \mid \end{bmatrix} \\ & - \frac{\mid B_m \mid \varsigma}{2\Gamma_2 \varrho}\tilde{w}_m^T(t)\tilde{w}_m(t) \\ & - \frac{\mid B_m \mid \varsigma}{2\Gamma_2 \varrho}[1-(\varrho+\upsilon)\Gamma_1^2]\tilde{w}_m^T(t-\xi)\tilde{w}_m(t-\xi) \\ & + \mid H_m \mid\mid x_t(t) \mid\mid x_g(t) \mid + \frac{\mid B_m \mid}{2\Gamma_2}(1+\Gamma_1 c)\Omega^T\Omega \end{aligned} \tag{5.20}$$

where $(\varrho+\upsilon) > 1$, $c = \varrho\Gamma_1^{-1}\upsilon^{-1}$ with $\upsilon > 0$ and there always exists a $(\varrho+\upsilon)$ for every $0 <\mid \Gamma_1 \mid< 1$ such that $(1-(\varrho+\upsilon)\Gamma_1^2 > 0)$. Since $x_t(t)$ is bounded, the fourth term is linear in $x_g(t)$ and the last term is also bounded. Then it follows from Equation 5.20 that

$$\left(A_t + \frac{1}{2\Gamma_2} \mid B_m \mid \right)A_g > \frac{1}{4}(\mid H_m \mid + \mid H_g \mid)^2 \tag{5.21}$$

is the sufficient condition for closed loop stability. Here the condition in the above equation not only depends on A_t but also Γ_2, the adaption gain. Generally A_t detects the bandwidth of the closed loop system and the robustness to plant uncertainties and unmodelled dynamics can be improved by tuning the gain Γ_2. Putting an upper limit on Γ_2 guarantees that the control output is uniformly bounded.

5.3 Predictor-corrector Adaptive Guidance Using an All-coefficient Adaptive Control Approach

Using adaptive control law augmentation, the integrated controller can handle the aero-parameter uncertainties and unmodelled dynamics largely and can achieve the terminal conditions accurately. However, in case of propulsion degradation or control surface saturation, the variation in terminal states may vary largely during the air-breathing phase. To handle these scenarios, an adaptive guidance algorithm using all-coefficient adaptive control theory is discussed here. Ascent guidance is an under-driven problem, which uses only the angle of attack command to achieve the terminal states-velocity, altitude and flight path angle. Flight path angle command is a derived command from altitude dynamics. In the

optimal ascent guidance algorithm control command-angle of attack is generated to optimize the fuel, taking velocity, altitude and mass as the state vectors for the optimization problem [94].

In all coefficient control theory, the complete guidance subsystem is modelled as a combination of different dynamics with specific control performance. The characteristic model should absorb all the dynamics required to meet the performance objective. In this problem, a combination of dynamics for velocity, altitude and flight path angle are used to represent the whole guidance such that the output of these dynamics and that of the complete guidance subsystem is same for the same input. Based on theory of characteristic modeling, the state output variables- velocity, altitude, flight path angle, the control variable-angle of attack and derivatives of these variables are bounded. Hence, the dynamics can be approximated by difference equation. The performance index, the system has to achieve and the easiness of implementation are the criteria for fixing the order of the difference equation for each dynamics. In order to improve the guidance accuracy, a first order difference equation is selected for defining each dynamics with control input.

In the present study the design objective is to achieve the terminal states namely altitude (h_f), velocity (V_f) and flight path angle (γ_f) at the end of the air-breathing phase of the flight. Now consider the velocity dynamics with control variable-angle of attack. The algorithm predicts the actual terminal velocity and velocity error ΔV is computed with desired terminal velocity of the nominal trajectory in each computation cycle. For the velocity error, the control command modification α_{ada_v} is computed using all coefficient theory. The velocity dynamics is represented by a first order difference equation as,

$$V(j+1) = g_v(j)V(j) + c_v(j)\alpha_{ada_v}(j) \tag{5.22}$$

where $V(j)$ is the velocity at j^{th} guidance cycle, α_{ada_v} is the modified part of the control variable-angle of attack at j^{th} time interval and g_v and c_v are the time varying parameters. The sum of the coefficients are unity, stating that all the unknown coefficients can be predicted online and converge to true values. For the first order difference equation since the unknown parameters is only two, parameter identification is faster. Thus, different low order discrete system with specific input and output are used to capture the features of the original higher order system. The time varying parameters $g_v(j)$ and $c_v(j)$ are bounded.

$$g_v(j) \in [g_{min}, g_{max}] \qquad c_v(j) \in [c_{min}, c_{max}] \tag{5.23}$$

A closed convex is defined such that

$$(g_v(j), c_v(j)) \in \Omega \tag{5.24}$$

where

$$\Omega = \begin{cases} (m_1, m_2)^T \in \mathrm{Re}^2 \begin{cases} m_1 \in [1-\overline{m}, 1-\underline{m}] \\ m_2 \in [\underline{n}, \overline{n}] \end{cases} \end{cases} \tag{5.25}$$

where $1 > \overline{m} > \underline{m} > 0, \overline{n} > \underline{n} > 0$. $g_v(j)$ and $c_v(j)$ are estimated on-line, using gradient based projection method. Let $\hat{g_v}(j)$ and $\hat{c_v}(j)$ be the estimated values of the parameters, estimated using the recursive least square algorithm. The estimation vector is

$$\hat{\vartheta}(j) = \begin{bmatrix} \hat{g_v}(j) & \hat{c_v}(j) \end{bmatrix} \tag{5.26}$$

and the regression vector is

$$\varphi(j) = \begin{bmatrix} V(j-1) & \alpha_{ada_v}(j-1) \end{bmatrix} \tag{5.27}$$

Now Equation 5.22 becomes

$$V(j+1) = \vartheta(j)\varphi(j)^T \tag{5.28}$$

Estimation of $\hat{\vartheta}(j)$ is given by

$$\begin{cases} \hat{\vartheta}(j) = \hat{\vartheta}(j-1) + L(j)\begin{bmatrix} V(j) - \hat{V}(j) \end{bmatrix} \\ \hat{\vartheta}(j) = \pi_\Omega \begin{bmatrix} \hat{\vartheta}(j) \end{bmatrix} \end{cases} \tag{5.29}$$

where

$$L(j)^T = \frac{P(j-1)\varphi(j-1)^T}{(\varphi(j-1))P(j-1)\varphi(j-1)^T + \mu}$$

$$P(j) = \frac{1}{\mu}[I - L(j)^T\varphi(j-1)]P(j-1)$$

estimated value of current cycle velocity is

$$\hat{V}(j) = \hat{\vartheta}(j-1)\varphi(j)^T$$

$P(0)$ is a positive definite matrix, $0 < \mu < 1$ and π_Ω is the orthogonal projection on the

convex set Ω. Using tracking control law

$$\alpha_{ada_v}(j) = \frac{V_r(j) - \hat{g_v}(j)V(j)}{\hat{c_v}(j) + \lambda_v} \tag{5.30}$$

where $V_r(j)$ is the expected velocity and $\lambda_v > 0$ denotes a constant design parameter.

Similarly modified control commands $\alpha_{ada_\gamma}(j)$ for the flight path angle dynamics and $\alpha_{ada_h}(j)$ for altitude dynamics are computed. Final adaptive control command is

$$\alpha_{ada}(j) = k_v\alpha_{ada_v}(j) + k_\gamma\alpha_{ada_\gamma}(j) + k_h\alpha_{ada_h}(j) \tag{5.31}$$

where k_v, k_γ and k_h are the gains designed for velocity, flight path angle and altitude respectively. Now the re-targeted angle of attack is given by

$$\alpha(j) = \alpha(j-1) + \alpha_{ada}(j) \tag{5.32}$$

Figure 5.1 illustrates the structural chart of all-coefficient adaptive guidance scheme. The augmented adaptive guidance is a non-iterative algorithm as it is formulated as a standard input-output control problem and modified adaptive control command $\alpha_{ada}(j)$ is computed only once in the guidance cycle.

Stability Analysis

In the adaptive algorithm, guidance subsystems- velocity, altitude and flight path angle are represented by first order difference equation where the characteristic coefficients are subset of the closed convex Ω as given in Equation 5.25 and are bounded. For the first order difference equation, it is easy to establish the the stability analytically and is distinct. Consider the time variant discrete system given by

$$y(j+1) = A(j)y(j) \tag{5.33}$$

where $A(j)$ is the system matrix and the solution is given by state transition matrix $\varphi(j, j_0)$. If the state transition matrix satisfies the constraint $\|\varphi(j, j_0)\| \leq k\Theta^{j-j_0}$ with $j, j_0 \in N$, $j \in (j_0, \infty)$ and $k \in (0, 1)$, then the system $y(j+1) = A(j)y(j)$ is exponentially stable. Now substituting the modified control Equation 5.30 in the characteristic Equation 5.22 we get

$$y(j+1) = g(j)y(j) + c(j)\frac{y_r(j) - \hat{g}(j)y(j)}{\hat{c}(j) + \lambda} \tag{5.34}$$

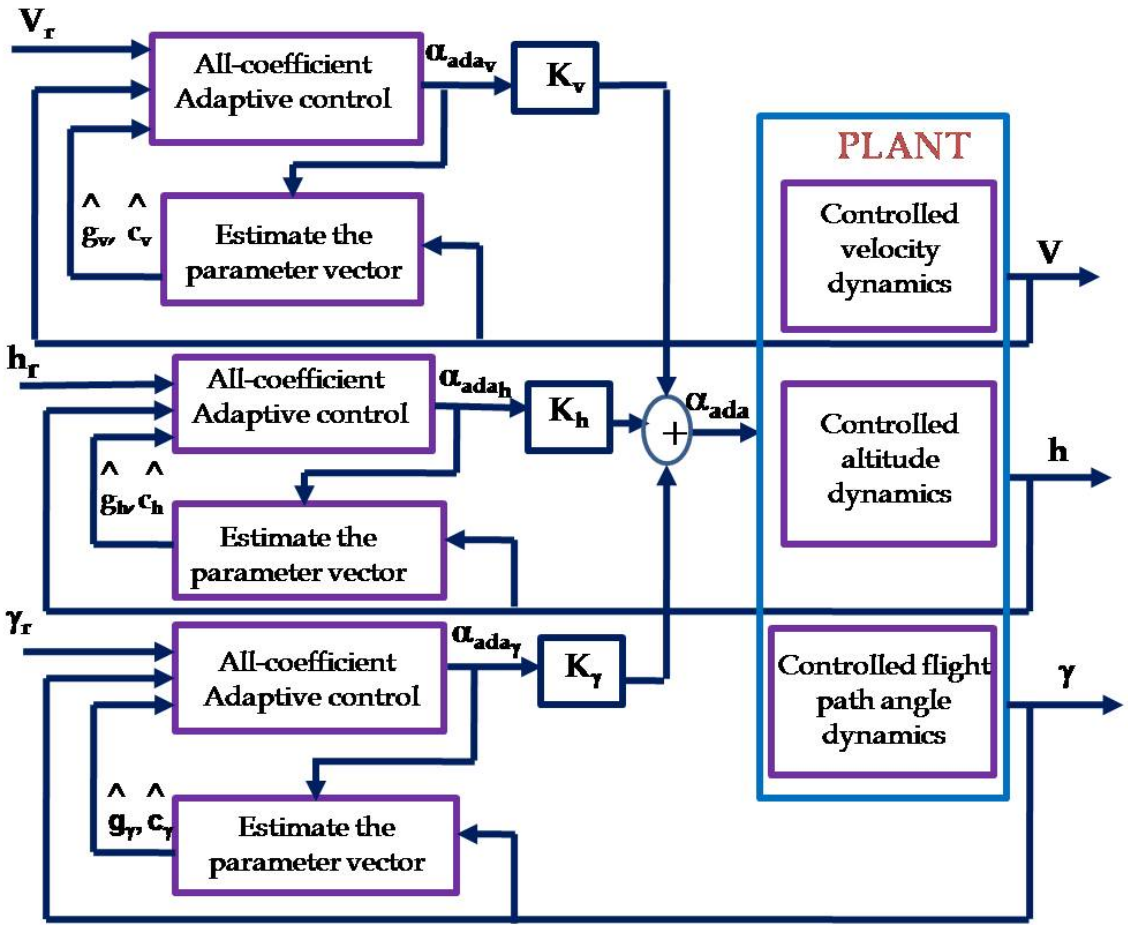

Figure 5.1: Augmented adaptive guidance scheme

$$y(j+1) = (g(j) - \frac{\hat{g}(j)c(j)}{\hat{c}(j)+\lambda})y(j) + c(j)\frac{y_r(j)}{\hat{c}(j)+\lambda} \tag{5.35}$$

Neglecting the reference command term, the above equation becomes

$$y(j+1) = (g(j) - \frac{\hat{g}(j)c(j)}{\hat{c}(j)+\lambda})y(j) \tag{5.36}$$

If

$$R(j) = (g(j) - \frac{\hat{g}(j)c(j)}{\hat{c}(j)+\lambda}) \quad \text{then} \quad y(j+1) = R(j)y(j) \tag{5.37}$$

Define

$$Q(j) = \frac{c(j)}{\hat{c}(j)+\lambda} \quad , \quad \lambda = k_\lambda \underline{q} \tag{5.38}$$

$$Q_{max}(j) = \max(Q(j)) = \frac{\overline{q}}{\underline{q} + k_\lambda \underline{q}} \tag{5.39}$$

$$Q_{min}(j) = \min(Q(j)) = \frac{\underline{q}}{\overline{q} + k_\lambda \underline{q}} \tag{5.40}$$

substituting these in Equation 5.36

$$R_{max}(j) = \max(R(j)) = 1 - \underline{p} - (1 - \overline{p})Q_{min} \tag{5.41}$$

$$R_{min}(j) = \min(R(j)) = 1 - \overline{p} - (1 - \underline{p})Q_{max} \tag{5.42}$$

For the system given by Equation 5.36 to remain stable, system matrix has to satisfy the constraint $\mid R(j) \mid \leq \Theta < 1$ which implies that the following inequalities have to be satisfied

$$1 - \underline{p} - (1 - \overline{p})Q_{min} \leq \Theta \tag{5.43}$$

$$1 - \overline{p} - (1 - \underline{p})Q_{max} \geq -\Theta \tag{5.44}$$

substituting for Q_{max} and Q_{min} from Equation 5.39 and 5.40, the inequalities modifies to

$$\frac{1 - \underline{p} - \Theta}{(1 - \overline{p})} \leq \frac{\underline{q}}{\overline{q} + k_\lambda \underline{q}} \tag{5.45}$$

$$\frac{1 - \overline{p} + \Theta}{(1 - \underline{p})} \geq \frac{\overline{q}}{\underline{q} + k_\lambda \underline{q}} \tag{5.46}$$

Now the inequality in Equation 5.45 gives the condition

$$k_\lambda \leq \frac{(1 - \overline{p})}{1 - \underline{p} - \Theta} - \frac{\overline{q}}{\underline{q}} \quad \text{when} \quad (1 - \underline{p} - \Theta) > 0 \tag{5.47}$$

and if $(1 - \underline{p} - \Theta) \leq 0$ the inequality in Equation **??** is satisfied if $k_\lambda > 0$. Similarly the inequality in Equation 5.46 gives the condition

$$k_\lambda \geq \frac{(1 - \underline{p})}{(1 - \overline{p} + \Theta)} \frac{\overline{q}}{\underline{q}} - 1 \tag{5.48}$$

summarizing, for the system to be stable the design parameter k_λ should satisfy the

$$\begin{cases} \max(0, \frac{(1-\underline{p})}{(1-\overline{p}+\Theta)} \frac{\overline{q}}{\underline{q}} - 1) \leq k_\lambda \leq \frac{(1-\overline{p})}{1-\underline{p}-\Theta} - \frac{\overline{q}}{\underline{q}}, & \text{if} \quad (1 - \underline{p} - \Theta) > 0 \\ \max(0, \frac{(1-\underline{p})}{(1-\overline{p}+\Theta)} \frac{\overline{q}}{\underline{q}} - 1) \leq k_\lambda, & \text{if} \quad (1 - \underline{p} - \Theta) < 0 \end{cases} \tag{5.49}$$

then

$$|y(j+1)| = |\varphi(j, j_0)y(j_0)| \leq k\Theta^{j-j_0}|y(j_0)| \tag{5.50}$$

and $|\varphi(j, j_0)| \leq k\Theta^{j-j_0}$, the closed loop system is exponentially stable.

5.4 Results and Discussions

To validate the augmented adaptive algorithm, time varying closed loop simulations has been carried out for different parameter perturbations. In the last chapter [94] it was already established that the hybrid controller shows robust performance for aero-disturbance coefficient perturbation up by 20%, control effectiveness perturbation down by 20% and for the combined perturbations. With adaptive augmentation, the controller is robust to more than 50% combined aero-perturbations. Table 5.1 gives the initial and final values of state vectors considered for the simulations. Following different cases are studied.

Table 5.1: Initial and final values of state parameters

Sl no	Parameters	Value	Unit
1	Initial Altitude	22500	m
2	Initial Velocity	1650	m/s
3	Initial Flight path angle	0.0	degree
4	Initial mass	127008	kg
5	Final Altitude	40080	m
6	Final Velocity	3080	m/s
7	Final Flight path angle	6.29	degree

5.4.1 Simulations with Adaptive Controller

Case 1: Aero-disturbance Coefficients $(m_\alpha, n_\beta, l_\beta, z_\alpha)$ +40% Variation

In this case, the aero-coefficients in the longitudinal and lateral dynamics are perturbed by +40% so that the effective aero-disturbance increases by more than 40%. Fig. 5.2 shows the comparison between with and without adaptive controller for the longitudinal states (altitude, velocity, α and flight path angle) and control parameters (elevon deflection and fuel equivalence ratio) during the entire air-breathing phase. Without adaptive controller, terminal state pill box conditions are achieved with an error in altitude, velocity, flight path angle (γ) as 94m, 0.54m/s, 0.00048deg respectively using high control effort on elevon (30deg deflection). However, using adaptive controller the pillbox conditions are met more accurately with less control effort (elevon deflection reduces to 20deg). Table 5.2 gives the terminal pillbox condition achieved for this perturbation with and without adaptive

control along with nominal. Without adaptive controller, the velocity control parameter - equivalence ratio (Φ) is reduced to near zero values to meet the terminal states.

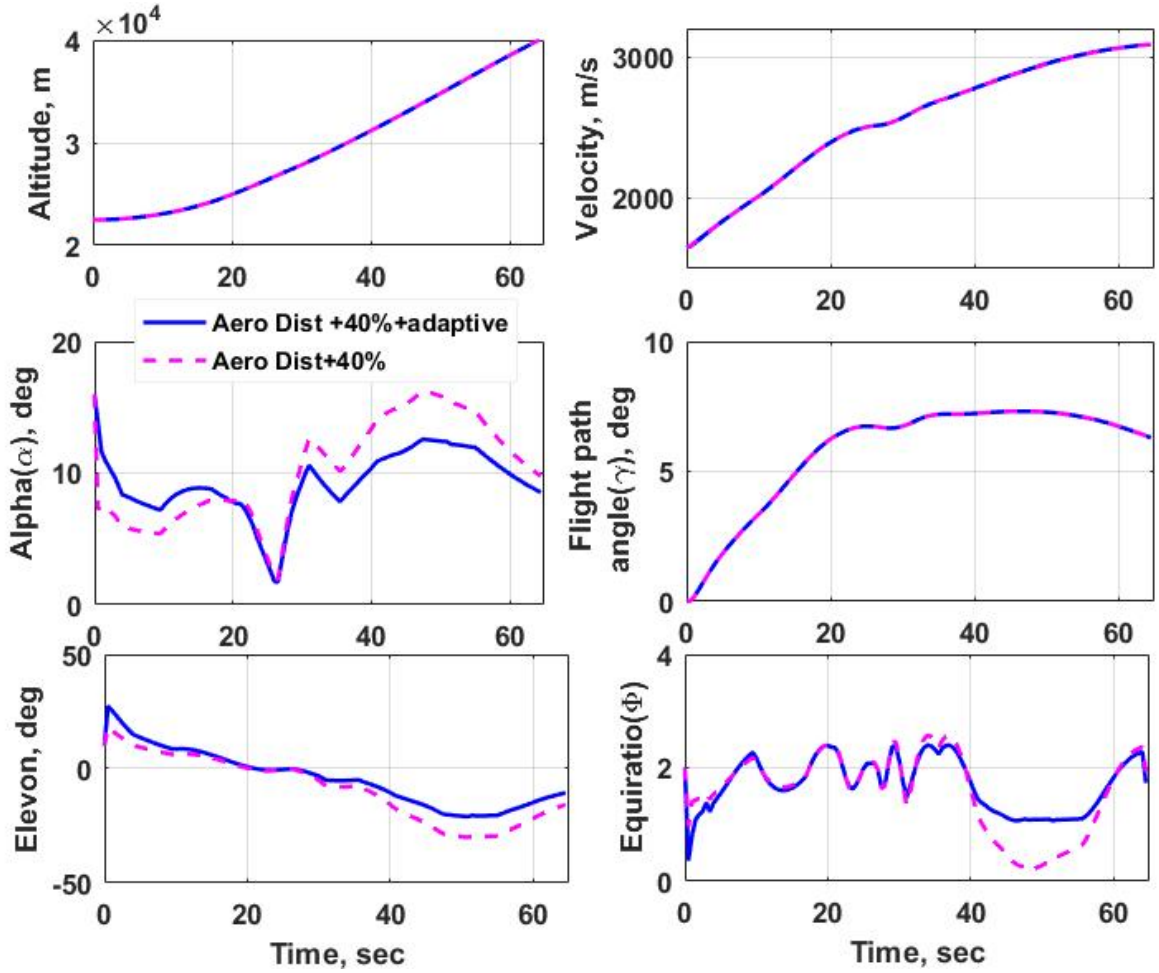

Figure 5.2: Case1: Aero-disturbance coefficient +40%

Figure 5.3 shows the comparison between with and without adaptive control after putting a lower limit of 0.5 on the equivalence ratio. Here without adaptive control, slight deviation is seen from nominal in velocity and flight path angle towards the end.

Case 2: Aero-disturbance Coefficients $(m_\alpha, n_\beta, l_\beta, z_\alpha) + 80\%$ Variation

In this case, the aero-coefficients are perturbed in the longitudinal and lateral dynamics by +80% thus increasing the effective aero-disturbance by more than 80%. Without adaptive augmentation, the controller is failing for this perturbation at 43s. However, using adaptive augmentation, the terminal conditions are achieved accurately, as summarized in Table 5.3. Figure 5.4 shows the comparison between this case and the nominal for longitudinal states

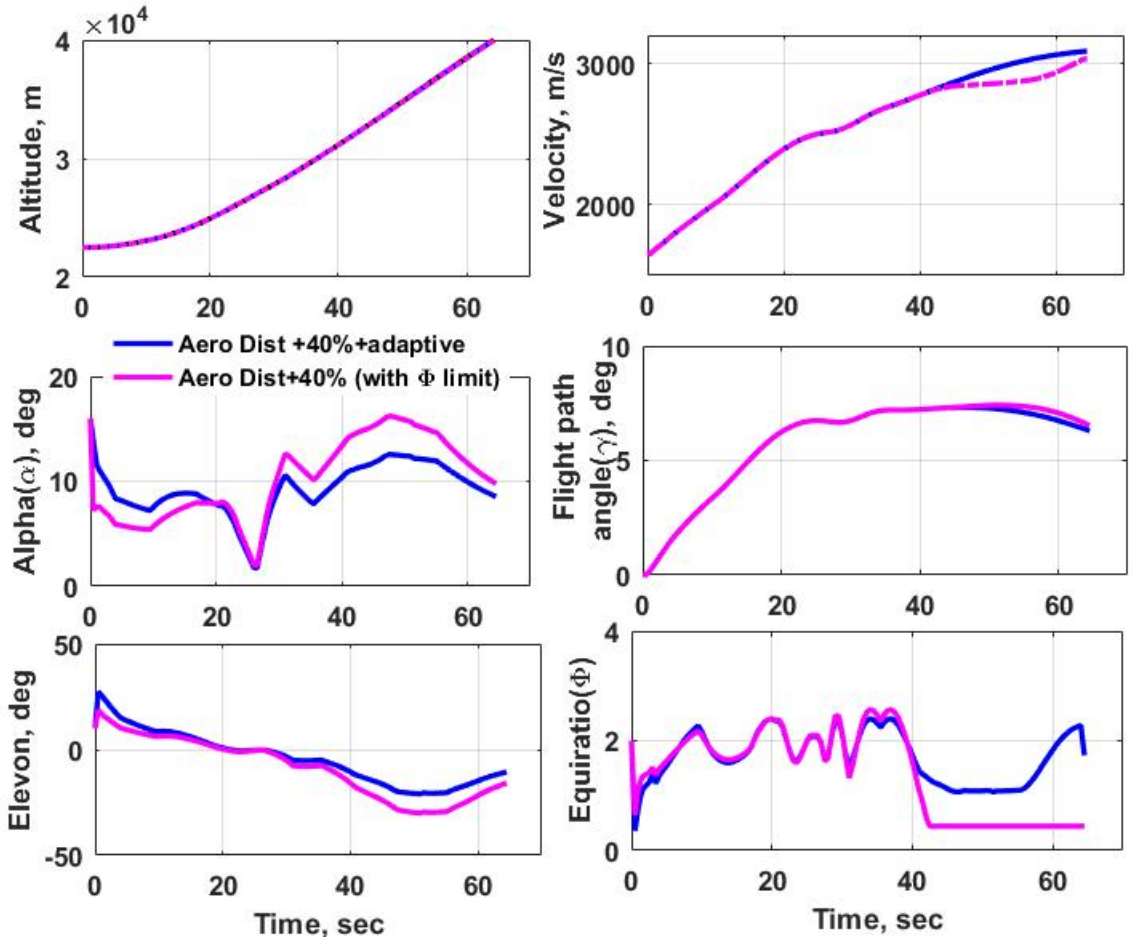

Figure 5.3: Case1: Aero-disturbance coefficient $+40\%$ with equivalence ratio limit

and control parameters. The tracking error in α ($\alpha_c - \alpha$) increases to 4.6 degrees in about 50 s, but at the end it reduces to less than 1.2 degrees. For the nominal case α perfectly tracks α_c as seen in Figure 5.4. The variation in β and rudder deflection is minimal compared to the nominal. For this particular perturbation, the variation in the lateral dynamics is shown in Figure 5.5. The rudder deflection is increased to 4deg around 55s from nominal 2deg to handle the perturbations on lateral dynamics.

Case 3: Aero-disturbance Coefficients $(m_\alpha, n_\beta, l_\beta, z_\alpha) + 80\%$ Variation and Aero-coefficients of Control Surfaces by -20%

Here the aero-coefficients are perturbed up in the longitudinal and lateral dynamics by 80% and that are perturbed down in the control surfaces by 20%. Effectively aero-disturbance increases by 80% and control effectiveness decreases by 20%. In the absence of adaptive controller, simulation fails at 34s while with adaptive controller, the end conditions are met

Table 5.2: Final state parameters for Case 1

Final pillbox parameters	Nominal	Aero-dis $+40\%$	Aero-dis $+40\%$ +adaptive control
Time(s)	64.5	64.5	64.5
Altitude(m)	40082.3016	40082.3598	40082.3567
Velocity(m/s)	3086.27	3086.81	3086.53
Flight path angle($^\circ$)	6.2961	6.29658	6.2962

Table 5.3: Final state parameters for Case 2

Final pillbox parameters	Nominal	Aero-dist $+80\%$	Aero-dist $+80\%$ +adaptive control
Time(s)	64.5	Controller fails	64.5
Altitude(m)	40082.3016	at 43s	40082.325
Velocity(m/s)	3086.27	-	3086.79
Flight path angle($^\circ$)	6.2961	-	6.2964

accurately. Figure 5.6 shows the comparison between this case and nominal for the longitudinal states and control parameters. The elevon deflection is demanding to near saturation of 60deg and throttle equivalence ratio is below zero. The tracking error in $\alpha(\alpha_c - \alpha)$ is of the order of 10deg around 50s which decreases towards the end to less than 4deg. After putting the limit of 0.5 on equivalence ratio, the state parameters are not meeting the terminal condition as shown in Figure 5.6. This indicates that this perturbation level defines the limit of performance for the adaptive controller. Table 5.4 gives the terminal pillbox condition achieved for this perturbation with and without limit on equivalence ratio along with nominal.

Table 5.4: Final state parameters for Case 3

Final pillbox parameters	Nominal	Aero-dis$+80\%$ cntrl-20%	Aero-dis$+80\%$ cntrl-20% +adacntl	Aero-dis$+80\%$ cntrl-20%+adacntl +clamp on Φ
Time(s)	64.5	Controller fails	64.5	64.5
Altitude(m)	40082.3016	at 34s	40082.034	39763.78
Velocity(m/s)	3086.27	-	3086.84	2772
Flight path angle($^\circ$)	6.2961	-	6.2987	7.297

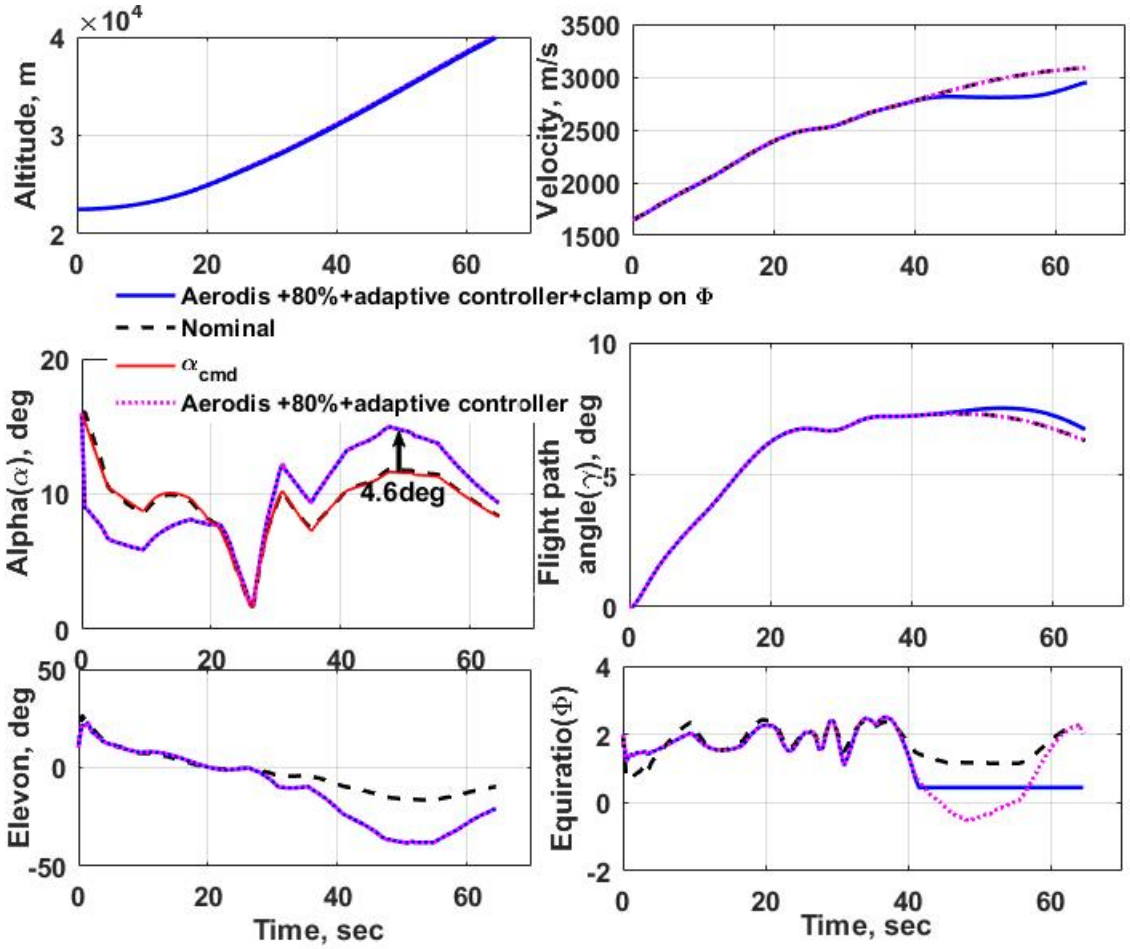

Figure 5.4: Case2: Aero-disturbance coefficient $+80\%$

5.4.2 Simulations with Adaptive Guidance Law

In this section, cases simulated are mainly to validate the adaptive guidance algorithm. The following cases are generated

1. thrust variation by tuning the propulsion coefficients.

2. saturation of the control surfaces by tuning the aero-coefficients.

Case 1: Lower bound thrust

Figure 5.7 shows the dispersion of the lower bound (LB) and upper bound (UB) in thrust with respect to the nominal value. Figure 5.8 shows the comparison between lower bound thrust perturbation and the nominal for the longitudinal states and control parameters. Here

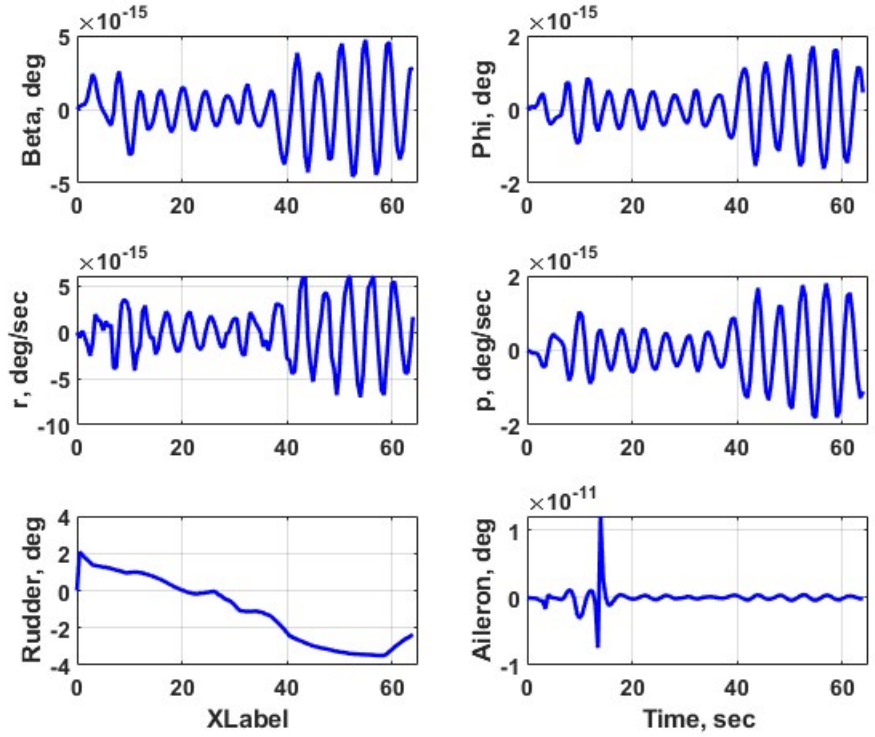

Figure 5.5: Case2: Aero-disturbance coefficient $+80\%$: Lateral dynamics

the α_c is re-targeted to meet the final conditions due to the reduction in thrust. Table 5.5 summarizes the final pillbox conditions achieved with and without adaptive guidance.

Table 5.5: Final state parameters for lower bound thrust perturbation

Final pillbox parameters	Nominal	Thrust LB	Thrust LB +adaptive Guidance law
Time(s)	64.5	64.5	64.5
Altitude(m)	40082.3016	39896.95	39905.634
Velocity(m/s)	3086.27	3077.33	3085.4
Flight path angle(°)	6.2961	6.45	6.4

Case 2: Elevon Actuator Saturation

In this case, aero-coefficients are tuned so that the elevon control demand is more than 60deg for 10s from 26s to 56s. Without adaptive guidance and with limit on control surface as 60deg, simulation fails at 48s. With adaptive guidance, α_c is re-targeted, which avoids

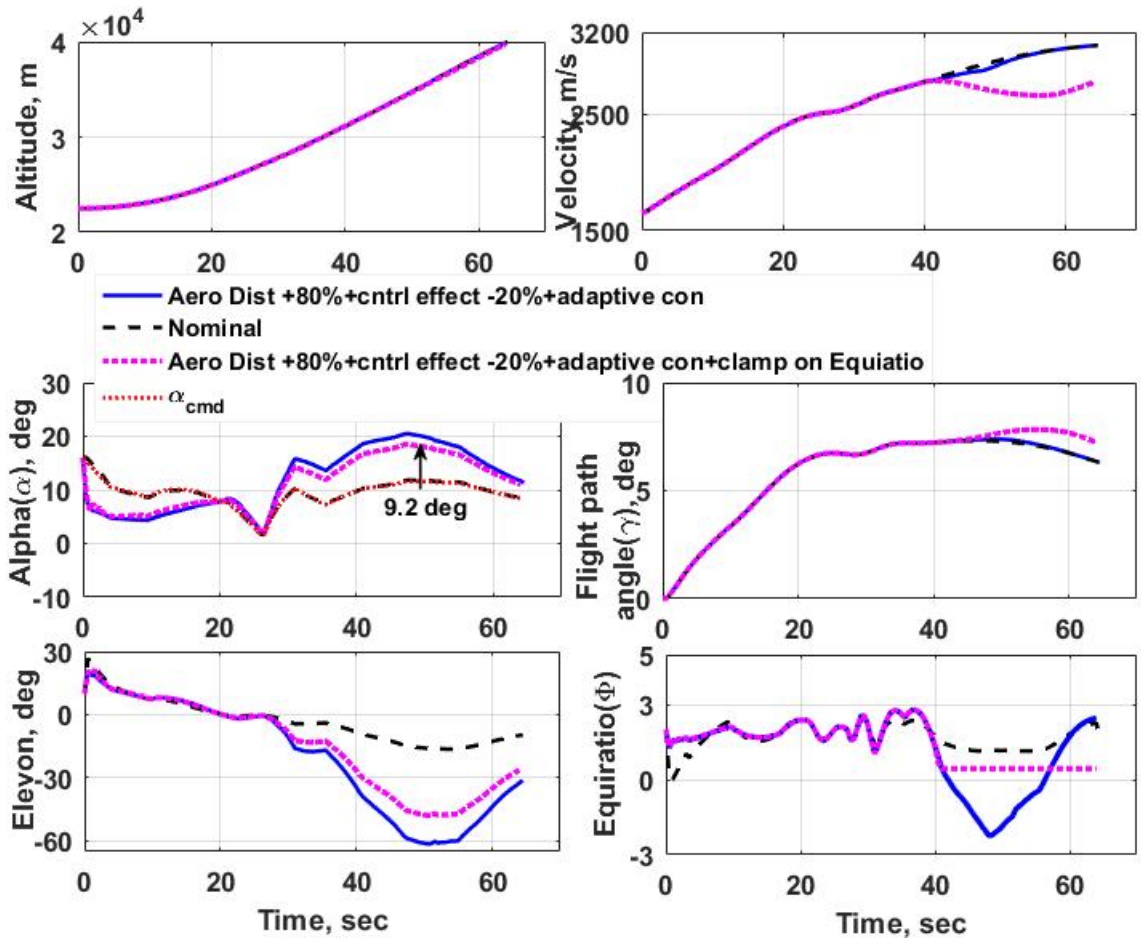

Figure 5.6: Case 3: Aero-disturbance coefficient $+80\%$ with control effectiveness -20%

the elevon saturation in meeting the terminal conditions. Figure 5.9 shows the comparison between the α_c re-targeting case and the nominal for the longitudinal states and control parameters.

5.4.3 Monte-Carlo Simulations

The model uncertainties and parameter dispersion have a large impact in the air-breathing phase of ABSLV. 6D MC simulations (MC) are done to assess the robustness and adaptability of the adaptive control guidance algorithm under wide range of random dispersion of parameters. Gaussian random dispersion is applied over the nominal value of the input parameters- propulsion, aero-coefficients, atmospheric density, initial mass, initial altitude, initial velocity and initial flight path angle. Table 5.6 gives the type of distribution and the variation 3σ applied to the mean value for the input parameters. Figure 5.10 illustrates

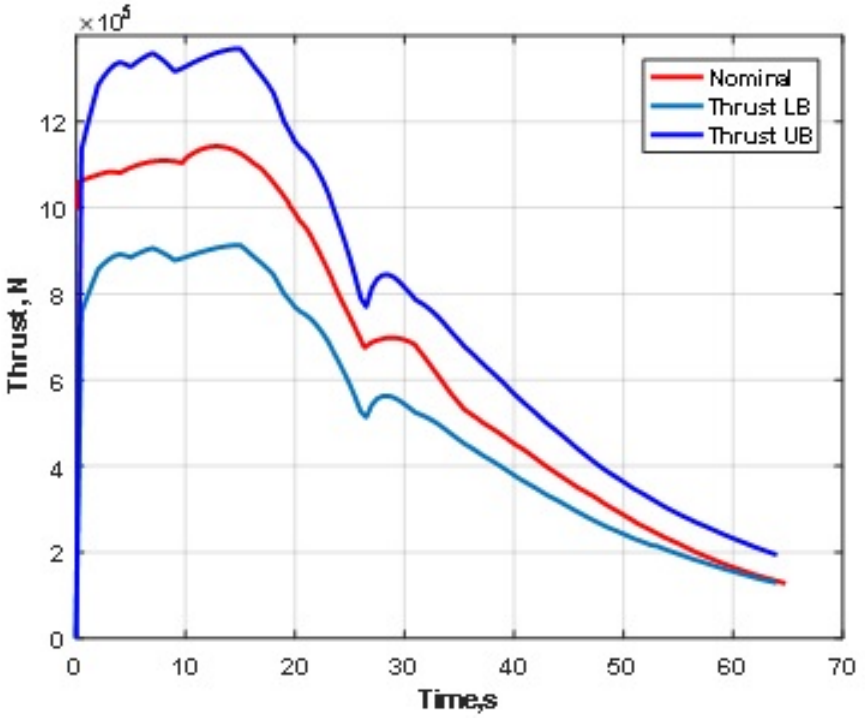

Figure 5.7: Variation of Nominal, upper and lower bound thrust profile

the spread of the longitudinal states and control parameters for 1500 MC simulations. MC variation of thrust, mass, moment coefficients (m_α, l_β), force coefficient ((z_α) and pitch rate is shown in Figure 5.11. Figure 5.12 gives the histogram of errors on terminal velocity, altitude and flight path angle and is less than 3m/s, 12m and 0.1deg respectively, which establishes the robustness of adaptive guidance algorithm. Table 5.7 gives the mean, minimum-maximum range and 95% confidence interval (is the range from 2.5 percentile to 97.5 percentile). Since the error distribution curves are not Gaussian, higher-order statistical moments like skewness and kurtosis are computed to assess how the samples disperse

Table 5.6: Parameter distribution and variation for MC simulation

State/Parameter	Mean	3σ	Distribution type
Initial Mass	127008kg	19000kg	Gaussian
Atmospheric Density	Nominal	15%	Gaussian
Thrust parameters	Nominal	10%	Gaussian
Initial Altitude	22.5km	6.3km	Gaussian
Initial Velocity	1650m/s	25m/s	Gaussian
Initial flight path angle	0°	0.5°	Gaussian

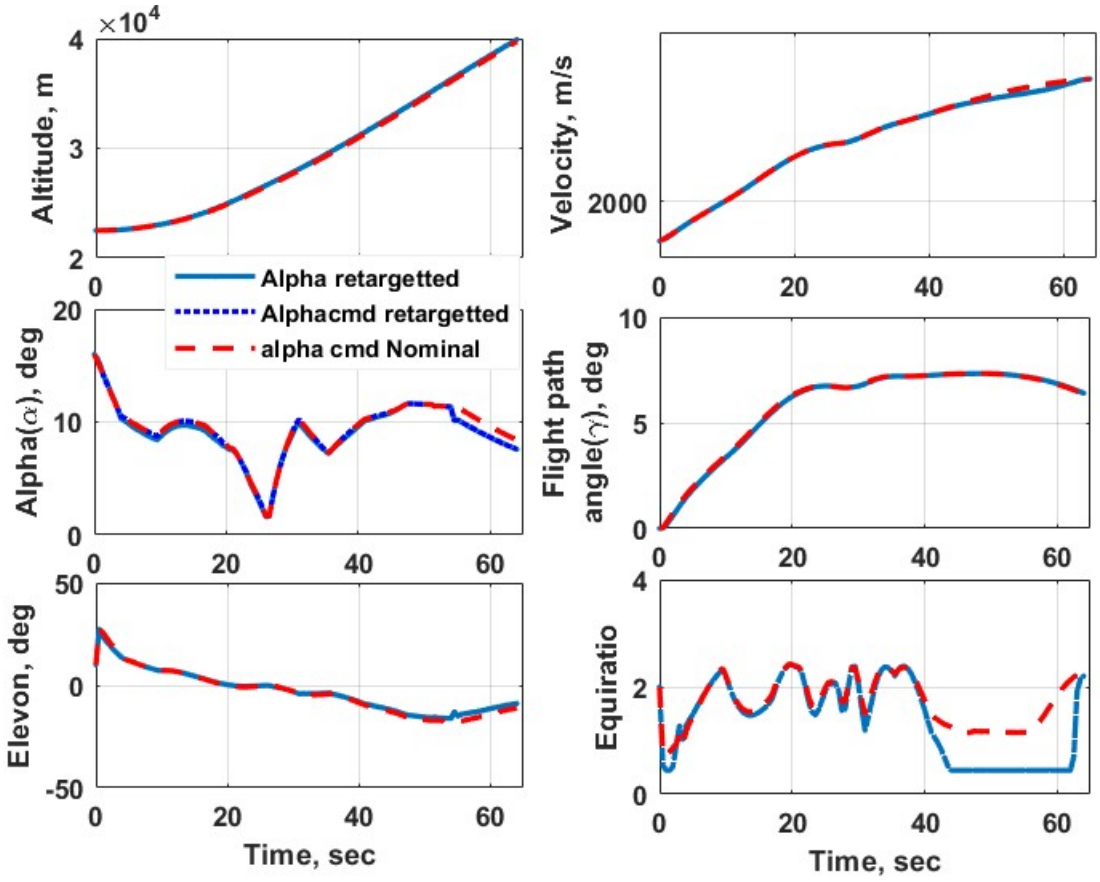

Figure 5.8: Angle of attack re-targeted for lower bound thrust perturbation

between a distribution's center and tails. Kurtosis is computed from the 4^{th} central moment (μ) as $Kurt = \mu^4/\sigma^4$. High value (normal distribution has kurtosis 3) denotes a distribution with thin tail and a high peak as seen in velocity error curve. Here skewness (measure of asymmetry) of the velocity error curve is -12.8 shows that it is left skewed curve. Similarly interquartile range gives the range of values that reside in the middle 50% of the dataset, given by the median of lower half and upper half of the dataset. Table 5.8, gives median, skewness, kurtosis and inter-quartile range of the three state error distribution curves.

Table 5.7: State error distribution specification for MC simulation

Parameter	Mean	Min	Max	95% confidence interval [2.5% to 97.5%]
Final velocity error, m/s	-0.012	-2.732	0.226	[-0.159 to 0.131]
Final altitude error, m	-0.306	-11.20	1.48	[-2.081 to 0.960]
Final flight path angle error, deg	+0.003	-0.001	0.087	[-0.0002 to 0.022]

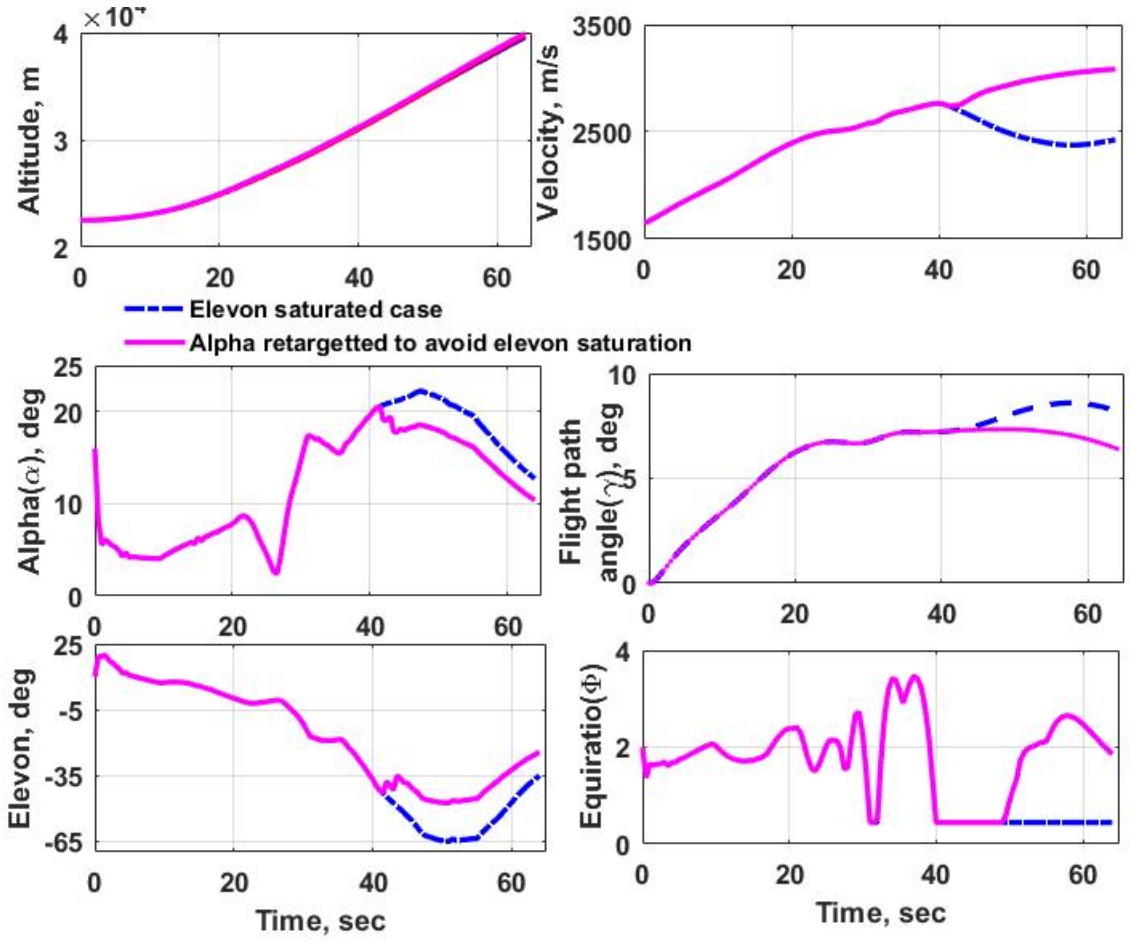

Figure 5.9: State parameters for elevon saturation case

Monte-Carlo simulation with wind perturbations

The wind perturbations over a typical measured wind in the upper atmosphere shown in Figure 5.13 is considered for simulation. The wind velocity in Geographic frame is converted to the ECI frame, and the relative velocity in the ECI frame is computed according to Equation 2.24. Figure 5.14 shows the state vectors, the deflection of the elevon, and the fuel equivalence ratio for the MC simulation. Here, the variation in α due to the velocity of the wind and the corresponding elevation deflection to achieve the desired α_c is clearly seen. Figure 5.15 gives the histogram of errors in the terminal velocity, altitude, and flight path angle with wind perturbations. The terminal error variation remains almost same with that of without wind perturbation.

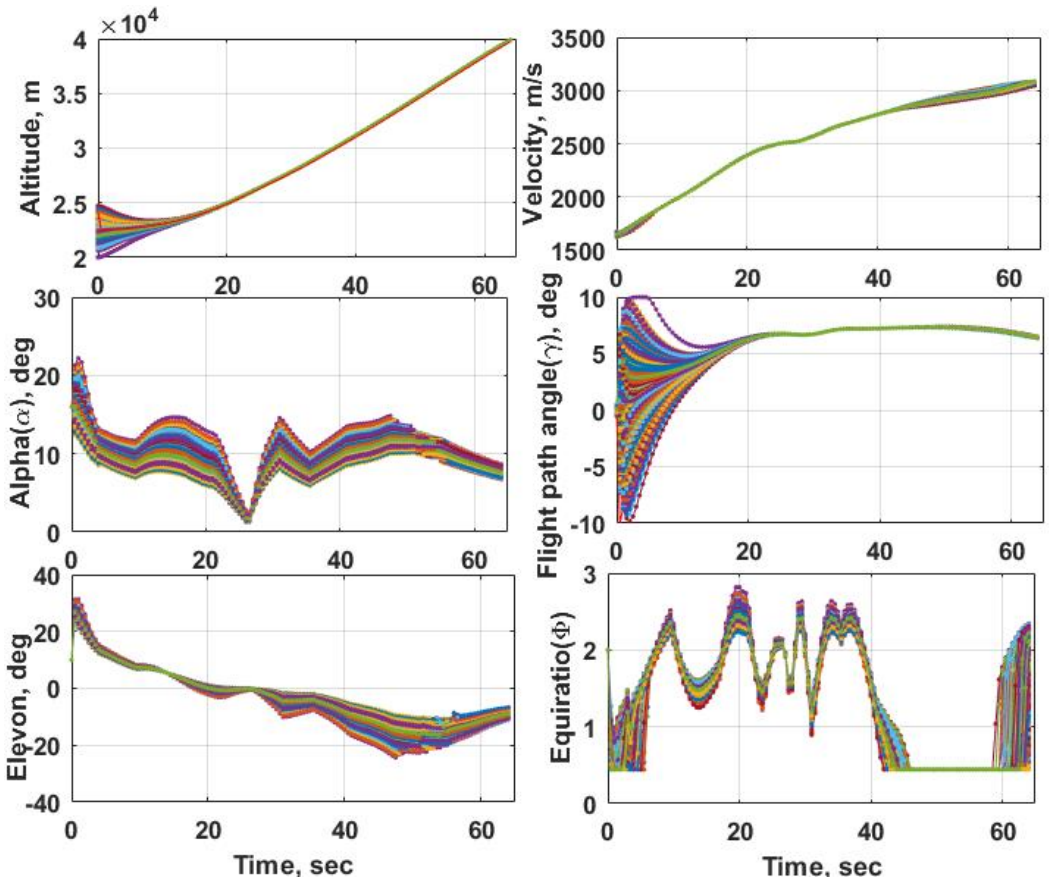

Figure 5.10: State vectors for MC simulation

5.5 Summary

During the air breathing phase, the hypersonic vehicle is subjected to a rapidly changing flight envelope. To handle uncertain dynamics and time-varying parameter uncertainties, existing integrated guidance and controller for this phase is augmented with adaptive controller and adaptive guidance law. The adaptive controller is based on derivative free adaption law which handles the time-varying uncertainties faithfully without compromising for closed-loop response. Stability analysis of the controller is done using Lyapunov-Krasovskii functional. Characteristic model-based all-coefficient adaptive guidance is used to re-target the vehicle to a sub-optimal trajectory for significant degradation in propulsion and performance. Quite a lot of numerical simulations are done to establish the performance of the new controller and the limits of performance. The robustness of the algorithm is demonstrated through MC simulations considering dispersion on initial state vectors, aero-coefficients, and propulsion parameters.

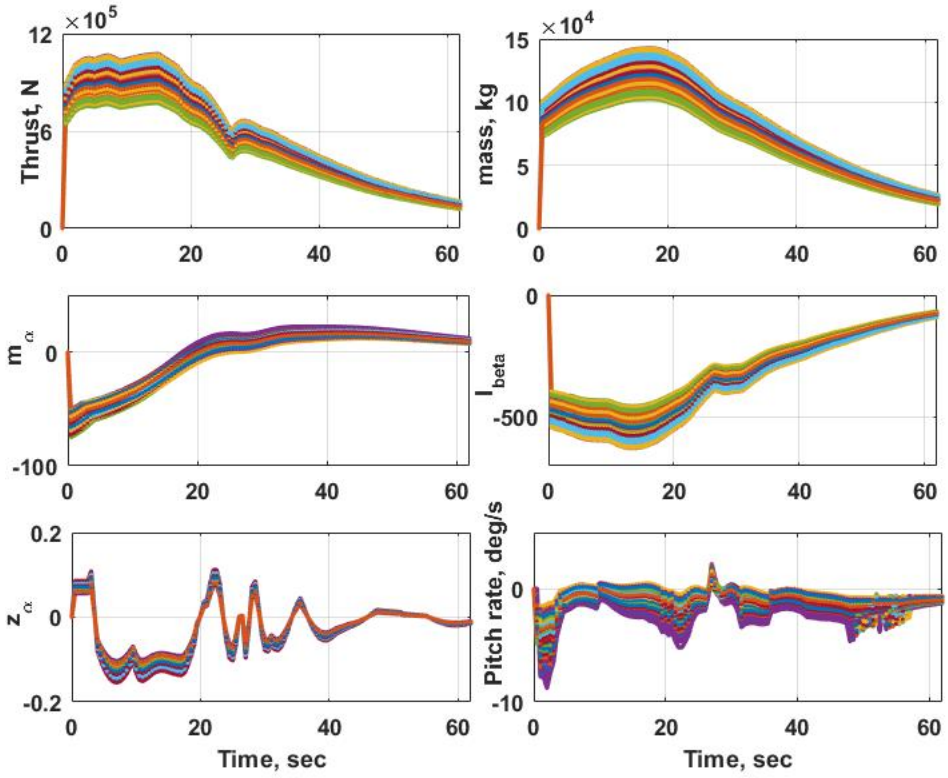

Figure 5.11: Parameters for MC simulation

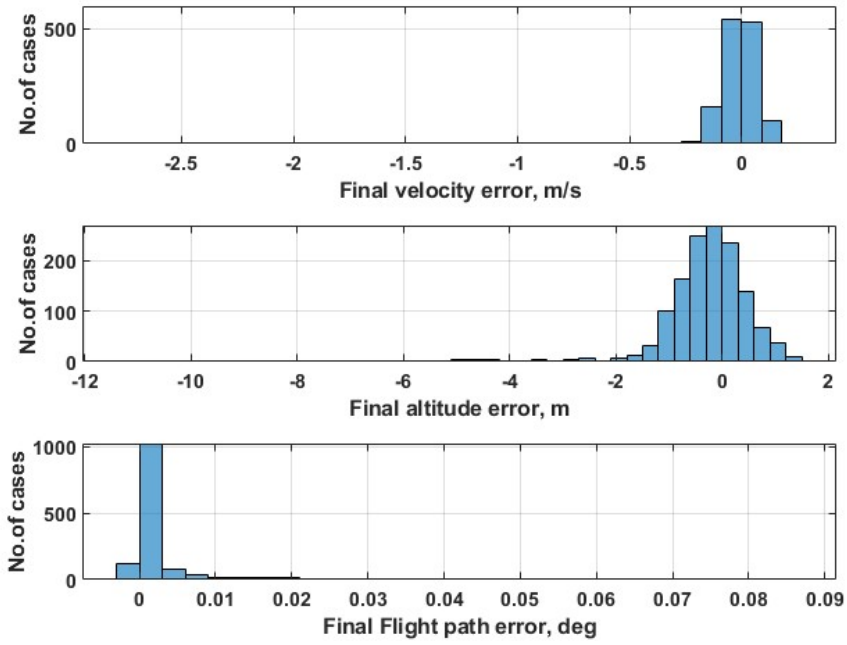

Figure 5.12: Final state vector error distribution diagram for MC simulation

Table 5.8: State error distribution specifications for MC simulation

Parameter	Median	Skewness	Kurtosis	Interquatertile range [25% to 75%]
Final velocity error, m/s	-0.005	-12.80	260.90	[-0.054 to 0.041]
Final altitude error, m	-0.211	-4.10	35.20	[-0.623 to 0.168]
Final flight path angle error, deg	-0.00	+6.16	51.20	[0.0003 to 0.0014]

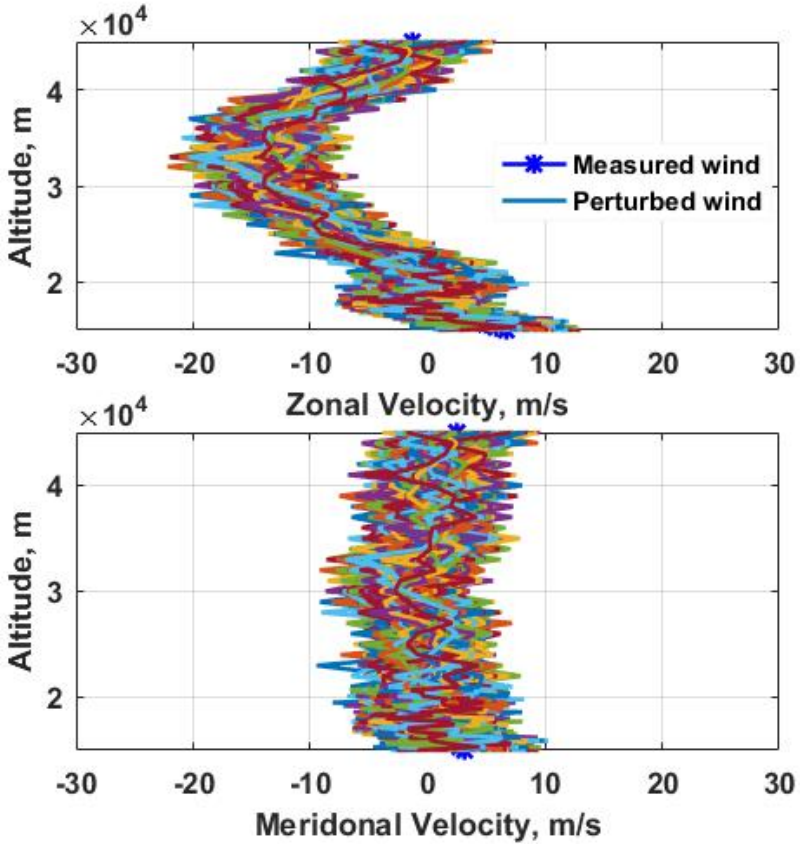

Figure 5.13: Wind perturbations considered for MC simulation

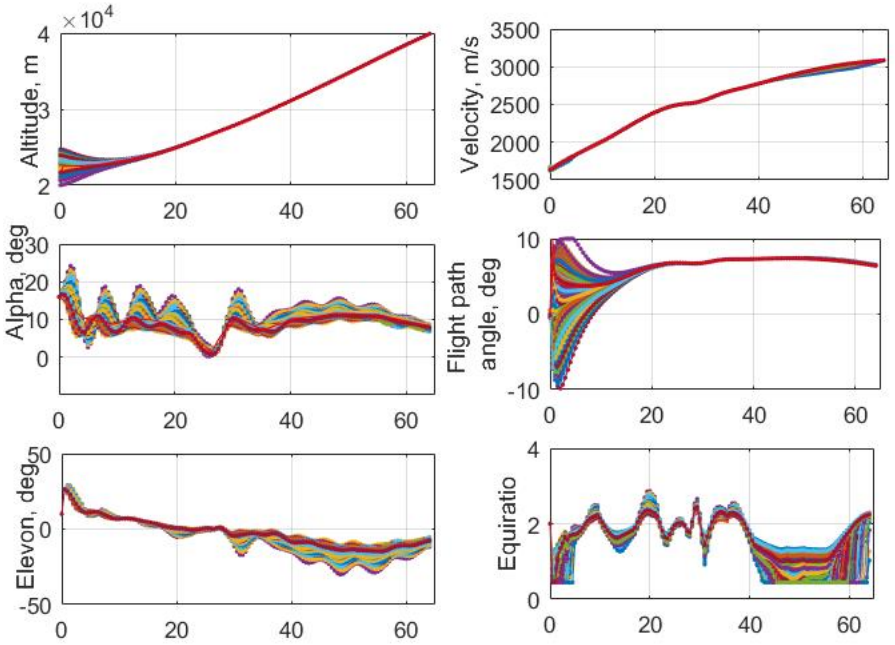

Figure 5.14: State parameters for MC simulation with wind perturbation

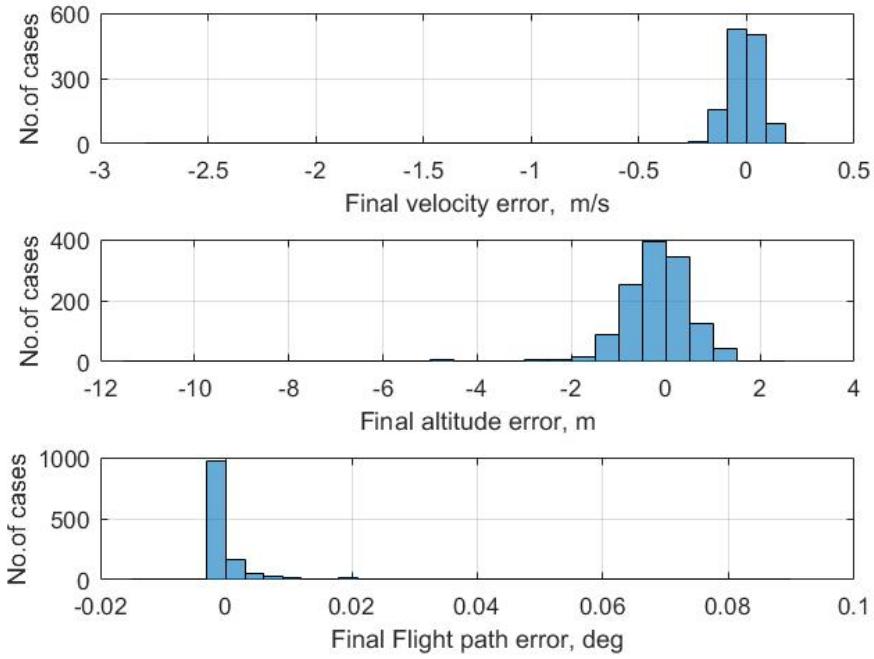

Figure 5.15: Final state vector error distribution diagram for MC simulation with wind perturbation

Chapter 6

Conclusions and Future Scope

This research work deals with the development of integrated guidance and control laws during the air-breathing phase of ABSLV. The summary of this research work is as follows.

1. A six-dimensional trajectory model for the winged cone configuration of ABSLV was developed addressing the coupling dynamics between various subsystems..

2. Using six-dimensional trajectory, guidance algorithm was formulated based on, optimal control law taking altitude, velocity and mass as states and angle of attack as control command, considering the effect of controller on guidance states. The algorithm was numerically solved using Gauss pseudo-spectral method.

3. Further, an integrated multi-input multi-output controller was designed with rotational states both longitudinal and lateral and translational states simultaneously. Controller design is based on hybrid control law with i) decoupling controller for input output decoupling through state feedback and ii) classical controller designed in each channel to ensure robustness.

4. An adaptive control law based on derivative free update law was augmented to the existing controller to handle a wide range of parametric uncertainties by tuning the adaption gain without compromising the stability of the overall system. Similarly an all-coefficient adaptive guidance law was developed to predict the terminal state and re-commanded the control inputs to achieve the predicted terminal states at air-breathing phase in case of control surface failure condition or for degraded propulsion performance.

5. The new adaptive integrated controller was validated through various parameter perturbations for aerodynamic parameters, control effectiveness, and propulsive parameters, and also evaluated the limit of perturbation that the overall system can handle.

Finally, the new scheme's robustness is demonstrated via Monte-Carlo (MC) simulations.

The future directions of the research work carried out in this thesis are as follows.

- Including the flexible effects in the control design level and its effects on propulsion and control structure interaction to be demonstrated through simulation.
- Structural modes can be modeled as unmodeled dynamics and its effects on adaptive controller can be studied.
- Modification terms to be added to the derivative free adaptive law to improve robustness.
- Wind gust, sensor/navigation errors can be included in the MC simulation.

Bibliography

[1] S. J.Y.Oh, F.Ma and V. Yang, "Interactions between shock and acoustic waves in a supersonic inlet diffuser," *Journal of Propulsion and Power*, pp. 486–495, 2005.

[2] W. E.Yong and K.He, "An adaptive predictor-corrector reentry guidance based on self-definition way-points," *Aerospace Science and Technology*, vol. 39, pp. 211–221, 2014.

[3] Y. C. Q. Z. Lin Cheng, Zhenbo Wang and K. Ni, "Multi-constrained predictor-corrector reentry guidance for hypersonic vehicles," *Journal of Aerospace Engineering*, vol. 232(16), pp. 3049–3067, 2018.

[4] L. X.Ming L., C. Kejun and T. Guojian, "Quasi-equilibrium glide adaptive guidance for hypersonic vehicles," *SCIENCE CHINA Technological Sciences*, vol. 55), pp. No.3: 856–866, March 2012.

[5] O. Jr and P. Lu, "Fast ascent trajectory optimization for hypersonic air-breathing vehicles," *AIAA Guidance, Navigation, and Control Conference, 2-5 August 2010, Toronto, Ontario Canada*, 2010.

[6] J. Heeg and A. S.Pototzky, "Active control of aerothermoelastic effects for a conceptual hypersonic aircraft," *Journal of Aircraft*, vol. 304, pp. 453–458, 1997.

[7] D.K.Schmidt, "Optimum mission performance and multivariable flight guidance for air-breathing launch vehicles," *Journal of Guidance, Control and Dynamics*, vol. 20, pp. 1157–1164, 1997.

[8] M.A.Bolender and D.B.Doman, "Nonlinear longitudinal dynamical model of an air-breathing hypersonic vehicle," *Journal of Spacecraft and Rockets*, vol. 44, no. 2, pp. 374–387, 2007.

[9] M.Kuipers, "Nonlinear longitudinal dynamical model of an air-breathing hypersonic vehicle," *American Institute of Aeronautics and Astronautics*, 2007.

[10] J. D.Schierman, "Integrated adaptive guidance and control for re-entry vehicles with flight-test results," *Journal of Guidance, Control and Dynamics*, vol. 27, November-December 2004.

[11] A. S. K.P.Groves, D.O.Sigthorssony and S.Yurkovichx, "Reference command tracking for a linearized model of an air-breathing hypersonic vechicle," *AIAA Guidance, Navigation and Control Conference and Exhibit*, pp. 15–18, 2005.

[12] M. Mirmirani and C. Wu, "Air-breathing hypersonic flight vehicle modeling and control, review, challenges and a cfd based example," *American Institute of Aeronautics and Astronautics*, pp. 152–167, 2005.

[13] L. Yongtao, "Analysis of longitudinal dynamic characteristics for air-breathing hypersonic flight vehicle." *21st AIAA International Space Planes and Hypersonics Technologies Conference*, 6-9 March 2017, Xiamen, China.

[14] M. A. B. Jason T. Parker and D. B. Doman, "Control-oriented modeling of an air-breathing hypersonic vehicle," *Journal of Guidance, Control and Dynamics*, vol. 30, May-June 2007.

[15] D. P. Thomas Jazra and M. K. Smart, "Design of an air-breathing second stage for a rocket-scramjet-rocket launch vehicle," *Journal of Guidance, Control and Dynamics*, vol. 50, March-April 20137.

[16] N. A. G. I. N.K.Gupta, B.K.Gupta and H.G.Yoon, "Integrated modeling and simulation of an air-breathing combustion system dynamics," *AIAA Modeling and Simulation Technologies Conference and Exhibit*, August 2007.

[17] K.G.Bowcutt, "Multidisciplinary optimization of air-breathing hypersonic vehicles," *Journal of Propulsion and Power*, pp. 1184–1190, 2001.

[18] R.Starkey and M.Lewis, "Critical design issues for air-breathing hypersonic wave-rider missles," *Journal of Spacecraft and Rockets*, 2001.

[19] S. Keshmiri, "Nonlinear and linear longitudinal and lateral-directional dynamical model of air-breathing hypersonic vehicle," *15th AIAA International Space Planes and Hypersonic Systems and Technologies Conference*, 2008.

[20] C. C. Engelund W.C., Holland S.D. and E. B. R.D., "Aerodynamic database development for the hyper-x airframe integrated scramjet propulsion experiment," *Journal of Spacecraft and Rockets*, pp. 803–810, 2001.

[21] H. Suzuki, "Optimal ascent trajectory and guidance law for aerospace plane," *37th AIAA Aerospace Sciences Mleeting and Exhibitand Exhibit*, January 1999.

[22] S. H. P.Lu and T. B., "Closed loop endo-atmospheric ascent guidance," *Journal of Guidance, Control and Dynamics*, vol. 26, pp. 283–294, 2003.

[23] Y. P.Huang, C.Wei and N.Cui, "Hybrid optimization approach for rapid endo-atmospheric ascent trajectory planning," *An International Journal of Aircraft Engineering and Aerospace Technology*, pp. 473–479, 2016.

[24] T. Yamamoto, "New real-time guidance strategy for aerodynamic ascent flight," *IAC-05-C1.8.02*, vol. 304, pp. 453–458, 1997.

[25] A. J.E.Corban and G.A.Flandro, "Optimal guidance and propulsion control for transatmospheric vehicles," *AIAA Guidance, Navigation and Control Conference and Exhibit*, Aug 1989.

[26] V. B. A.Mark and K. D. Mease, "Aerospace plane guidance using time-scale decomposition and feedback linearization," *Journal Of Guidance, Control and Dynamics*, vol. 15, no. 5, 1992.

[27] C. W. N. C. Yuan Li, Baojun Pang and Y. Liu, "Online trajectory optimization for power system fault of launch vehicles via convex programming," *Aerospace Science and Technology*, 2020.

[28] Q. Zhang and Z. Xu, "Autonomous ascent guidance with multiple terminal constraints for all-solid launch vehicles," *Aerospace Science and Technology*, 2020.

[29] N. M. A.J.Calise and S. Lee, "Design and evaluation of a three-dimensional optimal ascent guidance algorithm," *Journal Of Guidance, Control and Dynamics*, vol. 21, no. 6, 1998.

[30] G.Merkulov, "Minimum-effort impact-time control guidance using kinematics approximation," *Journal of Guidance, Control and Dynamics*, Sep-Oct 2021.

[31] M. J. Casey R.Heidrich and R. D.Braun, "Optimal information filtering for robust aerocapture trajectory generation and guidance," *Journal of Spacecraft and Rockets*, 2020.

[32] N. M. Bhavnesh Panchal and S. E. Talole, "Continuous-time predictive control-based integrated guidance and control," *Journal of Guidance, Control and Dynamics*, vol. 40, pp. 1579–1595, 2017.

[33] H.Buscket and A.J.Calise, "Uncertainty modeling and fixed-order controller design for a hypersonic vehicle," *Journal of Guidance, Control and Dynamics*, vol. 20, no. 1, pp. 42–48, 1997.

[34] R.Lind, "Linear parameter-varying modeling and control of structural dynamics with aerothermoelastic effects," *Journal of Guidance, Control and Dynamics*, vol. 25, no. 4, pp. 733–739, 2002.

[35] C.Tournesl, "Ramjet-powered reusable launch vehicle control by sliding modes," *Journal of Guidance, Control and Dynamics*, vol. 21, no. 3, pp. 409–415, 1998.

[36] Z.D.Wilcox, "Robust nonlinear control of a hypersonic aircraft in the presence of aerothermoelastic effects," *American Control Conference, IEEE Press,Piscataway, NJ*, pp. 2533–2538, 2009.

[37] A. S. M. D.Sigthorsson, P.Jankovsky and D.Doman, "Robust linear output feedback control of an air-breathing hypersonic vehicle," *Journal of Guidance, Control and Dynamics*, pp. 1052–1066, 2008.

[38] S. R. L. Z.D.Wilcox, W.MacKunis and W.E.Dixon, "Lyapunov-based exponential tracking control of a hypersonic aircraft with aerothermoelastic effects," *Journal Of Guidance, Control and Dynamics*, no. 4, July-August 2010.

[39] Z. Y. Hongfei Sun and J. Zeng, "New tracking-control strategy for airbreathing hypersonic vehicles," *Journal of Guidance, Control and Dynamics*, vol. 36, pp. 846–859, 2013.

[40] M. A. Bolender and D. B. Doman, "Flight path angle dynamics of air-breathing hypersonic vehicles," *AIAA Guidance, Navigation and Control Conference*, 2006.

[41] Y. S. B. M. Parker J.A., Serrani A. and D. D.B, "Approximate feedback linearization of an air-breathing hypersonic vehicle," *AIAA Guidance, Navigation and Control Conference*, 2006.

[42] C. C. and H. N., "Design and analysis of a novel adaptive control architecture with guaranteed transient performance," *IEEE Trans. Autom. Control*, pp. 586–591, 2008.

[43] M. H.Xu and P.A.Ioannou, "Adaptive sliding mode control design for a hypersonic flight vehicle," *Journal of Guidance, Control and Dynamics*, pp. 829–838, 2004.

[44] Y. T. and C. A.J., "Kalman filter modification in adaptive control," *Journal of Guidance, Control and Dynamics*, pp. 426–439, 2010.

[45] E. C. N. H. Yu Lei, Chengyu Cao and A. Kurdila, "Design of an l1 adaptive controller for air-breathing hypersonic vehicle model in the presence of unmodeled dynamics," *AIAA Guidance, Navigation and Control Conference and Exhibit*, August 2007.

[46] B.-N. M. Nguyen N. and Ishihira, "Robust adaptive optimal control with large adaptive gain," *Proc. American Control Conf.*, 2010.

[47] J. B.C.Gruenwald, T.Yucelen and D.Wagner, "Computing stability limits of adaptive controllers in the presence of high-order actuator dynamics," *IEEE Conference on Decision and Control*, 2016.

[48] E.Johnson and A.Calise, "Limited authority adaptive flight control for reusable launch vehicles," *Journal of Guidance, Control and Dynamics*, pp. 906–913, 2003.

[49] E.L.N.Hovakimyan, "Stable adaptation in the presence of actuator constraints with flight control applications," *Journal of Guidance, Control and Dynamics*, vol. 30, pp. 337–345, 2007.

[50] Z.D.Wilcox, "Nonlinear sequential loop closure control design for an air-breathing hypersonic vehicle mode," *American Control Conference, IEEE Press, Piscataway, NJ*, pp. 3458–3463, 2008.

[51] L.Fiorentini and A.Serrani, "Nonlinear robust adaptive control of flexible air-breathing hypersonic vehicles," *Journal of Guidance, Control and Dynamics*, vol. 32, no. 2, pp. 402–416, 2009.

[52] D. B. D. F. J. Ron Aditya, Mark J. Balas and F. x., "Multivariable direct adaptive stability and command augmentation of an air-breathing hypersonic vehicle," *AIAA SciTech Forum*, January 2017.

[53] B.J.Bialyl, "An adaptive backstepping controller for a hypersonic air-breathing missile," *AIAA Guidance, Navigation,and Control Conference*, Aug 2012.

[54] H.An and Q.Wu, "Adaptive control of variable geometry inlet configured air-breathing hypersonic vehicles," *Journal of Spacecraft and Rockets*, vol. 56, Sep-Oct 2019.

[55] T. Yucelen and A. J. Calise, "Robustness of a derivative-free adaptive control law," *Journal of Guidance, Control and Dynamics*, vol. 37, pp. 1583–1594, 2014.

[56] J.Tian and X.J.Xie, "Adaptive state-feedback stabilization for high-order stochastic non-linear systems with uncertain control coefficients," *International Journal of Control*, vol. 80, pp. 1503–1516, 2007.

[57] J. A.Lewis and E. N.Johnson, "Gain switching control law for dynamic inversion based adaptive control with unknown sign of control effectiveness," *AIAA SciTech Forum*, pp. 11–15, January 2021.

[58] T. Y. Benjamin C.Gruenwald and S. Sarsilmaz, "A new model reference adaptive control law to address actuator amplitude saturation," *AIAA Scitech Forum*, pp. 7–11, January 2019.

[59] B. C. K.Merve Dogan and T. Yucelen, "Robustness of an adaptive control law to uncertain input dynamics," *AIAA Guidance, Navigation, and Control Conference*, pp. 8–12, January 2018.

[60] K. A.Wise, "Design parameter tuning in adaptive observer-based light control architectures," *AIAA Information Systems-AIAA Infotech Aerospace*, pp. 8–12, January 2018.

[61] J. A.Muse, "An adaptive law with tracking error dependent adaptive gain adjustment mechanism," *AIAA Guidance, Navigation, and Control Conference*, vol. 6287, pp. 8–11, 2011.

[62] M. Kuipers, "Adaptive control of an aeroelastic airbreathing hypersonic cruise vehicle," *AIAA Guidance, Navigation and Control Conference and Exhibit*, vol. 6326, pp. 20–23, 2007.

[63] M. A. L. Fiorentini A.Serrani and D. B.Doman, "Nonlinear robust/adaptive controller design for an air-breathing hypersonic vehicle model," *AIAA Guidance, Navigation and Control Conference and Exhibit*, vol. 6329, pp. 20–23, 2007.

[64] M. Li and J. Hu, "An approach and landing guidance design for reusable launch vehicle based on adaptive predictor corrector technique," *Aerospace Science and Technology*, vol. 75, pp. 20–23, 2018.

[65] K. A.Joshi and S.S.Amma, "Predictor-corrector reentry guidance algorithm with path constraints for atmospheric entry vehicles," *Journal Guidance, Control and Dynamics*, vol. 30(5), pp. 1307–1318, 2007.

[66] A. G. Naresh Kumar and S.E.Talole, "Dynamic pressure based mid-course guidance scheme for hypersonic boost-glide vehicle," *Journal of Aerospace Engineering*, vol. 233(9), pp. 3211–3222, 2019.

[67] W. Y. H. W. B. Junshou Chen, A. Wang and H.Li, "Prediction-correction guidance algorithm for high velocity reentry capsules," *Proceedings of the 40th Chinese Control Conference*, pp. 26–28, July 2021.

[68] Z.S.Shui and J.Zhou, "On-line predictor-corrector reentry guidance law based on gauss pseudospectral methods," *Journal of Astronautics*, pp. 1249–1255, 2011.

[69] X. S. and L. P., "Constrained predictor-corrector entry guidance," *Journal of Guidance, Control and Dynamics*, pp. 1273–1280, 2010.

[70] K. Zou and X. Gou, "Characteristic model-based all-coefficient adaptive control of the drag-free satellites," *2020 Chinese Automation Congress (CAC) | 978-1-7281-7687-1/20/$31.00 ©2020 IEEE.*

[71] R. Rockwell, "Simulated scramjet shock train control using an all-coefficient adaptive control approach," *Journal of Propulsion and Power*, July August 2023.

[72] J. H. MaomaoLia and H. Huang, "A segmented and weighted adaptive predictor-corrector guidance method for the ascent phase of hypersonic vehicle," *Aerospace Science and Technology*, 2020.

[73] P. Lu, "Predictor-corrector entry guidance for low-lifting vehicles," *Journal of Guidance, Control and Dynamics*, pp. 1067–1075, 2008.

[74] P. Lu, "Entry guidance: A unified method," *Journal of Guidance, Control and Dynamics*, May June 2014.

[75] J. N. M. J.Schierman, D.Ward and D.Doman, "Integrated adaptive guidance and control for re-entry vehicles with fight-test results," *Journal of Guidance, Control and Dynamics*, pp. 975–988, 2004.

[76] Z. Q. Cheng Yang, Cheng Lin and P. Chu, "Predictor-corrector reentry guidance based on online model identification," *Proceedings of the 36th Chinese Control Conference*, July 26-28, 2017.

[77] Z. P. J. D. C. I. C. D.John, Shaughnessy S. and M.-L. Kelley, "Hypersonic vehicle simulation model:winged-cone configuration," *NASA TM-102610*, 1990.

[78] A.Maity and R.Padhi, "Non-linear sliding mode control design for an air-breathing engine with state estimation," *18th IEEE International conference on Control Application*, July 8-10 2009.

[79] D.K.Schmidt, "Dynamics and control of hypersonic aeropropulsive/aeroelastic vehicles," *AIAA Guidance, Navigation and Control Conference*, 1992.

[80] Blakelock and J. H, "Automatic control of aircraft and missiles," 1991.

[81] Nelson and R. C., "Flight stability and automatic control," 1998.

[82] F. F. Qi Gong and I. M. Ross, "Spectral algorithm for pseudospectral methods in optimal control," *Journal of Guidance, Control and Dynamics*, pp. 460–471, 2008.

[83] R. I.M. and F. F., "Pseudospectral knotting methods for solving optimal control problems," *Journal of Guidance, Control and Dynamics*, pp. 397–405, 2004.

[84] K. M. Elnagar G. and R. M., "The pseudospectral legendre method for discretizing optimal control problems," *IEEE Transactions on Automatic Control*, pp. 1793–1796, 1995.

[85] M. W. Gill P.E. and S. M.A, "Snopt: An sqp algorithm for large-scale constrained optimization," *SIAM Journal on Optimization*, pp. 979–1006, 2002.

[86] J.Davidson, "Flight control laws for nasa's hyper-x research vehicle," *American Institute of Aeronautics and Astronautics*, 1999.

[87] D.B.Doman and A.D.Ngo, "Dynamic inversion-based adaptive/re-configurable control of the x-33 on ascent," *Journal of Guidance, Control and Dynamics*, vol. 25, p. 275, 2002.

[88] A. S. K.P.Groves, D.O.Sigthorssony and S.Yurkovichx, "Nonlinear robust/adaptive controller design for an air-breathing hypersonic vehicle model," *AIAA Guidance, Navigation and Control Conference and Exhibit*, pp. 20–23, 2007.

[89] H.K.Khalil, "Nonlinear systems," *Prentice Hall, Upper Saddle River, N.J*, third edition, 2002.

[90] D.Ge, "Multi-loop gain scheduling control of flexible air-breathing hypersonic vehicle," *International Journal of Innovative Computing, Information and Control*, 2011.

[91] P. Paraskevopoulos and F. Koumbouli, "Decoupling and pole assignment in generalised state space systems," *IEEE Proceedings*, pp. 547–559, 1991.

[92] P.L.Falb and W.A.Wolovich, "Decoupling in the design and synthesis of multivariable control systems," *IEEE Transactions on Automatic Control*, pp. 651–659, 1967.

[93] P. M.Krstic and I. Kanellakopoulos, "Nonlinear and adaptive control design," *John Wiley and Sons, Inc., New York, NY*, 1995.

[94] H. Rani Radhakrishnan, Priyadarshanam H. and K.Sivan, "6d trajectory, guidance and control development for air-breathing phase of reusable launch vehicle," *International Journal of Control and Dynamics*, 7 February 2023.

[95] M. N. Calise A.J. and L. S., "Design and evaluation of a three-dimensional optimal ascent guidance algorithm," *Journal of Guidance, Control and Dynamics*, pp. 867–875, 1998.

[96] Y. T. Kim K. and C. A.J, "κ- modification in adaptive control," *Proc. AIAA Infotech Conf.*, 2010.

[97] M. J. Calise A.J., Yucelen T. and Y. B.J, "A loop recovery method for adaptive control," *Proc. AIAA Guidance, Navigation, and Control Conf.*, 2009.

Appendix A

Scramjet Engine Model

A short overview of the scramjet engine model is briefed here.

Scramjet Model

The scramjet engine forms the air breathing combustion system in which free stream air is compressed in the intake due to ram effect and then allowed into the combustion chamber where the fuel is injected and combustion take place. The hot gases after combustion are exhausted through convergent divergent nozzle to produce the thrust.

Scramjet model used in [1] consists of an inlet, an isentropic diffuser, a 1D Rayleigh flow combustor, and an isentropic internal nozzle. A single (long) fore-body compression ramp provides conditions to the rear-shifted scramjet inlet. Figure A.1 shows the schematic of a scramjet vehicle. The inlet is a variable geometry inlet but for this study the diffuser

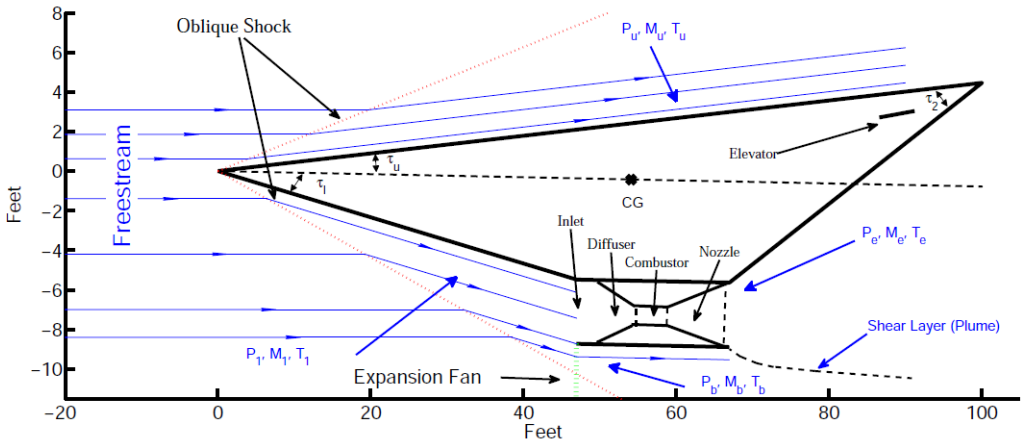

Figure A.1: Schematic of scramjet vehicle

area ratio $A_d = \frac{A_2}{A_1} = 1$. Figure A.2 shows the schematic of scramjet engine. The model assumes the presence of an infinitely fast cowl door which uses angle of attack to manage the shock-on lip condition.

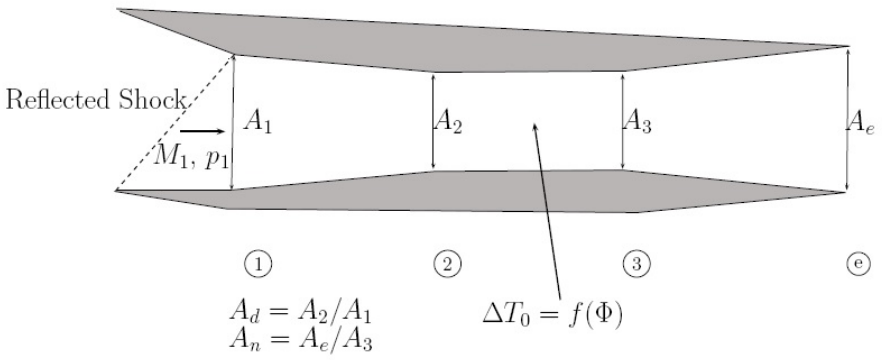

Figure A.2: Schematic of scramjet engine

At the design operating condition, the bow shock impinges on the engine inlet and at speeds below the design flight condition and/or larger flow turning angles, the cowl moves forward to capture the shock. At larger speeds and/or smaller flow turning angles, the bow shock is swallowed by the engine. In either case, there is a shock reflected from the cowl or within the inlet (i.e. we have a bow shock reflection). This reflected shock further slows down the flow and steers it into the engine. It should be noted that shock-shock interactions are not modeled. The model uses liquid hydrogen (LH2) as the fuel. It is assumed that fuel mass flow is negligible compared to the air mass flow. The model also captures linear fuel depletion.

Bow shock conditions: A bow shock will occur provided flow deflection angle δ_s is positive

$$\delta_s = \alpha + \tau_{1l} + \text{flexing angle} > 0\,\text{deg} \tag{A.1}$$

where $\tau_{1l} > 6.2\,\text{deg}$ is the lower fore-body wedge angle (see Figure A.1). If $\delta_s < 0$, a Prandtl-Meyer expansion will occur. Given the above, a bow shock occurs when the following flow turning angle (FTA) condition is satisfied

$$FTA = \alpha + \text{flexing angle} > 6.2\,\text{deg} \tag{A.2}$$

The properties (mach,temperature,pressure) across the bow shock inlet, diffuser exit, com-

bustor inlet and combustor exit can be computed using compressible flow dynamics. The bow reflection turns the flow parallel into the scramjet engine. If f denotes fuel-to-air ratio and f_{st} denotes stoichiometric fuel-to-air ratio, then the stoichiometric normalized fuel equivalence ratio is given by $\Phi = \frac{f}{f_{st}}$ which is the engine control. The purpose of the expanding internal nozzle is to recover most of the potential energy associated with the compressed (high pressure) supersonic flow. The thrust produced by the scramjet's internal nozzle is given by

$$Thrust_{internal} = \dot{m}_a(v_e - v_\infty) + (p_e - p_\infty)A_e \tag{A.3}$$

where $\dot{m}_a$ is the air mass flow rate through the engine, v_e is the exit flow velocity, v_∞ is the free-stream flow velocity, p_e is the pressure at the engine exit plane, A_1 is the engine inlet area, A_e is the engine exit area. The purpose of the expanding external nozzle is to recover the rest of the potential energy associated with the compressed supersonic flow. The length of the nozzle should be properly selected so that exit pressure is equal to free stream pressure and maximum thrust is produced.

$$Thrust_{external} = p_\infty L_a \frac{p_c}{p_\infty}\left[\frac{\ln\left(\frac{p_c}{p_\infty}\right)}{\frac{p_c}{p_\infty} - 1}\right]\tan(\tau_2 + \tau_{1u}) \tag{A.4}$$

Total thrust is $T_{tot} = Thrust_{internal} + Thrust_{external}$

Controller for Scramjet Engine

The main objective of the controller for scramjet engine is

1. dynamically produces the thrust by tracking the thrust command by regulating the fuel flow to the combustion chamber.

2. regulation of back pressure to manage the shock at the inlet as forward as possible so that the maximum pressure recovery is achieved with minimum fuel by varying the throat area of the nozzle.

The Figure A.3 shows the schematic air-breathing combustion system. Stations 1 through 4 form the intake; Station 2 is the cowl lip, and Station 3 is the notional location of the terminal shock. Stations 4 through 7 represent the combustor, Station 5 is the fuel injection point, and Station 6 is the dump behind which the pilot flame is maintained. The exhaust

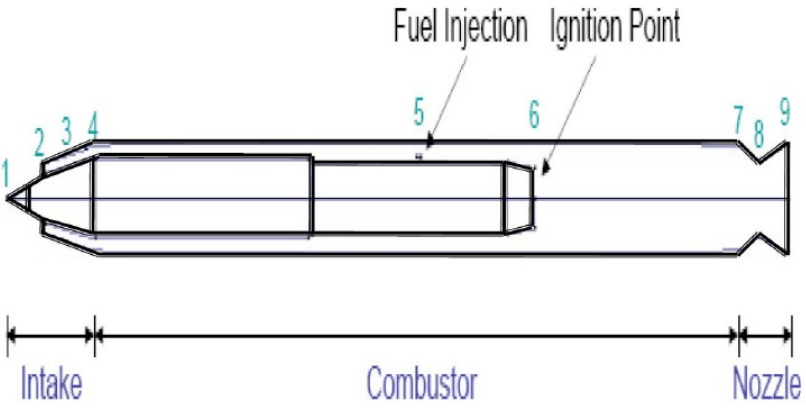

Figure A.3: Schematic of air-breathing combustion system

nozzle extends from Stations 7 to 9 with Station 8 being the throat. The dynamics of the combustion system is represented by following set of differential equation

$$\dot{P}_4 = \frac{1}{\tau_{54}}[P_{4ss} - P_4] \tag{A.5}$$

$$\dot{P}_5 = \frac{1}{\tau_{75}}[P_{4ss} - P_4] \tag{A.6}$$

$$\dot{T}_{05} = \frac{1}{\tau_{45}}[T_{05ss} - T_{05}] \tag{A.7}$$

$$\dot{m}_3 = \frac{1}{\tau_{45}}[\dot{m}_{5ss} - \dot{m}_5] \tag{A.8}$$

Using isentropic flow relations to compute the choked mass flow rate $\dot{m}_8$ through the throat with recovery factor $r_n = 0.98$ and $\gamma = 1.2$

$$\dot{P}_7 = \frac{1}{B}[\dot{m}_7 - A_{th}\frac{r_n P_{07}\sqrt{\gamma}}{\sqrt{RT_{07}}}(\frac{2}{\gamma+1})^{\frac{\gamma+1}{2(\gamma-1)}}] \tag{A.9}$$

$$\dot{P}_7 = \frac{1}{\tau_{57}}[P_{7ss} - P_7] \tag{A.10}$$

$$\dot{T}_{07} = \frac{1}{\tau_{57}}[T_{07ss} - T_{07}] \tag{A.11}$$

$$\dot{m}_7 = \frac{1}{\tau_{57}}[m_{7ss} - m_7] \tag{A.12}$$

where Pi is pressure at station i, $P0i$ and $T0i$ are stagnation pressure and temperature at station i respectively, $\dot{m}_i$ is the mass flow rate at station i, τ_{ij} is the time constant between stations i (1 to 9) and j (1 to 9), B is the back pressure factor, R is the universal gas constant and A_{th} is the throat area control. the interface between different components of air breathing combustion system is shown in Figure A.4

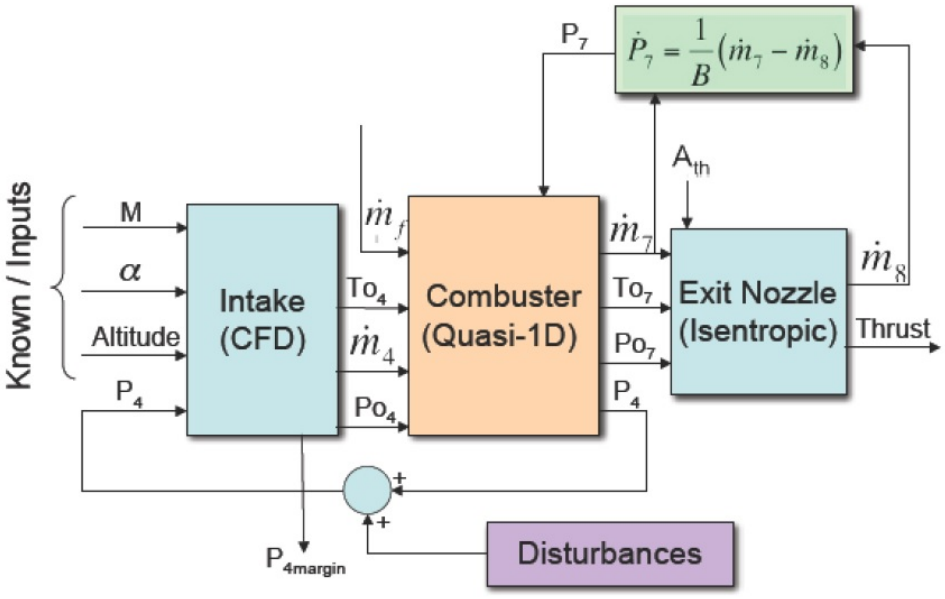

Figure A.4: Interface between different components of air-breathing combustion system

It is important for the controller to maintain the shock at the intake so that high air flow rate is achieved. This depends on the pressure P_4 at Station 4 at the given flight condition altitude, velocity and flight path angle. If P_4 exceeds a critical value P_{4c} then the air flow into the combustor is drastically reduced and thrust will be low. If the pressure is very low then pressure recovery is poor and fuel consumption will be more to produce the same thrust. Thus the controller has to maintain the pressure P_4 to a predefined value p_{4opt} which is marginally less than P_{4c}. This achieved by controlling the throat area A_{th}. The throat dimension is varied using throat area actuator based on A_{th} control.

Fuel flow rate controller is designed to control fuel flow rate into the chamber so that

thrust follows the commanded thrust. Thus in summary, the controller for air breathing combustion system has intake back pressure P_4 as the output with fuel flow rate and nozzle throat area as input. But the range of the thrust variation obtained with throat area is limited. The two controllers can be blended with single P_4 command input as both throat area and fuel flow rate influence almost the entire range of P_4 values. Strategy for the controller design is shown in Figure A.5.

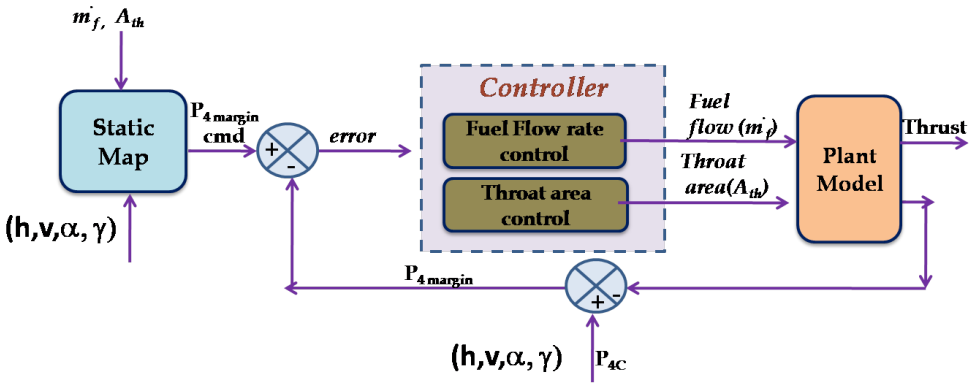

Figure A.5: Controller for air-breathing combustion system

Appendix B

Aerodynamic Force and Moment Coefficients

Aerodynamic force and moment coefficients of the basic vehicle and the control surfaces are generated from the data base of [77]. Aerodynamic force and moment coefficients of the basic vehicle as a function of angle of attack and Mach number are shown in Figure B.1 to Figure B.6.

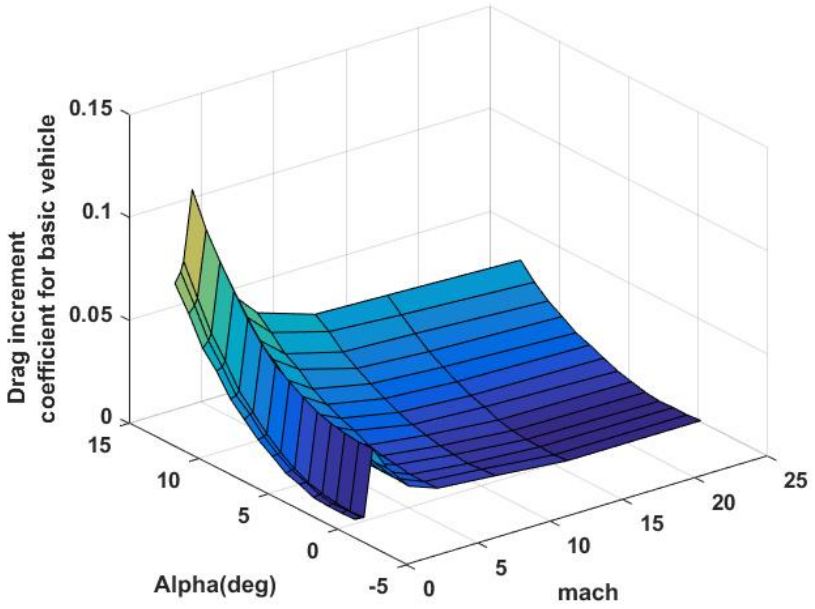

Figure B.1: Drag increment coefficient of basic vehicle (C_{D0}) as a function of α and M_a

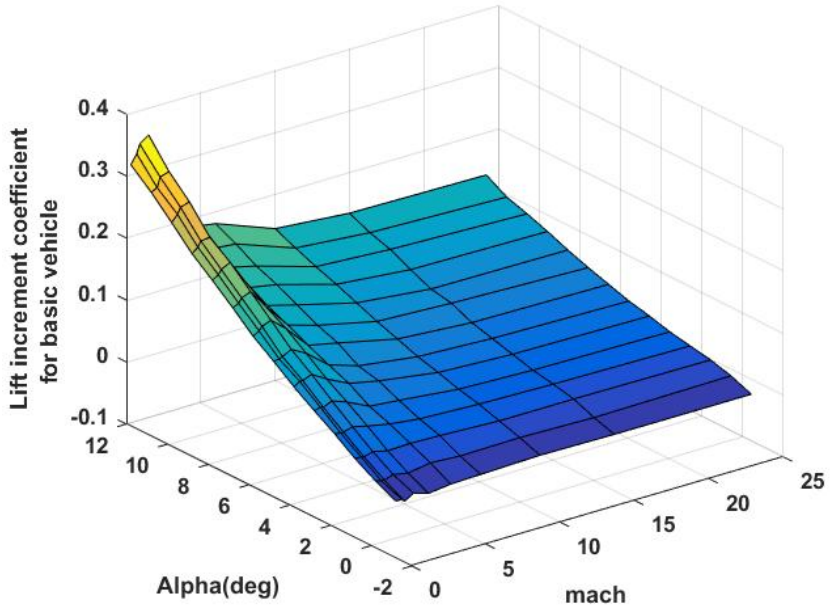

Figure B.2: Lift increment coefficient of basic vehicle (C_{L0}) as a function of α and M_a

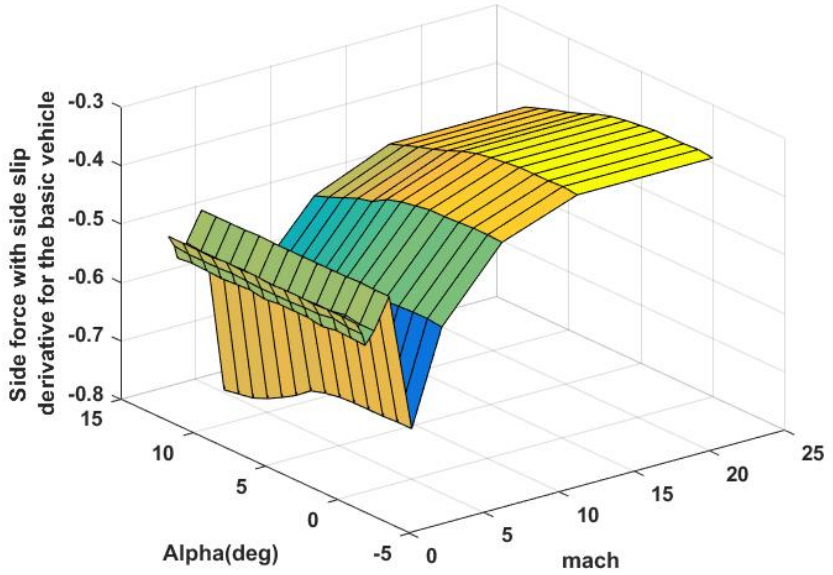

Figure B.3: Side force with side slip derivative of basic vehicle $(C_{Y\beta})$ as a function of α and M_a

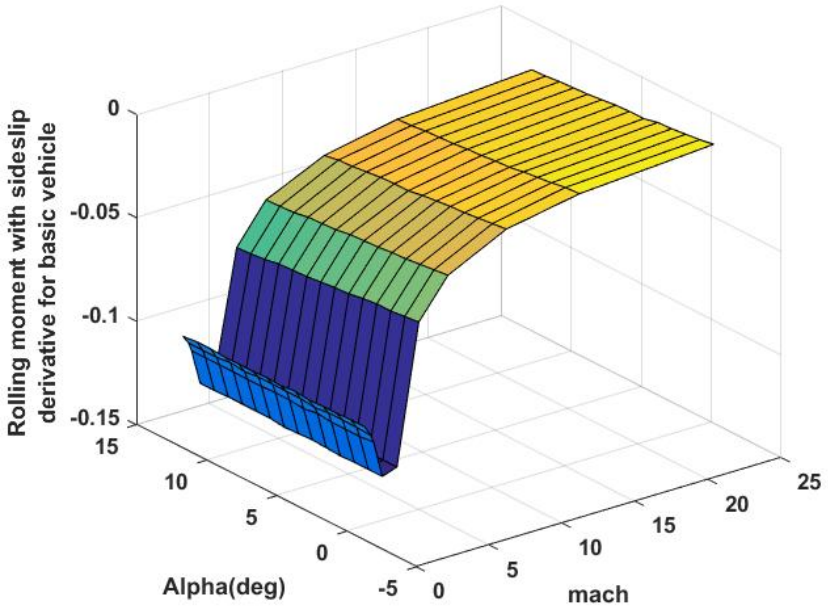

Figure B.4: Rolling moment with side slip derivative of basic vehicle $(C_{l\beta})$ as a function of α and M_a

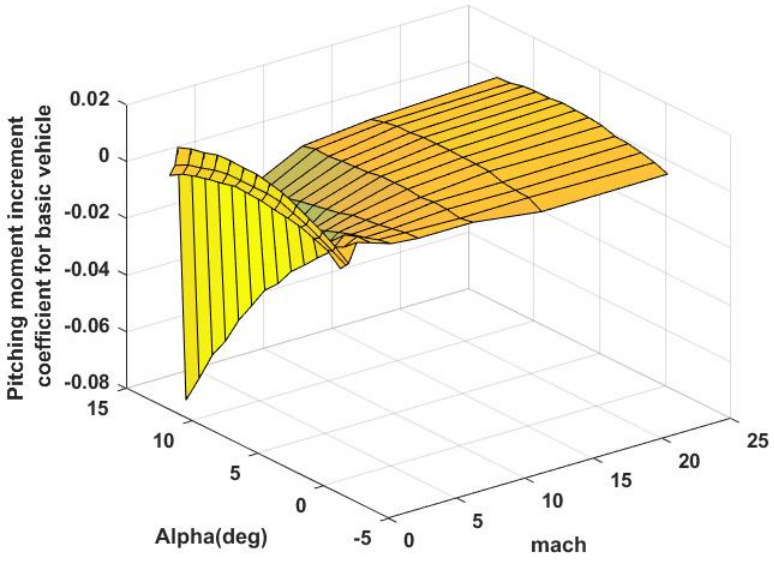

Figure B.5: Pitching moment increment coefficient of basic vehicle (C_m) as a function of α and M_a

The damping derivative for basic vehicle are shown in Figure B.7 to Figure B.9.

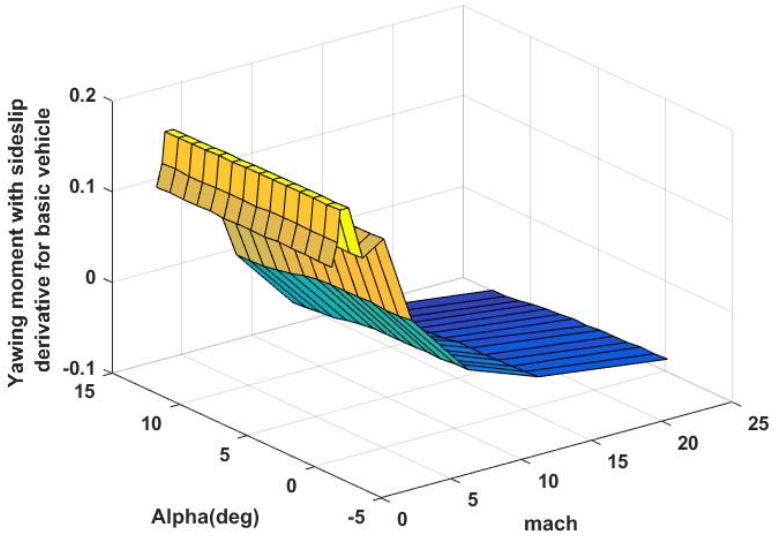

Figure B.6: Yawing moment with side slip derivative of basic vehicle $(C_{n\beta})$ as a function of α and M_a

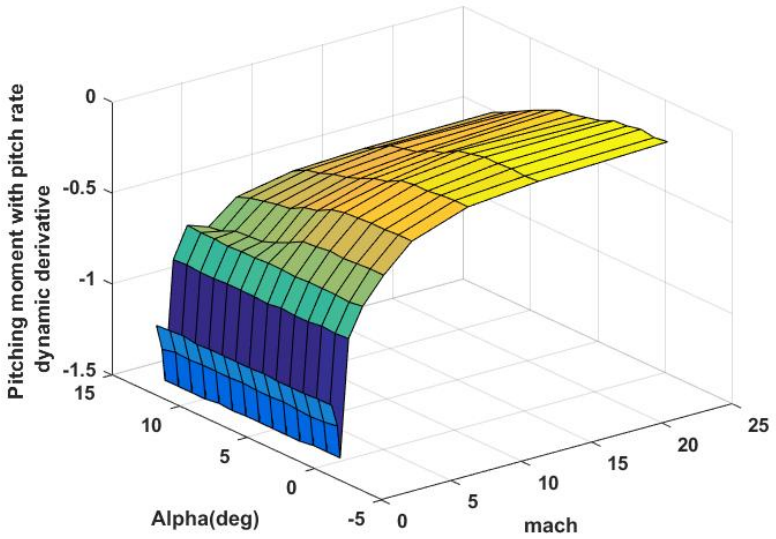

Figure B.7: Pitching moment with pitch rate dynamic derivative of basic vehicle (C_{mq}) as a function of α and M_a

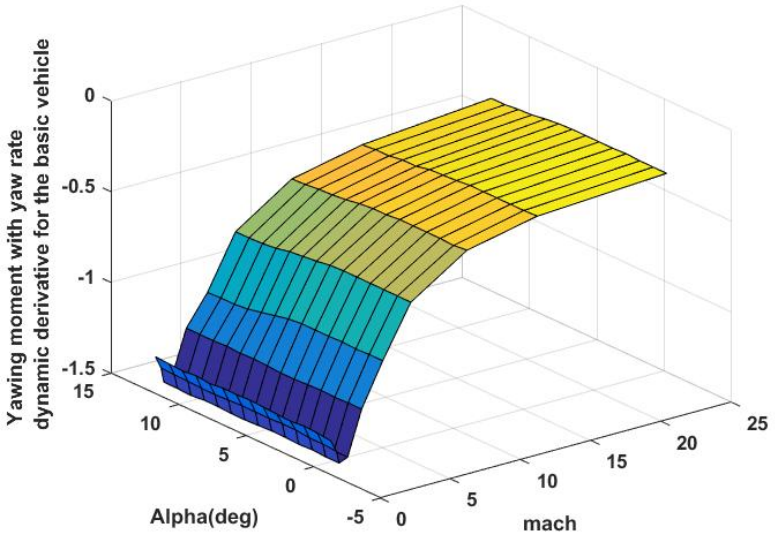

Figure B.8: Yawing moment with yaw rate dynamic derivative of basic vehicle (C_{nr}) as a function of α and M_a

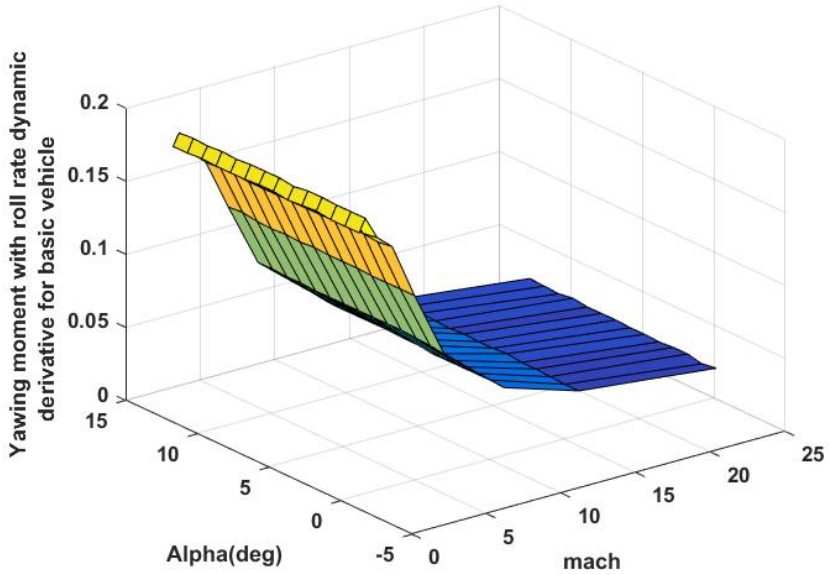

Figure B.9: Yawing moment with roll rate dynamic derivative of basic vehicle (C_{np}) as a function of α and M_a

The force and moment coefficient for left elevon are shown in Figure B.10 to Figure B.15.

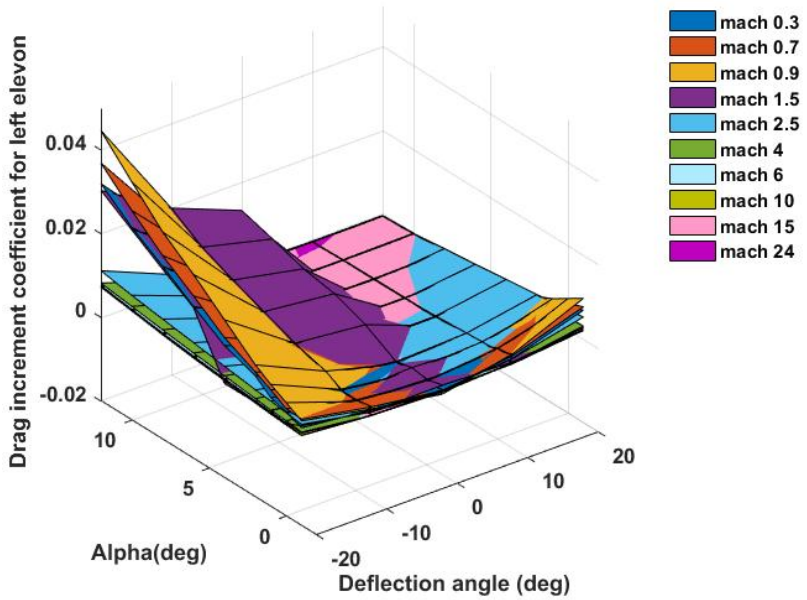

Figure B.10: Drag coefficient for left elevon $(C_{d\delta_l})$ as a function of α and M_a

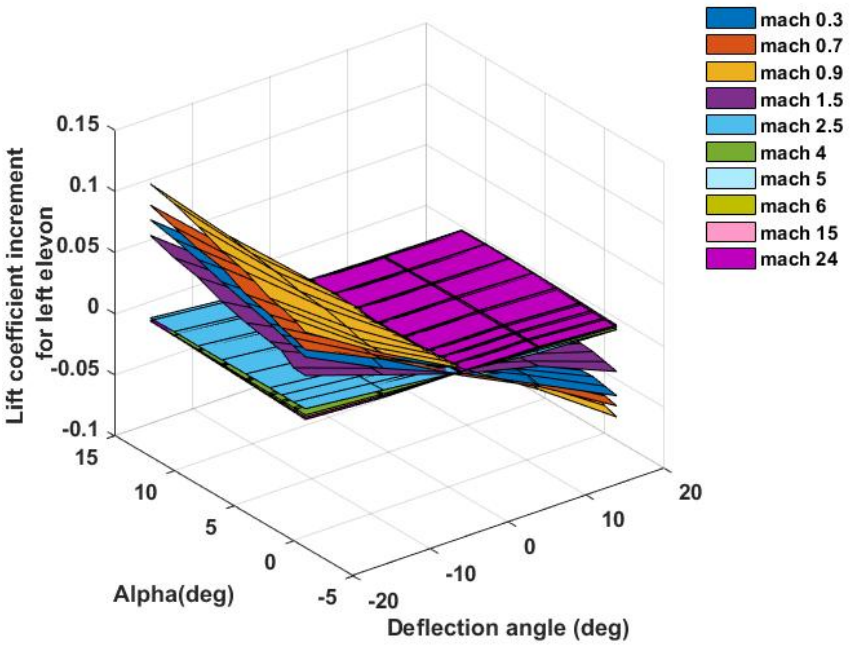

Figure B.11: Lift coefficient for left elevon $(C_{L\delta_l})$ as a function of α and M_a

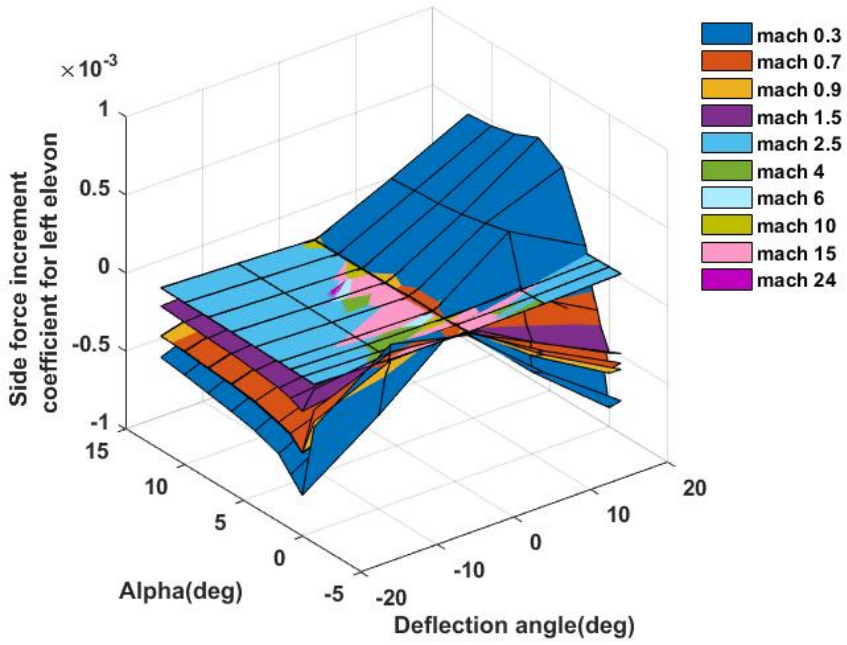

Figure B.12: Side force increment coefficient for left elevon $(C_{y\beta\delta_l})$ as a function of α and M_a

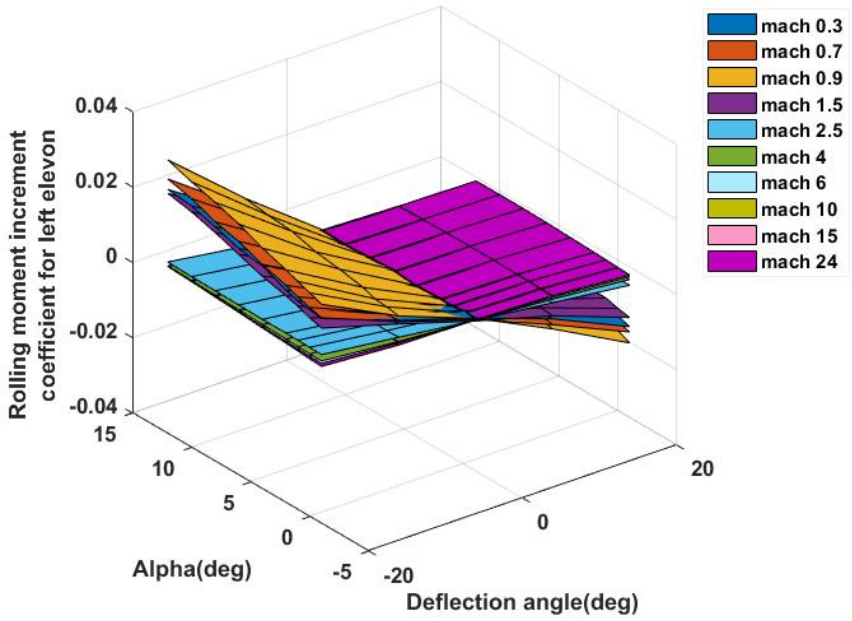

Figure B.13: Rolling moment coefficient for left elevon $(C_{l\delta_l})$ as a function of α and M_a

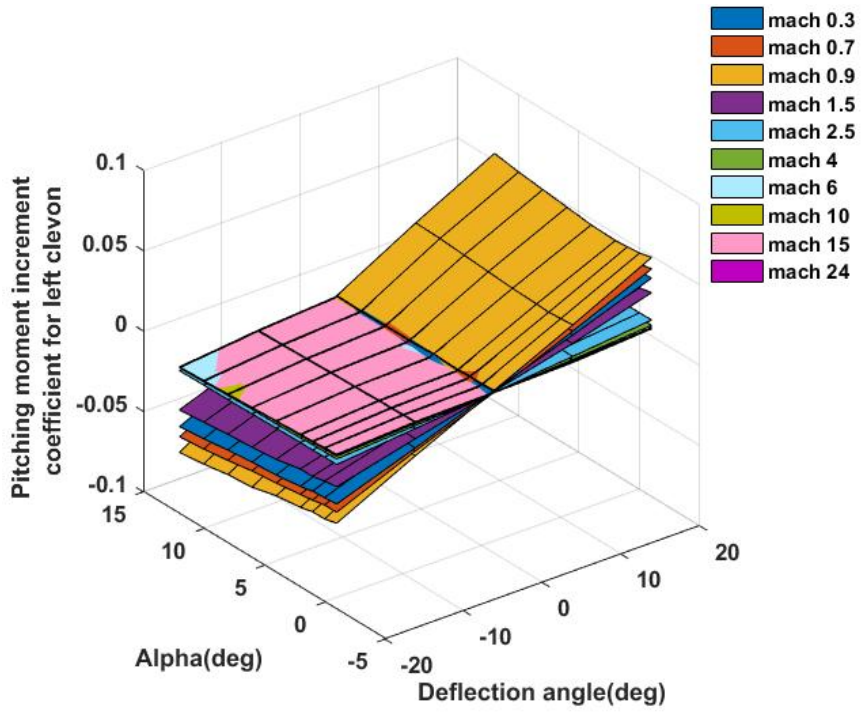

Figure B.14: Pitching moment coefficient for left elevon $(C_{m\delta_l})$ as a function of α and M_a

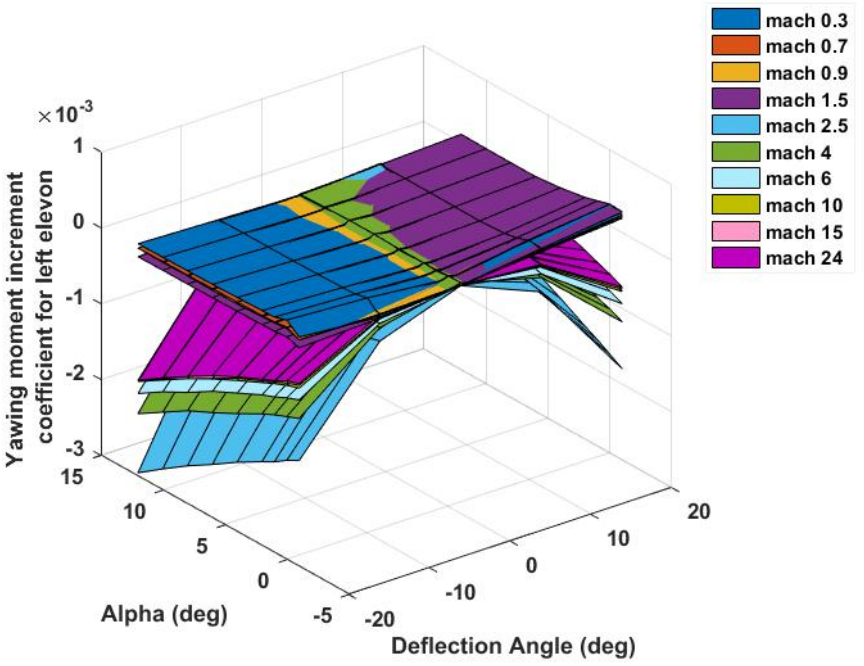

Figure B.15: Yawing moment coefficient for left elevon $(C_{n\delta_l})$ as a function of α and M_a

The force and moment coefficient for right elevon are shown in Figure B.16 to Figure

B.21.

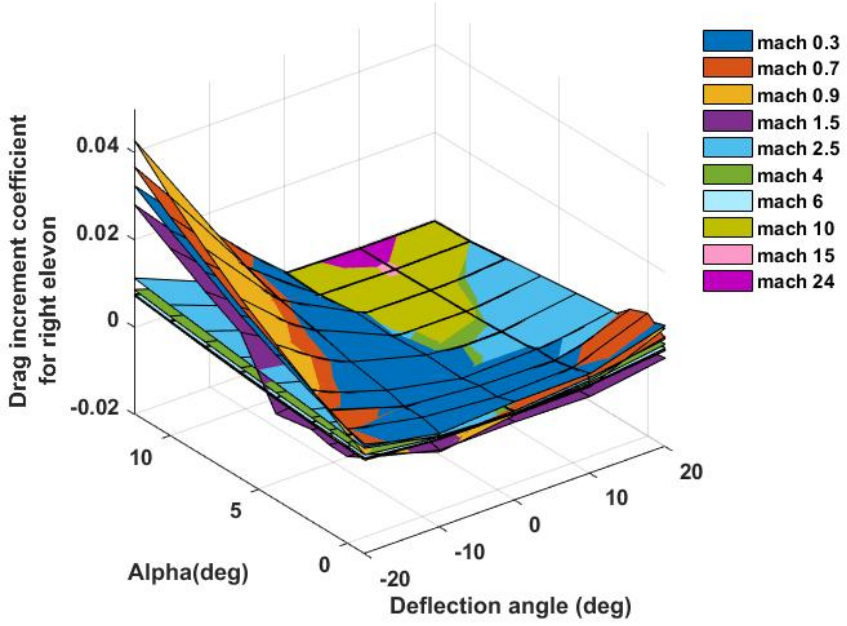

Figure B.16: Drag coefficient for right elevon $(C_{d\delta_r})$ as a function of α and M_a

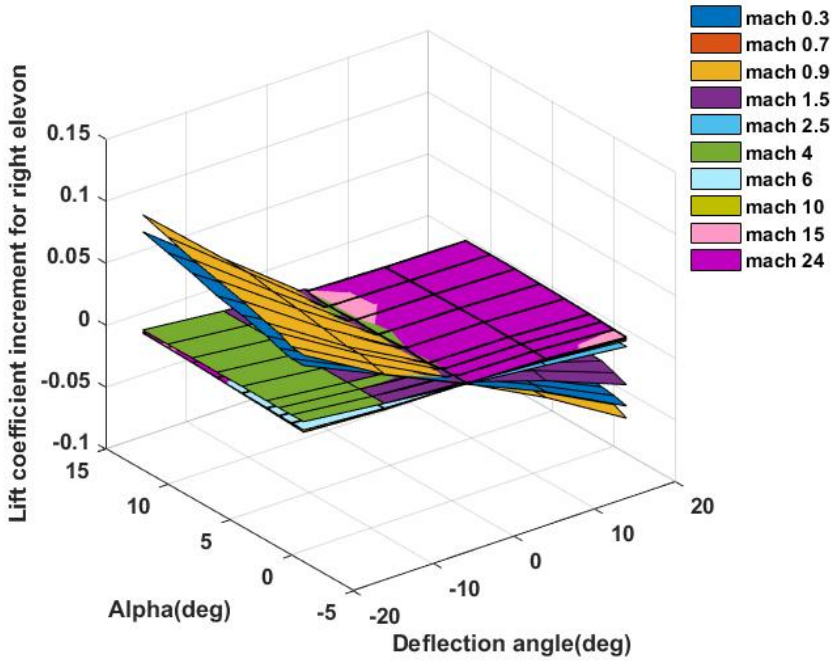

Figure B.17: Lift coefficient for right elevon $(C_{L\delta_r})$ as a function of α and M_a

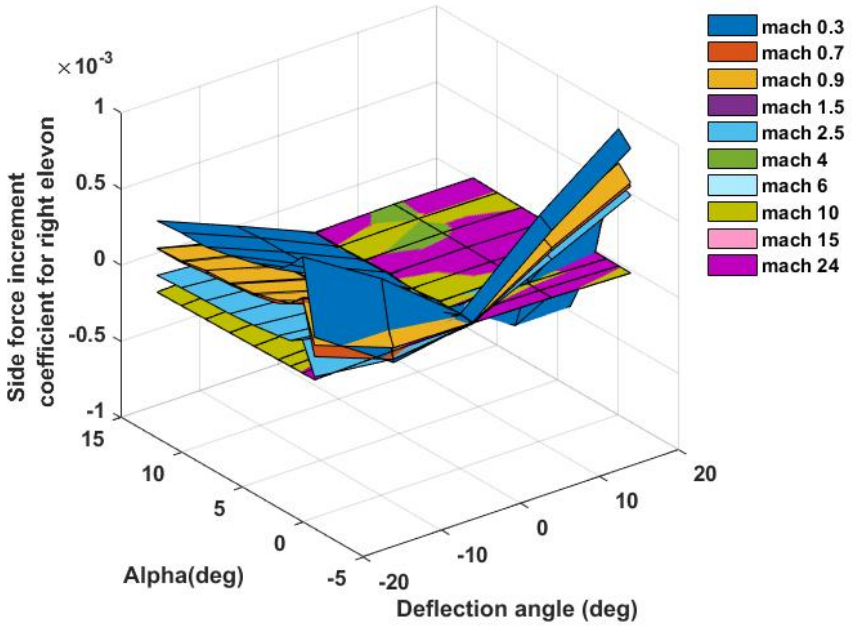

Figure B.18: Side force increment coefficient for right elevon $(C_{y\beta\delta_r})$ as a function of α and M_a

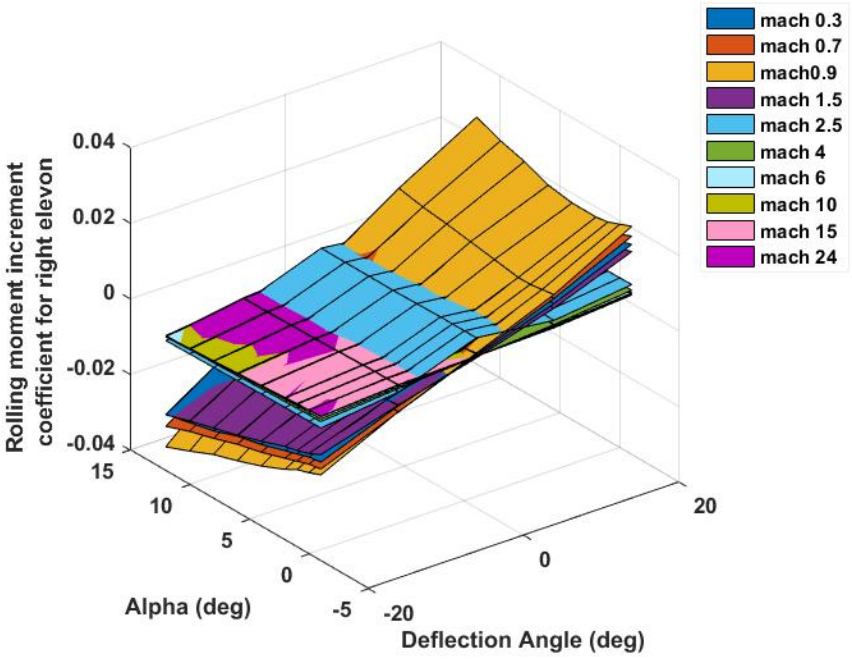

Figure B.19: Rolling moment coefficient for right elevon $(C_{l\delta_r})$ as a function of α and M_a

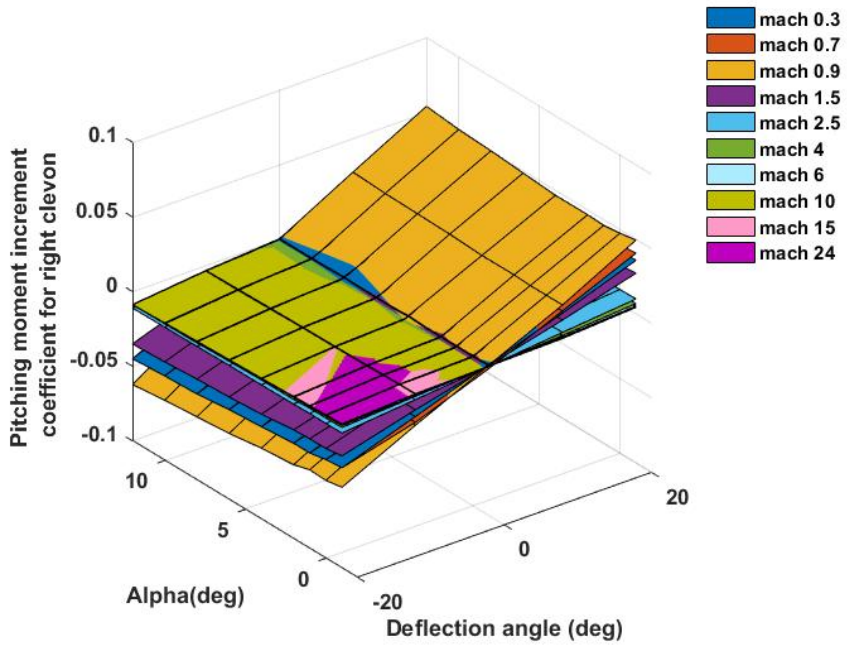

Figure B.20: Pitching moment coefficient for right elevon $(C_{m\delta_r})$ as a function of α and M_a

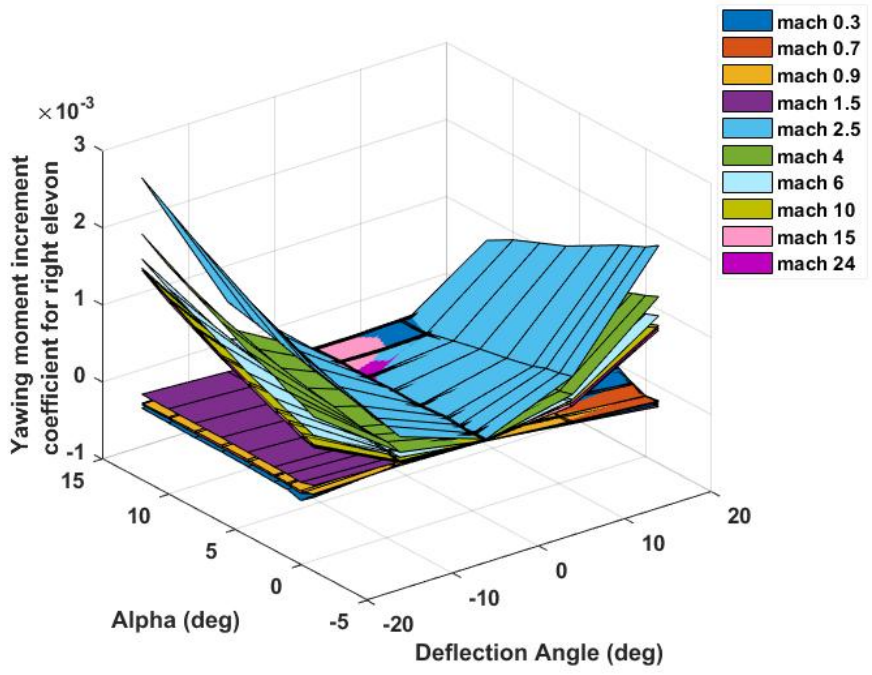

Figure B.21: Yawing moment coefficient for right elevon $(C_{n\delta_r})$ as a function of α and M_a

The force and moment coefficient for rudder are shown in Figure B.10 to Figure B.15.

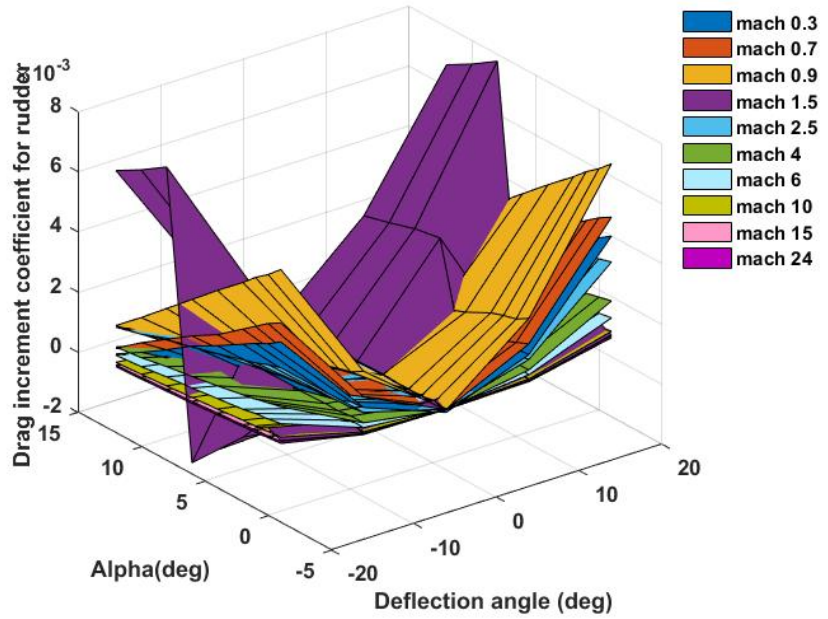

Figure B.22: Drag coefficient for rudder $(C_{d\delta_{ru}})$ as a function of α and M_a

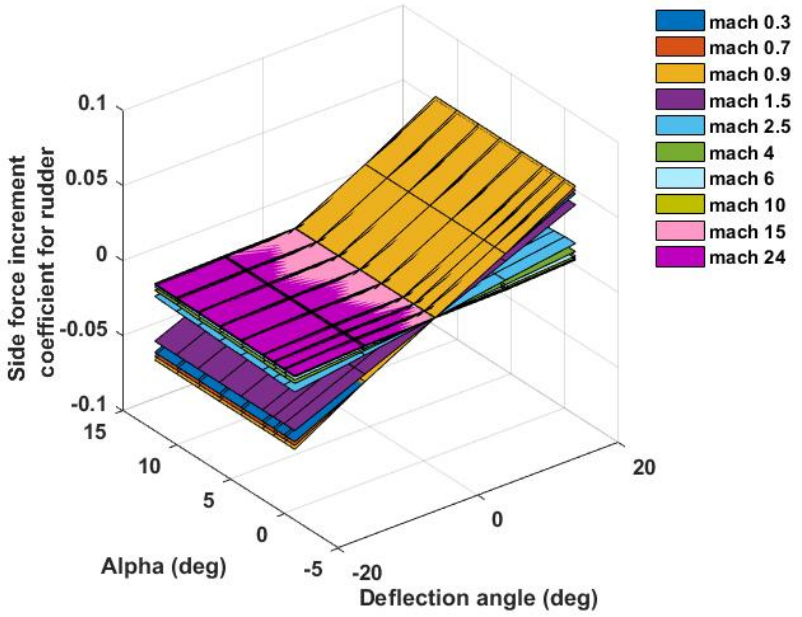

Figure B.23: Side force increment coefficient for rudder $(C_{y\beta\delta_{ru}})$ as a function of α and M_a

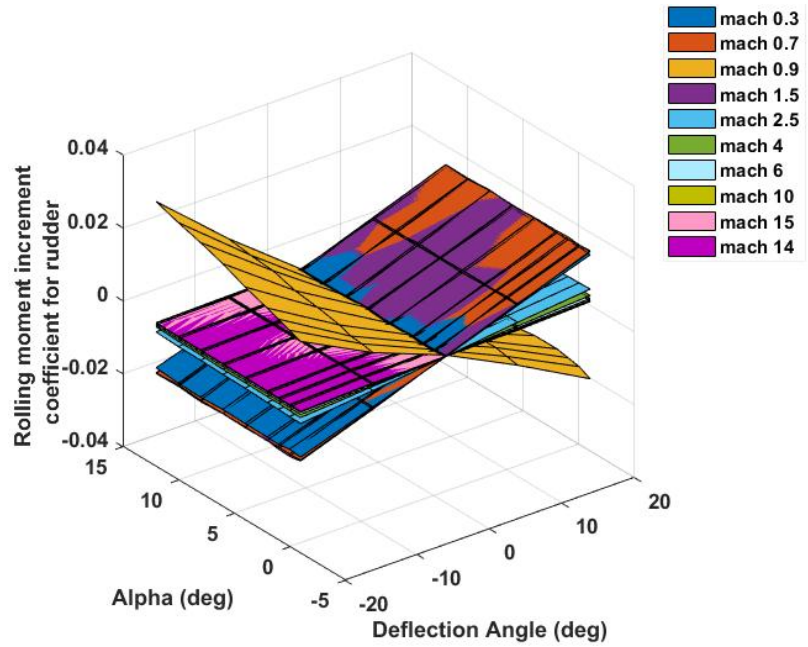

Figure B.24: Rolling moment coefficient for rudder $(C_{l\delta_{ru}})$ as a function of α and M_a

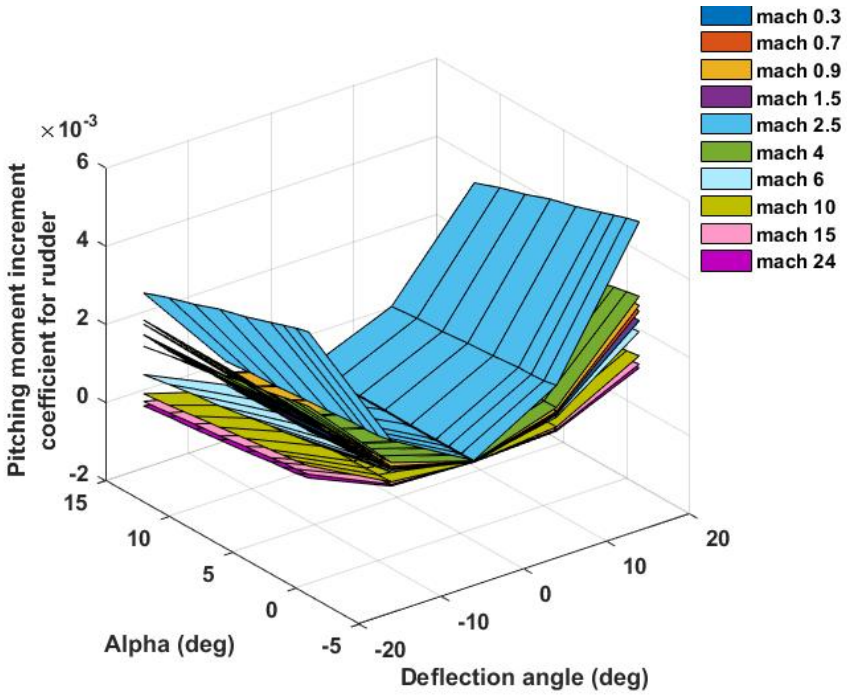

Figure B.25: Pitching moment coefficient for rudder $(C_{m\delta_{ru}})$ as a function of α and M_a

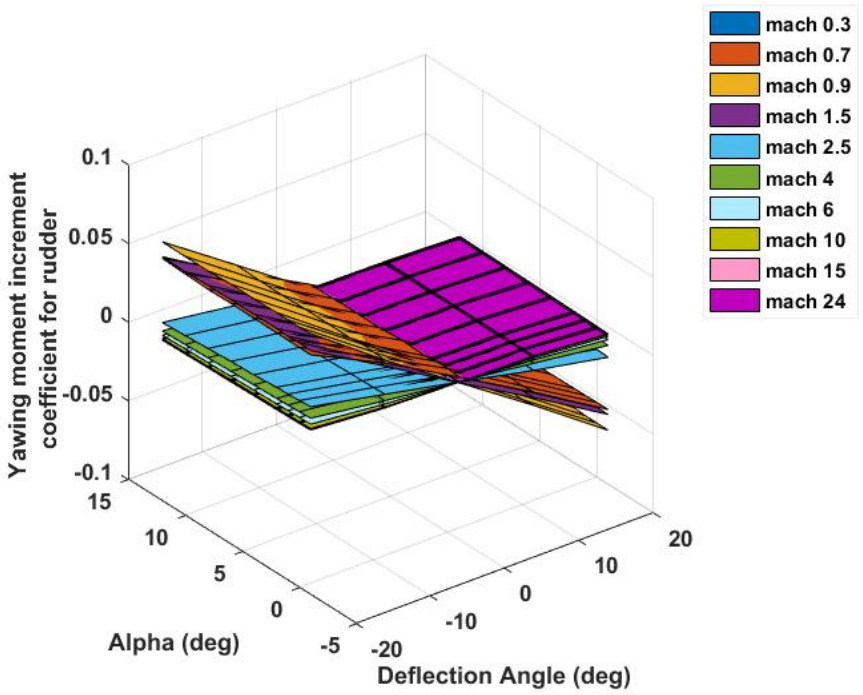

Figure B.26: Yawing moment coefficient for rudder $(C_{n\delta_{ru}})$ as a function of α and M_a

Appendix C

Vacuum Phase Guidance : Analytical Optimal Solution

Analytical solutions for optimal guidance problem in vacuum phase are available [95] over the past decades as summarized in [22]. The main features of the algorithm are

1. linear gravity gradient approximation

2. the closed form solution of co-state equation

3. the closed form solution of state equation using quadrature formulae

Let r_0 be the position vector. Then acceleration due to gravity g is approximated as a linear function of the position vector r as

$$g = \frac{\mu_E}{r_0^3} = -\omega^2 r \tag{C.1}$$

where μ_E is the gravitational parameter of the earth and ω is the Schuler frequency at r_0. This approximation preserves the change in direction of g with respect to r_0 and magnitude is slightly different from that of a Newtonian central gravity field. For the exo-atmosphere phase the axial aerodynamic force A and normal aerodynamic force L are zero, hence Equation 3.14 and 3.15 reduces to

$$\dot{r_I} = V_I \tag{C.2}$$

$$\dot{V_I} = g r_I + \frac{T I_b}{m} \tag{C.3}$$

Let $g_0 = \frac{\mu_E}{r_0^3}$ be the magnitude of acceleration due to gravity at r_0. Normalizing the equation with g_0 gives

$$\dot{V_I} = -r + T(\tau)I_b \tag{C.4}$$

where $T(\tau) = \frac{T_{vac}}{m(\tau)g_0}$ with τ as normalized time computed at the beginning of each guidance cycle. Considering the control constraint $\mu({I_b}^T I_b - 1)$, the Hamiltonian in Equation 3.18 reduces to

$$H = P_r^T V_I + P_v^T[-r + T(\tau)I_b] + \mu({I_b}^T I_b - 1) \tag{C.5}$$

The optimal condition $\frac{\partial H}{\partial \vec{I_b}} = 0$ gives

$$I_b^* = \frac{T(\tau)}{2\mu} P_v \tag{C.6}$$

The sufficient condition for optimal control is

$$\frac{\partial^2 H}{\partial {I_b}^2} = 2\mu I_3 < 0 \tag{C.7}$$

We have $\mu < 0$, hence the well proved concept that optimal thrust direction must be aligned to the direction co-state vector P_v. The co-state equations 3.19 and 3.20 now become

$$\dot{P_r} = P_v \tag{C.8}$$

$$\dot{P_v} = -P_r \tag{C.9}$$

The co-state equations have a closed loop solution of the form

$$\begin{bmatrix} P_v(\tau) \\ -P_r(\tau) \end{bmatrix} = \begin{bmatrix} \cos(\tau)I_3 & \sin(\tau)I_3 \\ -\sin(\tau)I_3 & \cos(\tau)I_3 \end{bmatrix} \begin{bmatrix} P_{v0}(\tau) \\ -P_{r0}(\tau) \end{bmatrix} = \Omega(\tau) \begin{bmatrix} P_{v0}(\tau) \\ -P_{r0}(\tau) \end{bmatrix} \tag{C.10}$$

where P_{v0}, P_{ro} are the initial values of co-state vectors at the beginning of each guidance cycle and I_3 denotes a 3x3 unit matrix. Now the thrust integrals can be defined as

$$I_c(\tau) = \int_0^\tau I_{pv} \cos\zeta T(\zeta) \mathrm{d}\zeta = \int_0^\tau \dot{I}_c(\zeta) \mathrm{d}\zeta \tag{C.11}$$

$$I_s(\tau) = \int_0^\tau I_{pv} \sin\zeta T(\zeta) \mathrm{d}\zeta = \int_0^\tau \dot{I}_c(\zeta) \mathrm{d}\zeta \tag{C.12}$$

Here the thrust varies with time as mass is changing. It is assumed that throttling of the engine is adjusted such that the axial acceleration constraint is met. Using this solution of thrust integrals, the state equations are given by

$$\begin{bmatrix} r(\tau) \\ V(\tau) \end{bmatrix} = \Omega \begin{bmatrix} r_0 \\ V_0 \end{bmatrix} + \Gamma(\tau) \begin{bmatrix} I_c(\tau) \\ I_s(\tau) \end{bmatrix} \tag{C.13}$$

where

$$\Gamma(\tau) = \begin{bmatrix} \sin(\tau) I_3 & -\cos(\tau) I_3 \\ \cos(\tau) I_3 & \sin(\tau) I_3 \end{bmatrix}$$

The the thrust integrals I_c and I_s are solved using numerical quadrature scheme. P.Lu etal uses Milne's rule for higher precision and low computational time with $\delta = \tau_{togo}/4$ where τ_{togo} is the time required to reach the engine cut off, which can be computed for optimal problem with free final time. With Milne's rule the thrust integrals are

$$I_i(\tau_{togo}) = \frac{\tau_{togo}}{90}[7\dot{I}_i(0) + 32\dot{I}_i(\delta) + 12\dot{I}_i(2\delta) + 32\dot{I}_i(3\delta) + 7\dot{I}_i(4\delta)] \quad i = c, s \tag{C.14}$$

Using this thrust integrals, co-states are solved using Equation C.14. Thus the state, co-state variables and the six terminal conditions as per Equations 3.30, 3.31 are functions of P_{r0}, P_{v0}. The time-to go τ_{togo} for engine shut off is computed from Equation 3.60. From the co-state Equation C.10 it can be shown that

$$\frac{\mathrm{d}\|P(\tau)\|}{\mathrm{d}\tau} = 0 \tag{C.15}$$

which follows $\|P(\tau)\| =$ constant. Thus the seventh terminal condition

$$\|P(\tau)\| = 1 \tag{C.16}$$

is satisfied if P_0 is scaled to have $\|P_0\| = 1$. To summarize the minimum time vacuum phase optimal guidance problem is a root finding problem with seven unknowns, terminal, transversal constraints and constraint given by Equation C.16, which can be solved using modified Newton method.

Appendix D

Derivative Based Adaptive Control

Consider the overall system represented by

$$\dot{x}_m(t) = A_m x_m(t) + B_m u(t) + H_g x_g(t) \tag{D.1}$$

$$\dot{x}_g(t) = A_g x_g(t) + H_m x_m(t) \tag{D.2}$$

where $x_m(t)$ is the modelled state vector, $u(t)$ is the control input vector, $x_g(t)$ is the unmodelled state vector and H_g, H_m and A_g are unknown parameters. To handle the parameter and model uncertainties, derivative based adaptive control law is used. The control input to plant is modified to continuously track the reference system as

$$u(t) = \nu(t) + u_{ada}(t) \tag{D.3}$$

where the adaptive part $u_{ada}(t)$ is

$$u_{ada} = -\hat{w}_m^T(t)\mu_m[x_m(t)] \tag{D.4}$$

Based on derivative based adaptive law, estimated weight function should satisfy the update law given by

$$\dot{\hat{w}}_m(t) = \Gamma \mu_m(x_m(t))\varepsilon^T(t)PB_m(\alpha, Q) \tag{D.5}$$

where

$$\varepsilon(t) = x_t(t) - x_m(t) \tag{D.6}$$

is the tracking error and Γ is the adaption gain with $\Gamma > 0$.

Stability Analysis

Using the Lyapunov functional the stability properties can be examined.

$$\begin{aligned}\mathcal{V}[\varepsilon(t), \tilde{w}_m(t), x_g(t)] = \frac{1}{2}\varepsilon(t)^2(t) + \frac{1}{2}{x_g}^2(t) \\ + \frac{\Gamma^{-1}B_m}{2}\tilde{w}_m(t)\tilde{w}_m^T(t)\end{aligned} \tag{D.7}$$

where

$$\tilde{w}_m(t) = w_m(t) - \hat{w}_m(t) \tag{D.8}$$

is the weight estimation error and $\varepsilon(t)$ satisfies

$$\varepsilon(t) = -A_t(\alpha, Q)\varepsilon(t) + B_m(\alpha, Q)w_m(t)\mu_m[x_m(t)] + H_g x_g(t) \tag{D.9}$$

Differentiating the above equation gives

$$\begin{aligned}\dot{\mathcal{V}}[\varepsilon(t), \tilde{w}_m(t), x_g(t)] \leq -\begin{bmatrix}|\varepsilon(t)| \\ |x_g(t)|\end{bmatrix}^T \begin{bmatrix}A_t & -\frac{1}{2}(|H_m| + |H_g|\end{bmatrix} \begin{bmatrix}|\varepsilon(t)| \\ |x_g(t)|\end{bmatrix} \\ -\frac{1}{2}(|H_m| + |H_g|) \quad A_g \\ + |H_m\|x_t(t)\|x_g(t)|\end{aligned} \tag{D.10}$$

then

$$\begin{bmatrix}A_t & -\frac{1}{2}(|H_m| + |H_g|\end{bmatrix} > 0 \tag{D.11}$$
$$-\frac{1}{2}(|H_m| + |H_g|) \quad A_g$$

which implies

$$A_t A_g > \frac{1}{4}(|H_m| + |H_g|)^2 \tag{D.12}$$

is the sufficient condition for closed loop stability as the last term in Equation D.9 is linear in $x_g(t)$. Hence the only way to improve the robustness to unmodelled dynamics is to increase A_t. Generally A_t detects the bandwidth of the closed loop system, it can not be chosen sufficiently large to improve the robustness to unmodelled dynamics as there is a likelihood of control saturation. Thus the adaptive gain law can generate high feedback gain for fast adaption which excites the unmodelled dynamics and leads to instability and unbounded solutions.

Modification terms for adaptive laws

Modification terms can be added to the adaptive laws to improve the robustness. The idea behind the leakage term is to modify the adaptive law in such a way that the time derivative of Lyapunov function is becomes negative when the the estimate of uncertain parameters exceeds certain limit. The various modifications for leakage term in $\dot{w}_m(t)$ equation are

1. with $e-$**modification**[2] term the Equation D.5 modifies to

$$\dot{\hat{w}}_m(t) = \Gamma \mu_m(x_m(t))\varepsilon^T(t)PB_m(\alpha, Q) - \Gamma_e \|\varepsilon(t)\|\hat{w}_m(t) \tag{D.13}$$

   where Γ_e is a fixed gain.

2. with $\sigma-$**modification** term the Equation D.5 modifies to

$$\dot{\hat{w}}_m(t) = \Gamma \mu_m(x_m(t))\varepsilon^T(t)PB_m(\alpha, Q) - \Gamma_\sigma \hat{w}_m(t) \tag{D.14}$$

   where Γ_σ is a fixed gain.

3. Another effective method of eliminating parameter drift and keeping the estimation of parameters to lie inside some known convex bound set in the estimation space is the gradient projection method.

   with **projection methods** D.5 modifies to

$$\dot{\hat{w}}_m(t) = \Gamma_p Proj[\hat{w}_m(t), \mu_m(x_m(t))\varepsilon^T(t)PB_m(\alpha, Q)] \tag{D.15}$$

   where Γ_p is a fixed gain.

   Projection operator-Proj: Consider a convex hyperspace of the form

   $\Omega = \left\{\theta \in \mathrm{Re}^n : (\theta_i^{min} \leq \theta_i \leq \theta_i^{max})_{i=1,2,\ldots,n}\right.$ where θ_i^{min} and θ_i^{max} respectively represent the minimum and maximum values of i^{th} component of the $n-$dimensional vector θ.

   Further consider a sufficiently small positive constant ϵ_0, consider another hyperspace of the form $\Omega_{\epsilon_0} = \left\{\theta \in \mathrm{Re}^n : (\theta_i^{min} + \epsilon_0 \leq \theta_i \leq \theta_i^{max} - \epsilon_0)_{i=1,2,\ldots,n}\right.$ where $\Omega_{\epsilon_0} \in \Omega$ then the projection operator $Proj :\in \mathrm{Re}^n\, \mathrm{Re}^n\, \mathrm{Re}^n$ is defined component

wise as

$$Proj[\theta, y] = \begin{cases} \frac{(\theta_i^{max} - \theta_i)y}{\epsilon_0}, & \text{if} \quad \theta_i > \theta_i^{max} - \epsilon_0 \quad \text{and} \quad y_i > 0 \\ \frac{(\theta_i - \theta_i^{min})y}{\epsilon_0}, \text{if} & \quad \theta_i < \theta_i^{min} + \epsilon_0 \quad \text{and} \quad y_i < 0 \\ y_i & \text{otherwise where} \quad y_i \in \mathrm{Re}^n \end{cases} \tag{D.16}$$

4. with κ**-modification** the system is desired to achieve a prescribed natural frequency and damping for error transients. This provides a filtering effect which helps to get smooth transient responses. Along with $\sigma-$modification term, κ-modification is also introduced with which D.5 modifies to

$$\dot{\hat{w}}_m(t) = \Gamma \mu_m(x_m(t))\varepsilon^T(t)PB_m(\alpha, Q) - \Gamma_\sigma \hat{w}_m(t) - \Gamma_\kappa \int_{t-T}^{t} \hat{w}_m(s)ds \tag{D.17}$$

   where Γ_κ [96] is the positive stiffness learning rate and $T > 0$ adding an integral form of stiffness to the first order weight update law. κ-modification is equivalent to having a T time delayed feedback of weight estimate so that oscillations in the adaptive control can be reduced by proper choice Γ_κ along with other adaption gains.

5. Similarly **Optimal control modification** [46], [97] also adds damping to the weight update law there by reducing the high frequency oscillations. The damping term depends on persistent excitation condition. With this excitation also the weight functions are bounded and exponentially stable. With optimal modification Equation D.5 modifies to

$$\begin{aligned} \dot{\hat{w}}_m(t) &= \Gamma \mu_m(x_m(t))\varepsilon^T(t)PB_m(\alpha, Q) \\ &\quad - \Gamma_{op}\mu_m(x_m(t))\mu_m(x_m(t))^T \hat{w}_m(t)B_m^T P A_t^{-1} B_m \end{aligned} \tag{D.18}$$

For derivative based adaptive law, high adaptive gain is required for the fast adaption which is expected to have adverse effect on robust stability and normal tracking performance. About the leakage terms added to improve the robustness, σ and $e-$modifications require no prior information about the plant. Projection based adaptive laws with dynamic normalization are robust with respect to the dynamic uncertainty.

List of Publications

Papers in Refereed International Journals

1. **Rani Radhakrishnan** and Priyadarsanam Hari, M.S. Harsha Simha and K.Sivan. *6D trajectory, guidance and control development for air-breathing phase of reusable launch vehicles*, International Journal of Dynamics and Control, January 2023 DOI: 10.1007/ s40435-023-01126-4.

2. **Rani Radhakrishnan** and Priyadarsanam Hari, M.S. Harsha Simha and K.Sivan. *Adaptive integrated guidance and control for air-breathing phase of reusable launch vehicles*, International Journal of Dynamics and Control, July 2024 DOI:10.1007/ s40435-024-01477-6.